



HYDRATION KINETICS AND SHRINKAGE BEHAVIOR OF  
HYBRID ALKALINE CEMENTS

A Thesis Submitted by

Lili Xue

For the award of

Doctor of Philosophy

2021

This page is intentionally blank

## ABSTRACT

Hybrid alkaline cement (HAC) which is composed of more than 70% supplementary cementitious materials (SCMs), less than 30% Portland cement and a small dosage of alkali activator is considered as a promising alternative material to Portland cement due to its low carbon emissions and excellent mechanical properties. An overview on the hydration mechanisms of HACs and durability is provided in this paper. It is evident that HAC is more durable than Portland cement in a number of environments; however, the lack of long-term track records in field is the barrier for application. The knowledge gap to facilitate the future research and development of HAC materials is also discussed.

In this study, HACs were prepared using 75% granulated blast furnace slag (GBFS) and/or fly ash (FA) and 25% Portland cement with external addition of 3%-5% alkali activator. The influence of precursors and  $\text{Na}_2\text{O}$  content on hydration heat, reaction extent and microstructural development were investigated to understand the early hydration kinetics. Increasing the  $\text{Na}_2\text{O}$  content improved the compressive strength and reaction extent gradually. The fly-ash based HAC shows slower hydration rate and lower reaction extent than that of slag-based HAC due to the much lower reactivity of fly ash, resulting in reduced compressive strength and slightly delayed setting.

One industrial by-product gypsum is used to retard the rapid setting of HAC. The influence of gypsum on setting time, hydration products and microstructure of HACs were investigated. The setting time of HACs were lengthened with the increase in the gypsum and reached their maximum when the dosage was 20%. The XRD and TG analysis results show that the monosulfate and thaumasite were generated in HACs with gypsum rather than ettringite. The incorporation of gypsum led to the reduction of hydration products and a loose microstructure. The retarding effect of gypsum was considered to be the decline of iron dissolution rate caused by chemical reaction instead of coverage theory.

Shrinkage is a vital factor for hybrid alkali activated cement (HAC) related to

durability. In this work, the drying shrinkage behavior of HAC mortars with various precursors, curing regimes and activator states was investigated. Portland cement mortar and alkali activated cement (AAC) mortar were used as control groups. Results showed that the drying shrinkage magnitude of HAC mortar is lower than that of AAC mortar but higher than that of Portland cement mortar. Slag-based HAC mortar shows the largest shrinkage value and the incorporation of fly ash could temper shrinkage slightly. The steam curing and solid activation could mitigate the magnitude of drying shrinkage for HAC mortar. MIP, SEM, and XRD analyses results show that the pore size distribution which is related to the capillary pressure, amount of crystalline phase and Ca/Si ratio in product gel are the primary factors affecting the shrinkage behavior of HAC.

The impact of Global Warming Potential (GWP) is employed to evaluate and quantify the carbon dioxide emissions of one cubic HAC concretes. The CO<sub>2</sub> footprint of HAC concrete is approximately 43-55% less than comparable concrete containing 100% OPC binder, whereas the carbon footprint of HACs is slightly higher than that of geopolymer concrete and AAC concrete. The carbon emission of HAC decreases when the fly ash is substituted for slag. Increasing the alkali contents of HAC results in an increase in carbon emissions. In terms of activator, HAC activated by waterglass shows the highest carbon emission, while HAC with sodium hydroxide shows the lowest. In conclusion, HAC can be considered as a low-carbon cementitious material due to its lower impact on global warming.

## **CERTIFICATION OF THESIS**

This Thesis is the work of Lili Xue except where otherwise acknowledged, with the majority of the authorship of the papers presented as a Thesis by Publication undertaken by the student. The work is original and has not previously been submitted for any other award, except where acknowledged.

**Student:** Lili Xue

**Principle supervisor:** Hao Wang

**Associate supervisor:** Zuhua Zhang

# STATEMENT OF CONTRIBUTION

## Journal papers

1. **Lili Xue**, Zuhua Zhang\*, Hao Wang: Hydration mechanisms and durability of hybrid alkaline cements (HACs): A review. *Construction and Building Materials*, 2021,266:121039.

The overall contribution of **Lili Xue** was 60% the concept development, analysis, drafting and revising the final submission; **others** contributed the other 40% to concept development, analysis, editing and providing important technical inputs.

2. **Lili Xue**, Zuhua Zhang\*, Hao Wang\*\*\*: Early hydration kinetics and microstructure development of hybrid alkali activated cements (HACs) at room temperature. *Cement and Concrete Composite*, 2021,123:104200.

The overall contribution of **Lili Xue** was 60% the concept development, analysis, drafting and revising the final submission; **others** contributed the other 40% to concept development, analysis, editing and providing important technical inputs.

3. **Lili Xue**, Zuhua Zhang\*, Hongfei Liu, Yuanhai Jiang, Hao Wang\*\*\*: Retarding mechanism of gypsum for hybrid alkali activated cements (HACs) at ambient temperature. *Construction and Building Materials* (Submitted).

The overall contribution of **Lili Xue** was 60% the concept development, analysis, drafting and revising the final submission; **others** contributed the other 40% to concept development, analysis, editing and providing important technical inputs.

4. **Lili Xue**, Zuhua Zhang\*, Hongfei Liu, Yuanhai Jiang, Hao Wang\*\*: Drying shrinkage behavior of hybrid alkali activated cements (HACs) mortars. Construction and Building Materials (Submitted).

The overall contribution of *Lili Xue* was 60% the concept development, analysis, drafting and revising the final submission; *others* contributed the other 40% to concept development, analysis, editing and providing important technical inputs.

### Conference Paper

5. **Lili Xue**, Zuhua Zhang\*, Hao Wang: Influence of precursor and activator state on hydration, mechanical properties and microstructure of hybrid alkaline cement (HAC), The 4<sup>th</sup> international conference on Chemically Activated Materials, to be held at Hefei, China, from 26<sup>th</sup> to 28<sup>th</sup> August, 2021.

The overall contribution of *Lili Xue* was 80% the concept development, analysis, drafting and revising the final submission; *others* contributed the other 40% to concept development, analysis, editing and providing important technical inputs.

## **ACKNOWLEDGEMENTS**

The training of doctoral study is a very important experience, which is a precious treasure for my whole life. I would like to thank everyone for supporting me to finish my PhD thesis. Firstly, I want to acknowledge my supervisors, Prof. Hao Wang and Dr. Zuhua Zhang. Their profound knowledge and keen insight have provided me with key inspiration and help in the topic selection and writing of my paper. In particular, my supervisors took pains to guide me in professional knowledge and scientific research through biweekly seminars and supervised me to complete my doctoral project. Thanks to their valuable advice and support, I was able to complete my doctoral thesis successfully.

I would like to acknowledge the financial support received from the USQ International Fees Research Scholarship. Also, the living stipend scholarship by Jiaxing University is acknowledged. In addition, the financial support from Zhejiang Longding company is acknowledged.

I also would like to acknowledge the Prof. Ganghua Pan team of Southeast University for providing me with a lot of help in the experiment. The laboratory of Nanjing Hydranlic Research Institute is also acknowledged for its experimental assistance.

Finally, I think of giving thanks to my family for their continuous support.

# TABLES OF CONTENTS

<b>ABSTRACT</b> .....	I
<b>CERTIFICATION OF THESIS</b> .....	III
<b>STATEMENT OF CONTRIBUTION</b> .....	IV
<b>ACKNOWLEDGEMENTS</b> .....	VI
<b>TABLES OF CONTENTS</b> .....	VII
<b>LIST OF FIGURES</b> .....	XI
<b>LIST OF TABLES</b> .....	XV
<b>LIST OF ABBREVIATIONS</b> .....	XVII
<b>CHAPTER 1: INTRODUCTION</b> .....	1
<b>CHAPTER 2: REVIEW ON THE HYDRATION MECHANISMS AND DURABILITY</b> .....	4
<b>2.1 Introduction</b> .....	4
<b>2.2 Hydration mechanisms of HACs</b> .....	6
<b>2.2.1 Hydration process of HACs</b> .....	6
<b>2.2.2 Microstructure features</b> .....	10
<b>2.2.3 Setting time</b> .....	15
<b>2.3 Resistance to aggressive solutions</b> .....	16
<b>2.3.1 Sulfate attack</b> .....	16
<b>2.3.2 Chloride penetration</b> .....	17
<b>2.3.3 Carbonation</b> .....	18
<b>2.4 Alkali-silica reaction (ASR)</b> .....	20
<b>2.4.1 Influence factors of ASR of AAMs and control</b> .....	20
<b>2.4.2 ASR of HACs</b> .....	21
<b>2.5 Resistance to high temperatures</b> .....	22
<b>2.6 Some hints on shrinkage behavior of HAC</b> .....	23
<b>2.6.1 Shrinkage behavior of AAMs</b> .....	24
<b>2.6.2 Influence factors and control</b> .....	24
<b>2.7 Some hints on efflorescence</b> .....	26

2.8 Perspectives for future research .....	28
2.9 Conclusions .....	29
<b>CHAPTER 3: RESEARCH PLAN AND METHODOLOGY .....</b>	<b>31</b>
3.1 Introduction .....	31
3.2 Research Plan .....	31
3.3 Materials .....	32
3.3.1 Solid materials .....	32
3.3.2 Alkali activator .....	33
3.3.3 Other materials and chemicals .....	34
3.4 Methodology .....	34
3.4.1 HAC hydration kinetics and control .....	34
3.4.2 HAC mortar shrinkage and strength .....	35
3.4.3 Microscopic characterization of HAC .....	36
3.5 Conclusions .....	37
<b>CHAPTER 4: EARLY HYDRATION KINETICS AND MICROSTRUCTURE</b>	
<b>DEVELOPMENT OF HAC AT ROOM TEMPERATURE .....</b>	<b>38</b>
4.1 Introduction .....	38
4.2 Materials and methods .....	39
4.2.1 Materials .....	39
4.2.2 Experimental method .....	41
4.3 Results and discussion .....	43
4.3.1 Setting time .....	43
4.3.2 Compressive strength .....	44
4.3.3 Hydration heat .....	44
4.3.4 Mineralogical analyses of hydration products .....	47
4.3.5 Microstructural development .....	53
4. 4 Conclusions .....	62
<b>CHAPTER 5: HYDRATION CONTROL-THE RETARDING MECHANISM OF</b>	
<b>GYP SUM FOR HACS .....</b>	<b>63</b>
5.1 Introduction .....	63

5.2 Materials and methods.....	64
5.2.1 Materials.....	64
5.2.2 Mixture proportions and specimen preparation .....	65
5.2.3 Experimental methods .....	66
5.3 Results and discussion .....	67
5.3.1 Setting time .....	67
5.3.2 Hydration heat characterization.....	68
5.3.3 XRD analyses of hydration products .....	70
5.3.4 TG analysis of hydration products.....	73
5.3.5 SEM-EDX analyses of hydration products .....	77
5.3.6 Retarding mechanism.....	81
5.4 Conclusions .....	82
<b>CHAPTER 6: SHRINKAGE BEHAVIOR OF HAC MORTARS .....</b>	<b>84</b>
6.1 introduction .....	84
6.2 Experimental programs.....	86
6.3 Results and discussion .....	89
6.3.1 Compressive strength .....	89
6.3.2 Drying shrinkage and water loss .....	89
6.3.3 Pore structure analysis.....	91
6.3.4 Mineralogical and morphological analysis.....	94
6.4. Conclusions .....	100
<b>CHAPTER 7: CARBON DIOXIDE EMISSIONS FOR HACs .....</b>	<b>102</b>
7.1 Introduction.....	102
7.2 Materials and methodology .....	102
7.2.1 Materials.....	102
7.2.2 Methodology .....	103
7.3 Results and discussion .....	104
7.3.1 Comparison of HACs, OPC, geopolymer and AAC concretes .....	105
7.3.2 Comparative analysis of HACs with different precursors and alkali contents .....	107

<b>7.3.3 Comparative analysis of HACs with different alkali activators</b> .....	108
<b>7.4 Conclusions</b> .....	109
<b>CHAPTER:8 CONCLUSIONS AND PERSPECTIVES</b> .....	110
<b>8.1 Conclusions</b> .....	110
<b>8.2 Perspectives</b> .....	112
<b>REFERENCES</b> .....	114
<b>APPENDIX</b> .....	130

# LIST OF FIGURES

## *Chapter 2*

Figure 2-1. A structural schematic diagram of the hydration process of HACs (García-lodeiro et al. 2013c).....	7
Figure 2-2. Heat flow of OPC, FA and M (OPC-FA70%) hydrated with (a) D1 (NaOH and Na <sub>2</sub> SiO <sub>3</sub> , pH 13.5); (b) D2 (Na <sub>2</sub> CO <sub>3</sub> pH 11.6)( García-Lodeiro et al. 2013b). ....	8
Figure 2-3. Activation model of HACs (70% FA+ 30% OPC) ( García-Lodeiro et al. 2013b). .....	9
Figure 2-4. Heat rate and total heat of OPC, HACs (OPC-GBFS80%) and OPC-GBFS blends (Angulo-Ramírez et al. 2017) .....	9
Figure 2-5. SEM micrographs of HACs a) OPC-GBFS 70%; b) OPC-FA 80% (Rivera et al. 2014). ....	10
Figure 2-6. SEM images of HACs (OPC-GBFS 80%) activated by NaOH and water glass (SS + NaOH) at 28 days (Angulo-Ramírez et al. 2017). ....	11
Figure 2-7. The molar percentage of gel composition determined by EDX (A) binder with liquid activator (B) binder with solid activator (Fernández-Jiménez et al. 2019).....	12
Figure 2-8. ITZ of (a) OPC concrete (Vargas et al. 2017) (b) HAC concrete (San Nicolas and Provis 2012). ....	14
Figure 2-9. XRD analysis of various hybrid OPC-geopolymer systems at 28 days (Legend: Q=Quartz, M=Mullite, P=Portlandite, C=Calcite, N=Nepheline, H=Hatruirite, □=CSH, △ =C(A)SH) (Askarian et al. 2018) .....	15
Figure 2-10. Structure and appearance of mortars exposed in Na <sub>2</sub> SO <sub>4</sub> solution (Bačuvčík et al. 2018). ....	17
Figure 2-11. Carbonation depth at different exposure time (Angulo-Ramirez et al. 2019) ....	19
Figure 2-12. ASR expansion of mortar bar in different test ages (Donatello et al. 2013b).....	21
Figure 2-13. ASR expansion in 6 months prismatic mortar at different conditions (HC eq HAC mortar; HM eq 70% PC and 30% HC mortar) (Palomo et al. 2019) .....	22
Figure 2-14. Visual changes in (a) FAN-4 and (b) MS pastes after temperature exposure.....	23

Figure 2-15. Time-dependent shrinkage of OPC and AAS under various RH conditions (Ye and Radlińska 2016) .....	25
Figure 2-16. Effect of Na <sub>2</sub> CO <sub>3</sub> to NaOH mole ratios and Na <sub>2</sub> O dosages on the drying shrinkage of AAS pastes (Jiao et al. 2018).....	26
Figure 2-17. Effect of curing condition on alkali leach ability and compressive strength of the geopolymer binder (Najafi Kani et al. 2012). .....	28

### ***Chapter 3***

Figure 3-1. XRD patterns of OPC, GBFS and FA: A: Alite; B: Belite; C: Calcite; T: Tricalcium aluminate; Q: Quartz; M: Mullite .....	33
Figure 3-2. XRD patterns of Gypsum. YH: CaSO <sub>4</sub> ·2H <sub>2</sub> O; Y: CaSO <sub>4</sub> .....	33

### ***Chapter 4***

Figure 4-1. XRD patterns of OPC, GBFS and FA: A: Alite; B: Belite; C: Calcite; T: Tricalcium aluminate; Q: Quartz; M: Mullite .....	41
Figure 4-2. Initial setting time and final setting time of OPC and HACs .....	43
Figure 4-3. Compressive strengths of OPC and HACs.....	44
Figure 4-4. Heat flow and cumulative heat of OPC and HACS with different Na <sub>2</sub> O contents .....	46
Figure 4-5. Heat flow and cumulative heat of OPC and HACs with different precursors.....	47
Figure 4-6. XRD patterns of HACS with different Na <sub>2</sub> O contents for 1-day and 7-day of curing. A: Alite; B: Belite; C: Calcite; H: Hydrocalumite (Mg <sub>6</sub> Al <sub>2</sub> (CO <sub>3</sub> (OH)) <sub>16</sub> ·4H <sub>2</sub> O); Ge: hydrated Gehlenite (C <sub>2</sub> ASH <sub>8</sub> ) .....	48
Figure 4-7. XRD patterns of HACs with different precursors at an early time, 2-day and 7-day of curing. A: Alite; B: Belite; C: Calcite; Q: Quartz; H: Hydrocalumite (Mg <sub>6</sub> Al <sub>2</sub> (CO <sub>3</sub> (OH)) <sub>16</sub> · 4H <sub>2</sub> O); Ge: hydrated Gehlenite (C <sub>2</sub> ASH <sub>8</sub> ); G: Gismondine; CSH: crystalline Calcium Silicate Hydrate.....	51
Figure 4-8. <sup>29</sup> Si NMR spectra of anhydrous OPC, GBFS, FA and 7-day cured HACS (a)with different Na <sub>2</sub> O contents;(b) with different precursors.....	54
Figure 4-9. Decomposition of the <sup>29</sup> Si NMR spectra of 7-day HACs pastes after subtraction of the signal from unreacted raw materials. ....	56

Figure 4-10. BESM images of HACS with different Na <sub>2</sub> O contents for 7 days of curing .....	58
Figure 4-11. BESM images of HACs with diverse precursors on 7 days of curing .....	59
Figure 4-12. Elemental distribution mapping of 7-day cured HACs with various precursors. .....	61

## ***Chapter 5***

Figure 5-1. XRD patterns of OPC, GBFS and Gypsum. A: Alite; B: Belite; C: Calcite; T: Tricalcium aluminate; YH: CaSO <sub>4</sub> ·2H <sub>2</sub> O; Y: CaSO <sub>4</sub> .....	65
Figure 5-2. Initial setting time and final setting time of OPC and HACs .....	68
Figure 5-3. Heat flow and cumulative heat of HACs with and without Gypsum .....	70
Figure 5-4. XRD spectra of OPC and HACs with and without Gypsum for initial setting and 24 h curing. A: Alite; B: Belite; C: Calcite; CSH: Calcium Silicate Hydrate; E: Ettringite; G: Gismondine (CaAl <sub>2</sub> Si <sub>2</sub> O <sub>8</sub> (H <sub>2</sub> O) <sub>4</sub> ); P: Portlandite; T: Thaumasite (Ca <sub>3</sub> Si (OH) <sub>6</sub> (CO <sub>3</sub> ) (SO <sub>4</sub> )(H <sub>2</sub> O) <sub>26</sub> ); S: Strätlingite (Ca <sub>2</sub> Al((AlSi) <sub>1.11</sub> O <sub>2</sub> ) (OH) <sub>12</sub> (H <sub>2</sub> O) <sub>2.25</sub> ); Y: Gypsum; Ms: Monosulphoaluminate (Ca <sub>4</sub> Al <sub>2</sub> (OH) <sub>12</sub> (SO <sub>4</sub> ) (H <sub>2</sub> O) <sub>6</sub> ); Mc: Monocarbonate. ....	72
Figure 5-5. TG and DTG analysis of hydrated OPC and HACs pastes at initial setting time, (a)TG and (b)DTG. ....	74
Figure 5-6. TG and DTG analysis of hydrated OPC and HACs paste after 24 h, (a)TG and (b)DTG.....	76
Figure 5-7. SEM images of OPC and HACs pastes at initial setting (a)OPC, (b)HAC, (c)HAC10, (d)HAC20, (e)HAC30.....	78
Figure 5-8. SEM micrographs of OPC and HACs pastes for 24 hours curing (a)OPC, (b)HAC, (c) HAC10, (d)HAC20, (e)HAC30.....	79
Figure 5-9. Element distribution in matrix of HACs .....	81

## ***Chapter 6***

Figure 6-1. XRD patterns of OPC, GBFS and FA: A: Alite; B: Belite; C: Calcite; T: Tricalcium aluminate; Q: Quartz; M: Mullite .....	87
Figure 6-2. Compressive strengths of OPC and HACs at different curing ages .....	89
Figure 6-3. Time-dependent drying shrinkage of OPC, AAC and HACs mortars.....	90
Figure 6-4. Water loss of OPC, AAC and HACs mortars .....	91

Figure 6-5. Total porosity and pore structure of OPC, AAC and HACs .....	92
Figure 6-6. Pore distribution of OPC, AAC and HACs pastes after 28 days curing.....	93
Figure 6-7. XRD patterns for OPC, AAC and HACs pastes after 28 days of curing. A: Alite; B: Belite; C: Calcite; P: Portlandite; E: Ettringite; G: calcium silicate hydrate; Q: Quartz; H: Hydrocalumite ( $Mg_6Al_2(OH)_{16}CO_3 \cdot 4H_2O$ ); Ge: hydrated Gehlenite ( $C_2ASH_8$ ).....	96
Figure 6-8. Microtopography of OPC, AAC and HACs pastes cured for 28 days .....	98

## ***Chapter 7***

Figure 7-1. A comparison of OPC, geopolymer, AAC and HAC binders on the impact of GWP of their concrete mixtures .....	106
Figure7-2. Summary of GWP100 for 1 m <sup>3</sup> HAC concretes with different precursors and different alkali contents.....	108
Figure 7-3. Comparison of GWP100 for 1 m <sup>3</sup> OPC and HAC concretes with different alkali activators .....	109

## LIST OF TABLES

### *Chapter 2*

Table 2-1. HACs reported in the literature: compositions, activators and compressive strengths .....	13
Table 2-2. Chloride permeability and Electrical Resistivity at 28 d of curing (Rivera et al. 2014). .....	18
Table 2-3. Si-O-(Si, Al) asymmetric stretch peak positions in FTIR spectra of P2 and P9 ( Najafi Kani et al. 2012). .....	27

### *Chapter 3*

Table 3-1. Technical indexes of Portland cement .....	32
Table 3-2. Chemical composition of Portland cement, GBFS and FA (wt.%).....	32
Table 3-3. Chemical composition of sodium silicate (wt.%).....	34

### *Chapter 4*

Table 4-1. Chemical composition of Portland cement, GBFS and FA (wt.%).....	40
Table 4-2. Composition of various HAC systems (wt.%).....	41
Table 4-3. XRD quantitative analysis of hydration products for HACS with different Na <sub>2</sub> O contents at 1 and 7 days age.....	49
Table 4-4. XRD quantitative analysis of HACs with different precursors at different ages ...	52
Table 4-5. Deconvolution results of <sup>29</sup> Si NMR spectra for 7-day HACs pastes after subtraction of the unreacted starting materials .....	57
Table 4-6. Elemental ratios of HACs hydration products .....	59

### *Chapter 5*

Table 5-1. Table 1 Chemical composition of Portland cement and GBFS (wt.%).....	64
Table 5-2. Proportions of HAC systems (wt.%) .....	66

### *Chapter 6*

Table 6-1. Chemical composition of Portland cement, GBFS and FA (wt.%).....	86
Table 6-2. Table 2 Composition of AAC and various HAC systems (wt.%).....	87

Table 6-3. Elemental ratios of OPC, AAC and HACs hydration gel .....100

***Chapter 7***

Table 7-1. Mix proportions for concretes (kg/m<sup>3</sup>).....104

Table 7-2. Inventory data and impacts associated with the raw materials, curing regime of  
OPC, geopolymer and HAC concretes. ....105

## LIST OF ABBREVIATIONS

AAC	Alkali Activated Cement
AAM	Alkali Activated Materials
ASR	Alkali-Silica Reaction
BSEM	Back Scatter Electron Microscopy
DTG	Derivative Thermogravimetric
FA	Fly Ash
GBFS	Granulated Blast Furnace Slag
HAC	Hybrid Alkaline Cement
HACS	Hybrid Alkaline Cement with Slag
HACF	Hybrid Alkaline Cement with Fly ash
HACSF	Hybrid Alkaline Cement with Slag and Fly ash
ITZ	Interfacial Transition Zone
MIP	Mercury Intrusion Porosimetry
NMR	Nuclear Magnetic Resonance
OPC	Ordinary Portland Cement
SCM	Supplementary Cementitious Materials (SCMs)
SEM	Scanning Electron Microscopy
SEM-EDS	Scanning Electron Microscopy with Energy Dispersive Spectroscopy
SP	Superplasticizer
TG	Thermogravimetric
XRD	X-Ray Diffraction
XRF	X-Ray Florescence

## CHAPTER 1: INTRODUCTION

As an indispensable building material, Portland cement makes great contribution to the global rapid development of infrastructure and urbanization in the past decades. Nonetheless, cement production also brings adverse impact to the global environment due to large emission of carbon dioxide and huge energy consumption (Schneider et al. 2011; Law et al.2012). Therefore, developing alternative cementitious materials with low carbon footprint but performance comparable to Portland cement is becoming a common objective for scientific and technical communities.

Hybrid alkaline cement (HAC) is a new promising cement alternative that comprises less than 30% Portland cement and more than 70% SCMs with a small dosage of activator (Palomo et al. 2007; García-Lodeiro et al.2016; Al-Kutti et al. 2018). Many investigations have been carried out on HACs, such as hydration process, mechanical properties and aspects of durability. HACs possess denser and more homogeneous microstructure than Portland cement and pure alkali activated cement due to more binding gels and coexisting of N-A-S-H and C-A-S-H, resulting in higher mechanical strength and lower permeability (García-Lodeiro et al. 2013c; Shi et al. 2011). It is worth mentioning that the hydration heat of Portland cement accelerates the alkali activation reaction of SCMs. As a result, HACs could set and develop strength at room temperature rather than high temperature curing that required by alkali activated cement (García-Lodeiro et al. 2013c; García-Lodeiro et al. 2011). In the current stage, HACs can be acceptable by the cement and concrete industry when the fully adoption of alkali-activated cementitious materials remains in doubt.

However, the issue of early hydration kinetics behavior which governs the workability, microstructure development (Cao et al. 2020) and mechanical properties of HACs is insufficiently understood. On the other hand, the shrinkage behavior and mechanism of HACs which is related to durability has not yet been well understood. To facilitate the application of HAC in practical engineering, it is necessary to address the hydration

kinetics control and shrinkage behavior of HACs. This study aims to understand and mitigate these problems. This work will provide fundamental knowledge about the hydration of hybrid alkaline cement and transfer technologies to industry. The innovation of this research lies in hydration kinetics and shrinkage behavior under the steam curing conditions or high temperature sealed conditions.

Chapter 2 provides an overview of the hydration mechanisms and some properties regarding durability of HACs, including resistance to aggressive solutions and high temperatures, carbonation and efflorescence, chloride ion penetration and alkali-aggregate reaction. It reports the influencing factors of hydration reaction and microstructure of HACs. It is evident that HAC is more durable than Portland cement in a number of environments; however, the lack of long-term track records in the field is the barrier for application. The knowledge gap to facilitate future research and development of HAC materials is also discussed.

Chapter 3 briefly introduces the research objectives and plans. The raw materials properties used in this thesis is given. The methodology and characterization procedures for the raw materials and HACs are outlined, especially the microanalysis.

Chapter 4 investigates the influence of precursors and Na<sub>2</sub>O content on setting time, mechanical properties, hydration heat, reaction extent and microstructural development in order to understand the early hydration kinetics. It is well known that type of precursors and alkali content are critical parameter of alkali-activated materials. The effective method to explore hydration kinetics of cementitious materials is isothermal conduction calorimetry. Moreover, the characterization of HAC via XRD quantitative analysis and <sup>29</sup>Si NMR spectroscopy is employed to explore the hydration kinetics of HACs. Correlate the hydration products with the kinetics of reaction.

In chapter 5, the hydration control of HACs is the focus. One industrial by-product gypsum is used to control the hydration and setting of HACs. The influence of gypsum on setting time, hydration products and microstructure of HACs were investigated via

isothermal calorimetric analysis, XRD, TG-DTG analysis and SEM-EDS analysis. And the retarding mechanism of gypsum on HACs was revealed.

In chapter 6, the drying shrinkage behavior of HACs mortars with various precursors, curing regimes and activator states is investigated, meanwhile the drying shrinkage behavior of HACs is compared to Portland cement and alkali activated cement (AAC). The microanalyses are undertaken to gain more insight into the mechanisms of drying shrinkage of HACs. The XRD, MIP and SEM-EDS analyses were employed to study the chemical composition, pore structure and microstructure of hydration products. The analysis of total porosity and pore structure is the key to shrinkage of hybrid alkali activated cement. The focus is to characterize the drying shrinkage behavior of HACs.

Chapter 7 analyses the CO<sub>2</sub>-e of HACs concrete extensively. It is unscientific to assume that HAC has a low carbon footprint without previously having carried out accurate calculation of carbon emissions. The GWP impact is employed to evaluate and quantify the carbon dioxide emissions of one cubic HAC concretes with different alkali contents, precursors and alkali activators. In addition, the comparison of CO<sub>2</sub> emission of HACs, geopolymers, alkali activated cement (AAC) and Portland cement is vital and significant to perform.

In chapter 8, the research conclusions involved in this thesis are summarized. Some problems in the research are presented. Perspectives for future research on HACs are also outlined.

## CHAPTER 2: REVIEW ON THE HYDRATION MECHANISMS AND DURABILITY

*Note: this chapter is based on the published paper entitled “Hydration mechanisms and durability of hybrid alkaline cements (HACs): A review”, by Lili Xue, Zuhua Zhang, Hao Wang, accepted for publication in **Construction and Building Materials**, 266(2021)121039.*

### 2.1 Introduction

The cement industry has an adverse impact on the global ecological environment and resources, not only because of the extensive consumption of limestone and clay and energy but also because of the large amount of CO<sub>2</sub> emissions. It is estimated that the cement industry emits 0.87~0.94 t of CO<sub>2</sub> when producing 1 t of cement clinker (Pacheco-Torgal et al. 2012;). As a result, the cement industry accounts for 7-8% of the global CO<sub>2</sub> emissions (Hossain et al. 2015). Worldwide cement production will have a twofold increase in the next 40 years (Hossain et al. 2015; García-Lodeiro et al. 2017), which will lead to great environmental impacts. Moreover, the high permeability of Portland cement (PC)-based concrete is one of the drawbacks which may induce early deterioration of reinforced concrete structures and eventually leads to poor durability. Therefore, seeking for alternative cementing materials with low carbon footprint and excellent performance has become a world-wide focus.

Alkali activated materials (AAMs) have been considered as promising alternatives to PC owing to their equivalent performances and much lower emissions of CO<sub>2</sub> than PC during the production (Shi et al. 2006; Zhang et al. 2014a; Davidovits et al. 1990). The role of the alkali activator is to enhance the potential pozzolanic reaction of SCMs. AAMs possess high early strength, superior resistance to acid and alkali, and outstanding performance against high temperature and freeze-thaw (Zhang et al.2017; Zhang et al. 2016.). However, even though AAMs are regarded as greener materials, there are still some technical issues when applied in construction, such as high shrinkage, too rapid setting, potential alkali-aggregate reaction and efflorescence as reported in the literature (Ye et al. 2017; Fernández-Jiménez and Puertas 2001; Zheng

et al.2019; El-Yamany et al. 2018). The primary cause for the above problems is likely to be the excessive alkalis and the hydration products which are low Ca/Si ratioed C-S-H and amorphous N-A-S-H (Jiao et al. 2018). Cost effectiveness is also a concern. These problems have hindered the marketability of AAMs.

Recently, one innovation to solve the aforementioned issues is to dilute PC with large dosages of SCMs and a small amount of alkali activator (Shi et al. 2011). Hence a new type of binder which is known as HAC has been proposed by some researchers, particularly after Angel Palomo from Eduardo Torroja Institute, Spain (Palomo et al.2007). HAC is formed by blending low proportions (<30%) of cement and high proportions (>70%) of SCMs with an alkali activator. Because this cementitious material takes advantage of PC and AAMs, it has more compact microstructure and almost no  $\text{Ca}(\text{OH})_2$  and ettringite in hydration products (García-Lodeiro et al. 2013a; Al-Kutti et al. 2018). Furthermore, the industrial production of HAC is easy to implement (Palomo et al. 2019). It has attracted greater attention in the context of the cement industry and scientific research (Donatello et al. 2014b; Kaja et al. 2018). Nonetheless, other researchers have argued that there are still some performance issues related to uncertain long-time durability, such as shrinkage, micro-cracking, carbonation, corrosion and potential alkali-silica reaction, which need to be investigated in further research (Juenger et al. 2011; Bernal and Provis 2014; Askarain et al. 2018). Palomo has also claimed that it was necessary to study the long-time behavior of HAC to establish the relationship with Roman cement in composition and microstructure (Palomo et al. 2019). On the other hand, permeability and water absorption, which depend on the hydration products and microstructure, are the critical parameters of durability (Davidovits et al. 1990). There is an obvious need to understand the hydration mechanism of HACs as well. Moreover, shrinkage is a vital property that affects the durability of cementitious materials (Hou et al. 2015). In this paper, the hydration mechanism, some durability performances and some hints on shrinkage behavior and efflorescence of HACs are reviewed. Furthermore, some questions that are crucial to the further research are proposed to develop the

fundamental knowledge about HACs and facilitate their application.

## **2.2 Hydration mechanisms of HACs**

### **2.2.1 Hydration process of HACs**

Hydration kinetics plays a crucial role in determining the product formation, microstructure development and mechanical properties of all cementitious systems. The study of hydration kinetics is not only important to understand the hydration mechanism, but is also useful to predict and improve the properties of HAC.

The hydration process of HAC is shown in Figure 2-1. At the first stage, the hydrated product of HAC is a mixture of C-S-H gel, the main reaction product of PC hydration, and N-A-S-H, the main hydration product of AAMs (García-lodeiro et al. 2013d). Nonetheless, C-S-H and N-A-S-H gels could alter their composition during reaction. When enough calcium (Ca) and alumina (Al) are present and the pH value is higher than 12 in solution, C-S-H and N-A-S-H gels will evolve into C-A-S-H and (N, C)-A-S-H respectively, which are three-dimensional structural gels with higher degrees of polymerization and more cross-linked Si (García-lodeiro et al. 2011; García-lodeiro et al. 2013c). Moreover, the hydration heat released by PC accelerates the alkali activation reaction of SCMs at room temperature. Therefore, the early strength and hardening rate of HAC are enhanced (García-lodeiro et al. 2016b).

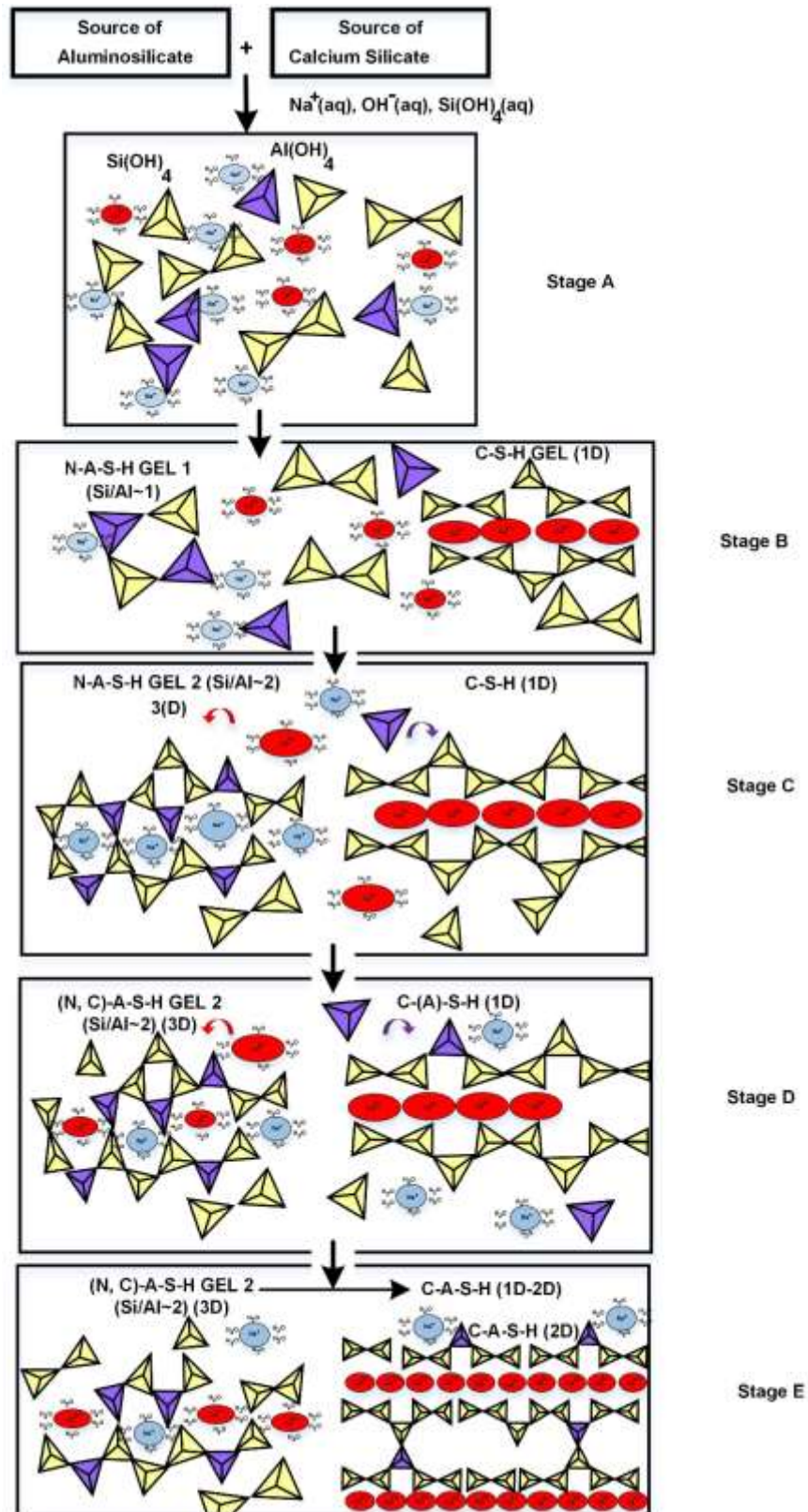


Figure 2-1. A structural schematic diagram of the hydration process of HACs (García-lodeiro et al. 2013c).

The hydration kinetics of HACs with different precursors has been studied by some researchers, and is usually conducted by isothermal conduction calorimetry via monitoring heat flow and cumulative heat at different ages. García-Lodeiro et al. (2013b) compared the heat flow of OPC, fly ash (FA) and M (OPC-FA70%) activated with D1 (NaOH and Na<sub>2</sub>SiO<sub>3</sub>, pH 13.5) and D2 (Na<sub>2</sub>CO<sub>3</sub>, pH 11.6).

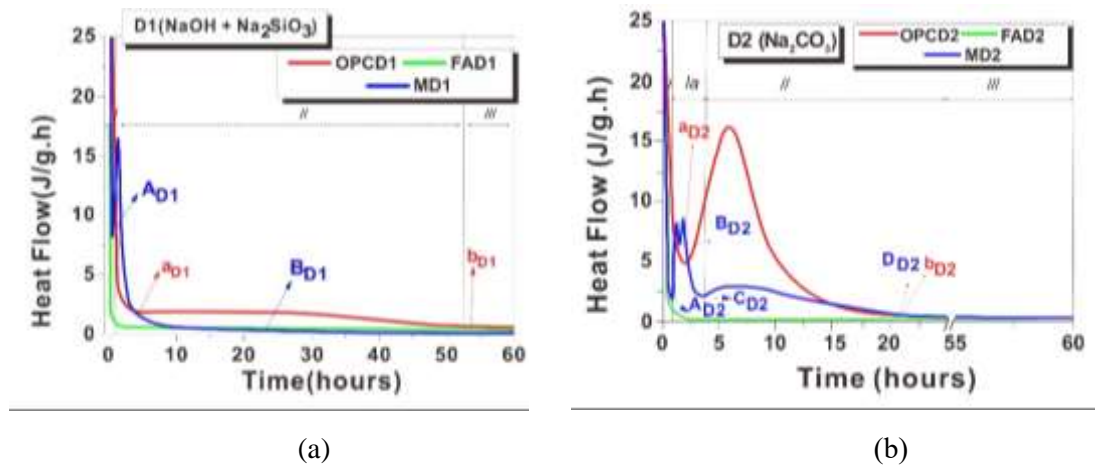


Figure 2-2. Heat flow of OPC, FA and M (OPC-FA70%) hydrated with (a) D1 (NaOH and Na<sub>2</sub>SiO<sub>3</sub>, pH 13.5); (b) D2 (Na<sub>2</sub>CO<sub>3</sub> pH 11.6)( García-Lodeiro et al. 2013b).

As shown in Figure 2-2, there was an exothermic peak in period II on the OPCD2 curve (Figure 2-2 b), while the peak did not appear on the OPCD1 curve (Figure 2-2 a). indicating that the OPC tend to hydrate slowly in high alkali content solution. No exothermic peak appeared on FAD1 and FAD2 curves during the whole trial, signifying that fly ash systems had difficulty hydrating at ambient temperature despite the presence of alkali. In terms of HACs, the MD1 curve showed a narrow peak in period II, which suggested that the alkali activator inspired synergies between the fly ash and Portland cement. The double peak on the MD2 curve was related to the Na<sub>2</sub>CO<sub>3</sub>. The main peak on the MD2 curve was lower than that of the MD1 curve, which meant a delayed hydration in the Na<sub>2</sub>CO<sub>3</sub> solution. And an activation model of HACs (OPC 30% and FA70%) was proposed in Figure 2-3.

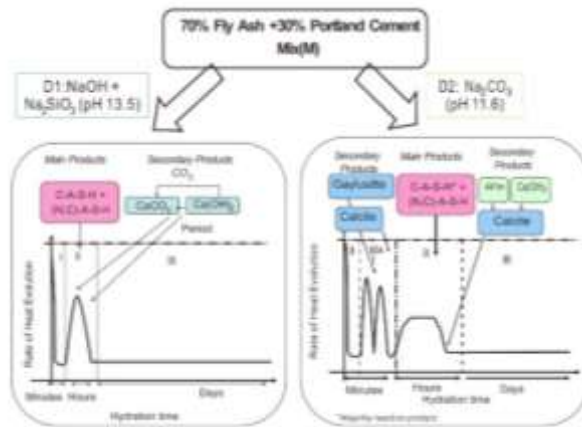


Figure 2-3. Activation model of HACs (70% FA+ 30% OPC) (García-Lodeiro et al. 2013b).

Angulo-Ramírez et al. (2017) studied the heat rate release and cumulative heat of OPC, OPC-GBFS blend and HACs by NaOH and sodium silicate (SS)+ NaOH activated OPC-GBFS blends, which is shown in Figure 2-4. The initial peak and acceleration peak of the OPC-GBFS 80% blend hydration in the water were both lower than that of OPC100% because the OPC was diluted

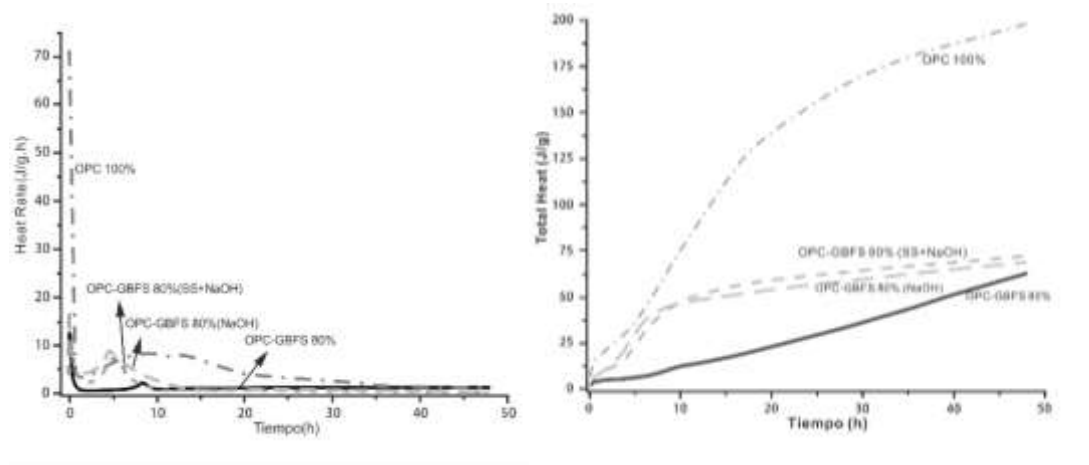


Figure 2-4. Heat rate and total heat of OPC, HACs (OPC-GBFS80%) and OPC-GBFS blends (Angulo-Ramírez et al. 2017)

by slag and then the hydration rate was slowed down. The hydration behavior of HACs was similar to the OPC, which included a first peak that was associated with hydration and dissolution of GBFS, and an acceleration peak which was related to precipitation of reaction products. In terms of total heat, due to the lower cumulative heat than OPC,

the HACs could be regarded as low hydration heat cements.

### 2.2.2 Microstructure features

In hybrid alkaline systems, the reaction products and microstructure mainly depend on the composition of precursors (high-Ca or low-Ca), the nature of activators and the curing regimes.

#### 2.2.2.1 Effect of precursors

In high - Ca systems (PC-blast furnace slag blended systems), the main gels are C-S-H and C-A-S-H while when calcium is low in the blend (PC-fly ash blended system), the C-A-S-H and (N, C)-A-S-H gels are formed as reaction products (García-Lodeiro et al. 2013b; Palomo et al. 2013). The microcosmic analysis showed that the microstructure of HACs presented a dense matrix in both high -Ca systems and low - Ca systems (see Figure. 2-5). The mechanism was hypothesized to be a cross-linked network mixture composed of C-S-H gel and N-A-S-H gel formed in the hydration process, which could make the matrix more compact due to the more binding gels and coexistence of N-A-S-H and C-A-S-H in comparison to geopolymer (Angulo-Ramírez et al. 2017; Rivera et al.2014). The EDS analysis of Zone 1 indicated that the gel in Figure. 2-5 a) was C-(A)-S-H and in Figure. 2-5 b) was N-A-S-H.

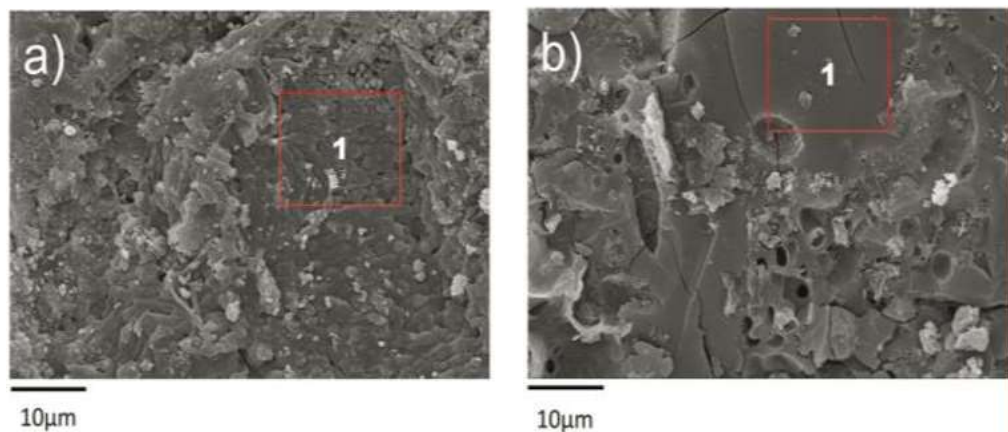


Figure 2-5. SEM micrographs of HACs a) OPC-GBFS 70%; b) OPC-FA 80% (Rivera et al. 2014).

Compared with traditional C-S-H gel, these mixed gels C-A-S-H and C-(A)-S-H, have higher aluminum content and a higher degree of polymerization (Qu et al. 2016). Moreover, the content of dissoluble silicates also influences the microstructure of

HACs (Fernández-Jiménez et al. 2014). It was reported that products with higher  $\text{SiO}_2/\text{Al}_2\text{O}_3$  could form a denser microstructure (Mejía et al. 2015).

#### 2.2.2.2 Effect of alkali activators

Water glass, NaOH,  $\text{Na}_2\text{CO}_3$  and  $\text{Na}_2\text{SO}_4$  are commonly used in HACs (Palomo et al. 1999). Previous studies found that dense and compact microstructures can be obtained by activating slag with water glass (see Figure 2-6) in spite of some small cracks due to high drying shrinkage (Angulo-Ramírez et al. 2017; Jiao et al. 2019). In other studies it was stated that  $\text{Na}_2\text{SO}_4$  can increase the strength of HAC by reaction with  $\text{Ca}(\text{OH})_2$  generate  $\text{CaSO}_4 \cdot 2\text{H}_2\text{O}$  and NaOH, which improved the alkalinity in the solution (Pratiwi et al. 2017).

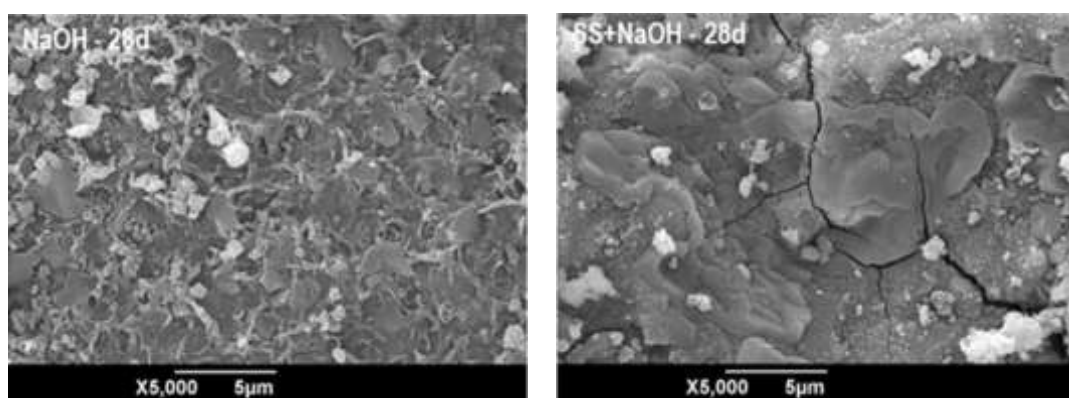


Figure 2-6. SEM images of HACs (OPC-GBFS 80%) activated by NaOH and water glass (SS + NaOH) at 28 days (Angulo-Ramírez et al. 2017).

As the concentration of activator increased, HACs presented a more compact and denser matrix (García-Lodeiro et al. 2018b; Acevedo-Martinez et al. 2012). In terms of the state of the activator, Fernández-Jiménez et al. (2019) reported that more homogeneous distribution of the hydration products can be obtained by a solid-state chemical activator than a liquid activator. Because the solid activator has to dissolve before reacting, while the liquid activators react directly, and the HAC with solid activators sets more slowly than that of liquid activators, the composition of the gel was likely to remain stable. The molar composition distributed in binders with liquid activator (B2) and solid activator (B3) is shown in Figure 2-7.

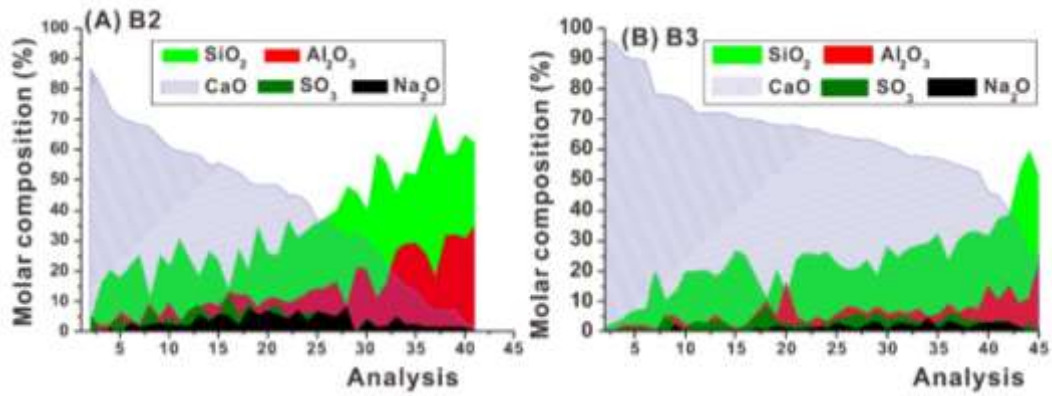


Figure 2-7. The molar percentage of gel composition determined by EDX (A) binder with liquid activator (B) binder with solid activator (Fernández-Jiménez et al. 2019).

However, various activators alter only the proportions of gels in the main hydration products rather than the types. The above-mentioned HACs with different precursors and activators in the literature are shown in Table 2-1.

Table 2-1. HACs reported in the literature:compositions,activators and compressive strengths

System	Activators	2 d CS (MPa)	3 d CS (MPa)	7 d CS (MPa)	28 d CS (MPa)	Ref.
30% OPC+70% FA	NaOH	4.83	-	-	24.72	(Palomo et al. 2007)
30% OPC+70% FA	SS + NaOH	12.91	-	-	36.94	(Palomo et al. 2007)
30% OPC+70% FA	SS + NaOH	-	-	-	30	(García-Lodeiro et al. 2013c)
30% OPC+70% FA (Si/Al=5)	SS + NaOH	-	-	-	47.0	(Mejía et al. 2015)
30% OPC+70% FA (Si/Al=6)	SS + NaOH	-	-	-	51.7	(Mejía et al. 2015)
20% OPC+80% FA	Na <sub>2</sub> SO <sub>4</sub>	-	17	20	28	(Pratiwi et al. 2017)
20% OPC+80% FA	SS + Na <sub>2</sub> SO <sub>4</sub>	-	5	9	12	(Pratiwi et al. 2017)
20% OPC+80% FA	Na <sub>2</sub> CO <sub>3</sub>	21	-	-	30	(Fernández-Jiménez et al. 2014)
20% OPC+80% FA	Na <sub>2</sub> SO <sub>4</sub>	25	-	-	42	(Fernández-Jiménez et al. 2014)
20% Portland clinker +80% FA	Na <sub>2</sub> SO <sub>4</sub> +Na <sub>2</sub> CO <sub>3</sub>	17	-	-	30	(García-Lodeiro et al. 2017)
50% OPC+50% FA	Na <sub>2</sub> SO <sub>4</sub>	30.33±0.5		41.32±0.29	52.53±1.70	(Fernández-Jiménez et al. 2019)
20% OPC+80% GBFS	Liquid SS-4%Na	-	-	18.4	27.5	(Bilim and Ati 2012)
20% OPC+80% GBFS	Liquid SS-6%Na	-	-	45.3	57.1	(Bilim and Ati 2012)
20% OPC+80% GBFS	Liquid SS-8%Na	-	-	58.3	70.1	(Bilim and Ati 2012)
20% OPC+80% GBFS	NaOH	-	-	21	27.5	(Angulo-Ramírez et al. 2017)
20% OPC+80% GBFS	SS + NaOH	-	-	45	53	(Angulo-Ramírez et al. 2017)
20% OPC+80% Boiler slag	SS + NaOH	-	-	-	25	(Rivera et al. 2014)
30% OPC+70% Boiler slag	SS + NaOH	-	-	-	33	(Rivera et al. 2014)

\* CS eq Compressive Strength, FA eq Fly ash, GBFS eq granulated blast furnace slag, SS eq Sodium Silicate

### 2.2.2.3 Effect of curing regimes

Regarding the curing regime, HACs usually develop high early strength under thermal curing conditions due to the low porosity and higher densification microstructure of matrices (García-Lodeiro et al. 2018a; Escalante-Garcia et al.2014). It is well known that high curing temperature and the presence of alkalis could expedite the hydration of calcium silicates in clinker and nucleation of C-S-H gel. Meanwhile, the solubility of the Si and Al will be improved (Thomas et al. 2003; Escalante-Garcia et al. 2000). Hence, the aqueous phase would contain more Si and Al ions as the increase of curing temperature. When initial curing regime was 85 °C for 20 h, the precipitation of C-A-S-H was enhanced, and a higher amount of hydration products were formed compared to C-S-H, and as a consequence, the formation of ettringite was inhibited (Qu et al. 2016). The effect of the type of activators on HACs microstructure lie on the curing regimes is an interesting research topic that is worth further study.

### 2.2.2.4 ITZ of HAC concrete

HAC concrete possesses more compact and uniform ITZ (San Nicolas and Provis 2012; Shi and Xie 1998) than that of PC-based ITZ (Vargas et al. 2017). The SEM micrographs of PC concrete ITZ and HAC concrete ITZ are shown in Figure 2-8.

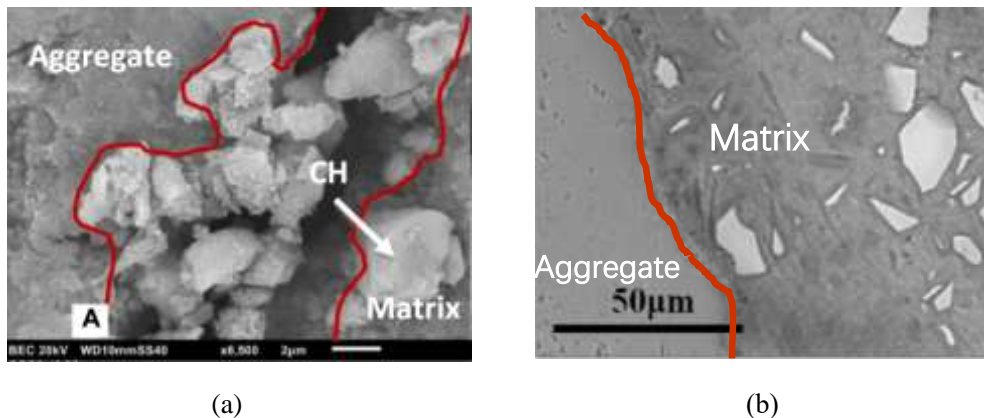


Figure 2-8. ITZ of (a) OPC concrete (Vargas et al. 2017) (b) HAC concrete (San Nicolas and Provis 2012).

It is well known that Portlandite and ettringite are typical crystals in PC hydration products which tend to concentrate at the interfacial transition zone (ITZ) and forms coarse grains. This can decrease the interface adhesion and result in low strength and

poor durability. While  $\text{Ca}(\text{OH})_2$  crystal has only a small presence in HACs because it is consumed by alkaline activated reaction (Escalante-Garcia et al. 2014). The formation of ettringite in HACs may depend on the type of activator. When  $\text{Na}_2\text{SO}_4$  was used as activator, the HACs would generate ettringite and monosulfoaluminate. Sometimes the U-phase ( $3\text{CaO}\cdot\text{Al}_2\text{O}_3\cdot\text{CaSO}_4\cdot 0.5\text{Na}_2\text{SO}_4\cdot 15\text{H}_2\text{O}$ ) may exist, which is considered as the result of ettringite conversion in highly alkaline solution. However, the amount of ettringite and U-phase are small in HACs (Fernández-Jiménez et al. 2019). If activators in addition to sulfate are used, the amount of ettringite in the HACs is likely too low to be detectable. As shown in Figure 2-9, no Portlandite was detected in HACs (GP10, GP20, GP30). Therefore, the ITZ of HACs is compact.

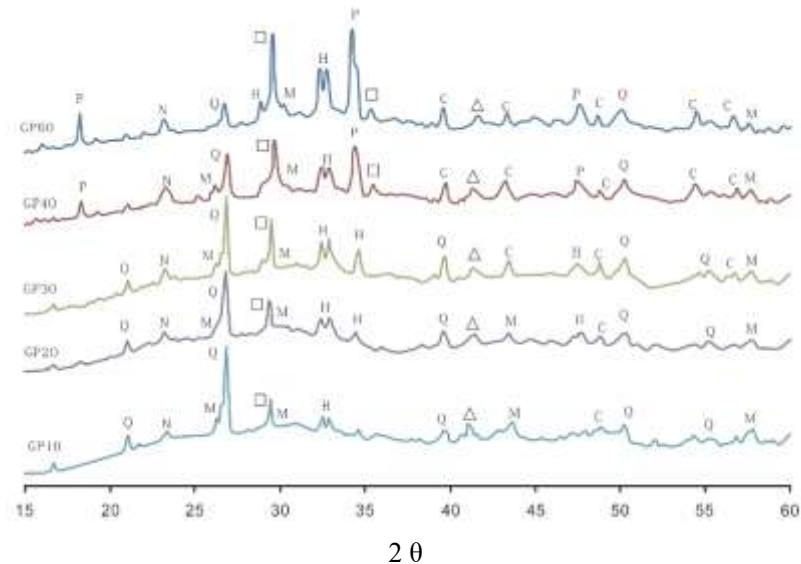


Figure 2-9. XRD analysis of various hybrid OPC-geopolymer systems at 28 days (Legend: Q=Quartz, M=Mullite, P=Portlandite, C=Calcite, N=Nepheline, H=Hatruirite, □=CSH, △=C(A)SH) (Askarian et al. 2018).

In summary, the microstructure of HACs is denser and more homogeneous than PC and geopolymer, which results in higher mechanical strengths and lower permeability. The more compact microstructure of HAC can be achieved by increasing the concentration of the activator and using solid activator or water glass (SS + NaOH) as activators.

### 2.2.3 Setting time

In HAC systems, theoretically, the hydration of Portland cement will accelerate

because of presence of activators, and the setting time is usually shortened. It has been reported that as the OPC content increased, setting time of HACs was reduced gradually (Askarian et al. 2018). This is unfavorable for industrial practice. However, there is not much information regarding the control of setting time of HACs so far.

Setting retarders are commonly used to extend the setting time of OPC, particularly in hot season, hot weather and for long distance deliver of ready mixed concrete. Retarders could be organic and inorganic chemicals, and the choose of a proper type depends on the purpose and cost consideration. The organic retarders for OPC are carbohydrates, hydroxy carboxylic acids and polyols. The mechanism is that carbohydrates and their derivatives mainly retard the hydration of C<sub>3</sub>S and the formation of C-S-H via adsorption and complexation. Hydroxyl carboxylic acids retard the hydration process by retarding the crystallization of cement hydration products (Yu et al. 2018; Cheung et al. 2011). Citric acid was effective to prolong the setting time of OPC (Askarian et al. 2018).

It is important to adjust the setting time of HAC, however, in highly alkaline environment these carbohydrates, acids and polyols may be none effective because of the destroy of their molecular or the neutralization reaction between acid and alkalis. There have been studies on the effect of activator type on setting behavior in AAMs, and it shows that Na<sub>2</sub>CO<sub>3</sub> could delay the initial setting time due to the forming of calcium carbonate in the Na<sub>2</sub>SiO<sub>3</sub> activated AAMs (Li et al. 2019). Therefore, the control of the setting time of HAC may be achieved by altering the type of activators. Besides, the influence of gypsum which is usually used in OPC on the setting time of HACs is worth to study further.

## **2.3 Resistance to aggressive solutions**

### **2.3.1 Sulfate attack**

The sulfate resistance of AAMs is generally better than that of OPC in many cases due to the compact structure, the low permeability, and the absence of Ca (OH)<sub>2</sub> (which is an inducement of sulfate attack) in hydration products (Davidovits et al. 1990; Donatello et al. 2013b; Donatello et al. 2014a; Janotka et al. 2014; Bačuvčík et al.

2018).

The excellent resistance sulfate of HACs has been reported in recent years. Donatello et al. (2013b) studied the behavior of HAC (80% FA and 20% OPC) that was immersed in 0.1N HCl, 4.4% Na<sub>2</sub>SO<sub>4</sub> and seawater for a period up to 90 d. The HACs presented adequate resistance to Na<sub>2</sub>SO<sub>4</sub> solution and seawater, which could be comparable to commercially available sulfate resistant cement (Donatello et al. 2014a). Janotka et al. (2014) investigated the performances of HAC which was exposed for 360 days in 5% Na<sub>2</sub>SO<sub>4</sub> solution and MgCl<sub>2</sub> solution. The results showed that the HAC exhibited superior chemical resistance relative to the reference OPC. Bačuvčík et al. (2018) also reported the excellent sulfate resistance of HAC which was eroded by 5% Na<sub>2</sub>SO<sub>4</sub> solution. Figure 2-10 shows the structure and appearance of mortars exposed in Na<sub>2</sub>SO<sub>4</sub> solution for long period.



(a) OPC mortar immersed 4 years in Na<sub>2</sub>SO<sub>4</sub> (b) HAC mortar immersed 5 year in Na<sub>2</sub>SO<sub>4</sub>

Figure 2-10. Structure and appearance of mortars exposed in Na<sub>2</sub>SO<sub>4</sub> solution (Bačuvčík et al. 2018).

Fernández-jiménez and García-lodeiro (2013) explored the sulfate resistance of HACs via exposing them to 4.4% Na<sub>2</sub>SO<sub>4</sub> solution; meanwhile a kind of high durability OPC was used as a control. The results showed that the behavior of HAC exposed to Na<sub>2</sub>SO<sub>4</sub> solution was comparable to the high durability OPC. Microscopic characterization indicated that no portlandite was detected in HACs.

To sum up, the HACs display excellent resistance to sulfate attack.

### 2.3.2 Chloride penetration

Chloride ions could destroy the steel passivation film, and then cause corrosion of the steel bar and quickly result in serious damage to concrete structures (Wang et al. 2019).

Studies have shown that the chloride penetration depth of alkali-activated cement concrete is lower than OPC concrete due to the denser structure. In alkali activated systems, chloride ion permeability showed a linear decline trend with the increase in NaOH solution concentration and Na<sub>2</sub>SiO<sub>3</sub> content (Lee and Lee 2016).

Until now, the chloride penetration of HACs has not been studied widely. Some research has indicated that the resistance to chloride penetration of HACs is associated with its precursor nature (Rivera et al. 2014). High-Ca systems show higher resistance to chloride penetration than low-Ca system, which is attributed to the denser calcium silicate gel C-A-S-H generated in the hydration of slag compared with the porous sodium silicate gel N-A-S-H. As shown in Table 2-2, the hybrid slag system exhibits the lowest chloride permeability, followed by FA-geopolymer, and hybrid fly ash system presents the highest penetration of chloride.

Table 2-2 Chloride permeability and Electrical Resistivity at 28 d of curing (Rivera et al. 2014).

System	Chloride Permeability (coulombs)	Electrical Resistivity (Ohm-m)
FA-geopolymer	1478	15.8
HFA20 (20% OPC+80% FA)	2877	10.3
HBS30 (30% OPC+70% BS)	963	122.0

\*BS eq Boiler slag, FA eq Fly Ash, H eq Hybrid

However, the leaching test showed that the concentration of chloride in the HAC (blends with OPC clinker, fly ash and bottom ash) exceeded the upper limit according to the standard (García-Lodeiro et al. 2016a), which could lead to possible reinforcement corrosion when HACs are applied to manufacture structural concrete. Therefore, the systematic and extensive study of chloride penetration of HACs is essential in future research.

### 2.3.3 Carbonation

The existence of Ca (OH)<sub>2</sub> in PC concrete is to ensure the high PH (over 14) of pore solution to prevent steel reinforcement from corrosion. So the decreasing alkalinity in concrete could make the steel reinforcement more vulnerable to corrosion (Bilim 2011).

It is reported that the AAMs are more susceptible to carbonation than OPC mortars even though their microstructures were more compact and less permeable (Puertas et al. 2006; Bilim and Ati 2012; Angulo-Ramirez et al. 2019).

HACs concrete showed higher sensitivity to carbonation than OPC. Bilim and Ati (2012) studied carbonation resistance of HACs mortars. The results showed that the carbonation depths of HAC mortars were higher than OPC mortar, especially at long-term carbonization. Angulo-Ramírez et al. (2019) determined the carbonation resistance of 100% OPC concrete, HB concrete (HAC: 80% GBFS/20% OPC) and CE (GBFS concrete without alkaline activator:80% GBFS/20% OPC). The results indicated that HB and CE concretes exhibited less resistance to carbonation than OPC concrete; meanwhile the HB concrete displayed only slightly better resistance to carbonation than CE (see Figure 2-11).

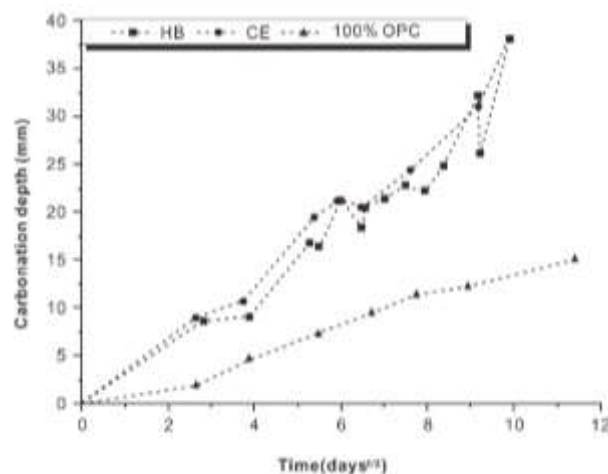


Figure 2-11. Carbonation depth at different exposure time (Angulo-Ramirez et al. 2019)

This behavior can be explained as follows: there is not enough  $\text{Ca}(\text{OH})_2$  to neutralize with  $\text{CO}_2$ , then C-A-S-H gel reacted with  $\text{CO}_2$  and caused the degradation of C-A-S-H gels by decalcification, resulting in the deeper carbonation depth (Gruyaert et al. 2013). Some researchers suggested that the higher susceptibility of the carbonation process was correlated with the content of GBFS, especially in concretes with more than 70% GBFS (Gruyaert et al. 2013; Borges et al. 2010). Other researchers attributed the high susceptibility carbonation of AAMs to micro-cracks caused by the drying

shrinkage that these materials usually suffer (Bernal et al. 2014; Aperador et al. 2012). The type of activator was also reported to affect the resistance of carbonation, for example, AAMs activated by water glass showed higher susceptibility (Puertas et al. 2006; He et al. 2018).

As is clear from the above descriptions, the carbonation depth of HACs is likely to be reduced by controlling the proportion of precursors and the type of alkali activators. In addition, mitigating the drying shrinkage of HACs could be an effective way to lessen the carbonation depth of HACs.

## **2.4 Alkali-silica reaction (ASR)**

AAMs usually contain larger amounts of alkalis than OPC concrete, which raises the concerns in relation to potential ASR (Fernandez-Jimenez et al. 2007; Provis et al. 2015). However, the question of whether ASR happens in AAMs has been debated. Some research states that ASR could not possibly occur in AAS mortars because the alkalis from the activator were combined in hydration products; meanwhile the alkaline concentration decreased with the reaction process until equilibrium was reached (García-Lodeiro et al. 2016b; Talling et al. 1989). San Nicolas et al. (2014) reported that there was no indication of cracking and expansive products caused by ASR in the microscopic images of 7-years' old AAS concrete. Other researches argued that ASR existed in AAMs, although the ASR degree was less than that of OPC (Abdollahnejad et al. 2014; Shi et al. 2015a; Shi et al. 2015b; Ichikawa 2009; Thomas 2011). Therefore, ASR of AAMs still need to be considered.

### **2.4.1 Influence factors of ASR of AAMs and control**

The type and dosage of activators could influence ASR of AAMs. The expansion rank of AAMs with different activators was as follows: waterglass > Na<sub>2</sub>CO<sub>3</sub> > Na<sub>2</sub>SO<sub>4</sub> > NaOH (Chen et al.). Shi et al. (2017 and 2018a) investigated the influence of alkali dosage on the ASR of slag mortars activated by NaOH. Their research indicated that the ASR expansion decreased with the increment of alkali dosage, which was consistent with a previous study (Al-Otaibi 2008). Precursor type was also reported to affect the degree of ASR (Al-Otaibi 2008; Krivenko et al. 2014). Krivenko et al. (2014)

stated that the additional quantities of active Al (metakaolin and fly ash) can effectively control ASR expansion. Shi et al. (2018b) confirmed that the ASR expansion of water glass activated slag mortars can be controlled by fly ash and metakaolin. And the main factor governing the ASR expansion was the alkalinity of pore solution in the AAS mortars.

#### 2.4.2 ASR of HACs

There are a small number of studies about the ASR behavior of HACs. Donatello et al. (2013b) investigated the ASR expansion of MS (Portland cement) and FAN-4 (HAC) in compliance with the method in ASTM 1260. The test results are shown in Figure 2-12.

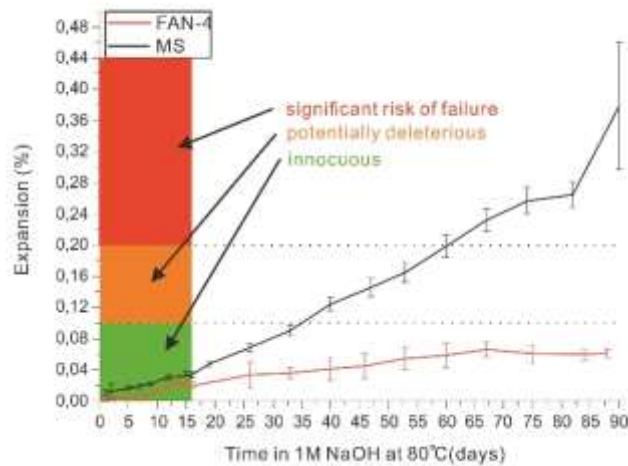


Figure 2-12. ASR expansion of mortar bar in different test ages (Donatello et al. 2013b).

It can be seen that ASR expansion values of both cements were less than 0.1% after 16 days, which was in accord with the ASTM 1260 requirement. But the distinction of expansion became more noticeable with the testing time, and the HAC presented greater dimensional stability. Angulo-Ramírez et al. (2018) investigated the ASR expansion of three types of binder: OPC, blend cement, and HAC. The result showed that OPC was the most vulnerable to ASR attack, followed by the HAC and the blend cement presented the best dimensional stability. Compared with the blend cement, a rose-shaped gel with expansive nature in a pseudo rose-shaped structure was observed

in HAC, but the ASR expansion value was not beyond the limits of specified value. The basicity of pore solution is also the main factor affecting the ASR of HAC. Palomo et al. (2019) also stated that HAC could restrain the ASR. As Figure 2-13 shows, the expansion of HC (HAC mortar) remains below 0.100% in the period of 6 months.

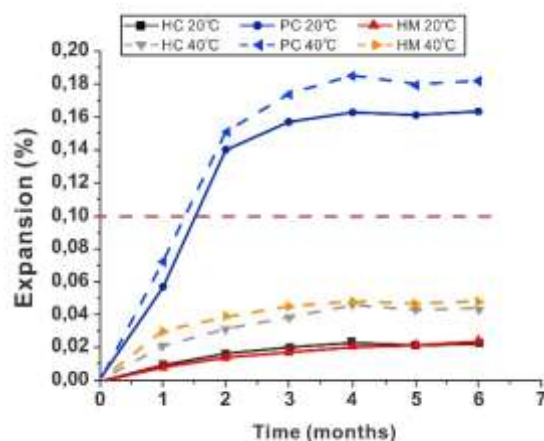


Figure 2-13. ASR expansion in 6 months prismatic mortar at different conditions (HC eq HAC mortar; HM eq 70% PC and 30% HC mortar) (Palomo et al. 2019).

In summary, ASR exists in HAC, albeit the expansion value which is within the allowable value.

## 2.5 Resistance to high temperatures

HACs are characterized as having high resistance to temperature according to the literature (Donatello et al. 2013b; Strigáč and Martauz 2014; Fernández-Jiménez et al. 2010). Strigáč and Martauz (2014) stated that HACs demonstrated high resistance to thermal stress when they were heated up to 400 °C. Donatello et al. (2013b) examined the resistance to high temperatures of MS (OPC) and FAN-4 (HACs). The results indicated that the compressive strength of HACs nearly doubled their initial strength after exposure to 800 or 1000 °C, along with 5% shrinkage beginning at 700 °C and also in accord with color change in Figure 2-14. This situation was attributed to the sinter processes occurring in HACs. By contrast, the compressive strength of Portland cement declined linearly with increasing temperature.

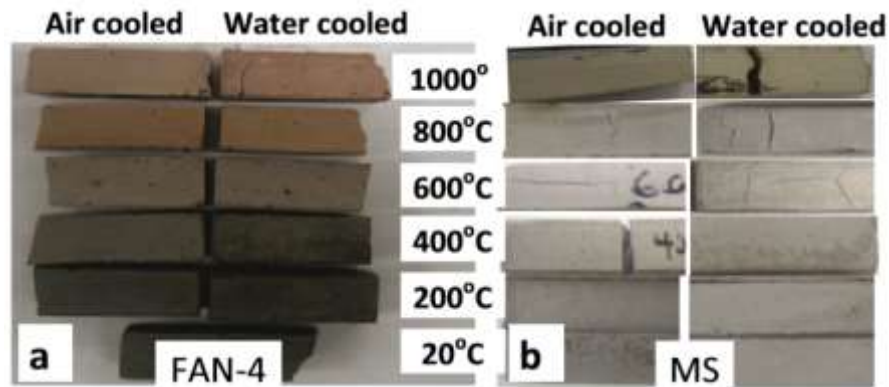


Figure 2-14. Visual changes in (a) FAN-4 and (b) MS pastes after temperature exposure (Donatello et al. 2013b).

Fernández-Jiménez et al. (2010) studied the mechanical behavior of three type of cements at high temperature: OPC geopolymer and HACs (70% fly ash and 30% clinker). The results showed that geopolymer exhibited excellent mechanical properties under high temperature, especially at 600 °C due to the formation of a molten phase while the strength of HACs began to decline when temperature was higher than 600 °C, but the strength was higher than that of OPC. Over all, the high temperature resistance of HACs is superior to Portland cement, but worse than geopolymer.

## 2.6 Some hints on shrinkage behavior of HAC

Shrinkage is a key property affecting the durability of cementitious materials. Cracks caused by shrinkage may increase the permeability, which leads to infiltration of water and corrosive materials and ultimately destroys the structure. Shrinkage behavior involves autogenous shrinkage, chemical shrinkage, drying shrinkage and carbonation shrinkage (Mastali et al. 2018). The autogenous shrinkage is accompanied by chemical shrinkage (Lee et al. 2014). To date very few works have been undertaken to address the shrinkage of HAC. Martauz et al. (2016) reported that the shrinkage of HAC concrete was reduced by 48% to 58.4% in comparison to OPC, but the shrinkage mechanism was not clarified. Little is known regarding to the shrinkage behavior of HAC, especially the shrinkage behavior of HAC with different precursors and activators under steam curing or high temperature sealed conditions, so this deserves

future research. However, there are studies on the shrinkage behavior of AAMs and the approaches of control.

### **2.6.1 Shrinkage behavior of AAMs**

The AAMs usually show high-magnitude shrinkage than PC. It can be attributed to high capillary stress which results from an increased refinement of pore size caused by alkali activators (Melo Neto et al. 2008). In terms of drying shrinkage, more water in AAMs exists as interstitial water within the gel rather than hydration products, hence the loss of unbound water over time leads to significant drying shrinkage (Chi and Huang 2013). In addition, the more refined pores in AAMs, the higher the capillary stress, which leads to high drying and autogenous shrinkage (Ye and Radlińska 2016). Furthermore, the major hydration product C-A-S-H is more amorphous than the C-S-H generated in OPC hydration, which results in excessive autogenous shrinkage (Jia et al. 2018). The reason is that the Ca/Si ratio plays a significant role in the cluster morphologies of cementing materials: the calcium is conducive to form an ordered structure whereas the silicon contributes to increase the amorphous state of the structure (Mataalkah et al. 2019). The C-A-S-H with low Ca/Si ratio is unfavorable to the formation of stable structures in AAMs so it exhibits higher shrinkage compared with PC. According to Ye and Radlińska (2016), drying shrinkage is also attributed to the structural combination of alkali cations in C-A-S-H, which reduce the stacking regularity of C-A-S-H layers, resulting in the easier collapse and redistribution of C-A-S-H.

### **2.6.2 Influence factors and control**

The shrinkage kinetics of AAMs is governed by the RH during the drying process. Ye and Radlińska reported the different shrinkage values of OPC and AAS (alkali activated slag) cement under various RH condition (Ye and Radlińska 2016). It can be seen from Figure 2-15 that AAS exhibited substantially higher shrinkage than OPC. The OPC showed higher shrinkage when the RH was lower, whereas the AAS cement demonstrated higher shrinkage when under higher RH conditions, and the highest shrinkage of AAS was measured at 50% RH (16500 $\mu\text{m}/\text{m}$ ). It is related to the redistribution and rearrangement of C-A-S-H nanoparticles (Ye et al. 2017). Moreover,

the ultimate shrinkage of AAMs is also dependent on the drying rate and drying procedure.

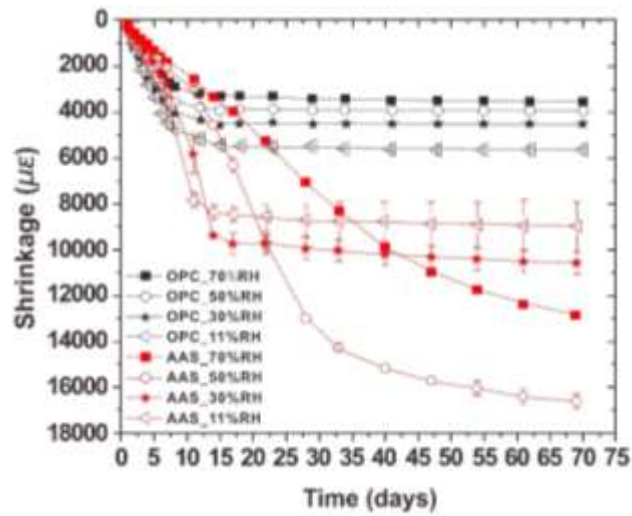


Figure 2-15. Time-dependent shrinkage of OPC and AAS under various RH conditions (Ye and Radlińska 2016).

In terms of the alkali activator, the shrinkage behavior of AAMs is affected via altering the solution chemistry and hydration products. The nature, dosage and composition of activators could result in diverse shrinkage behavior. Slag mortar activated with water glass had the highest shrinkage (six times of PC mortar), while solid hydroxide activator showed a lower shrinkage (triple PC mortar), the lowest shrinkage could be obtained by  $\text{NaCO}_3$  which is comparable or lower to PC mortar (Duran et al. 2009). When the mixing proportion of  $\text{NaCO}_3$  to  $\text{NaOH}$  mole ratio is 3:2 and the dosage of  $\text{Na}_2\text{O}$  is 8%, the lower shrinkage of AAS cement can be achieved, as shown in Figure 2-16 (Jiao et al. 2018).

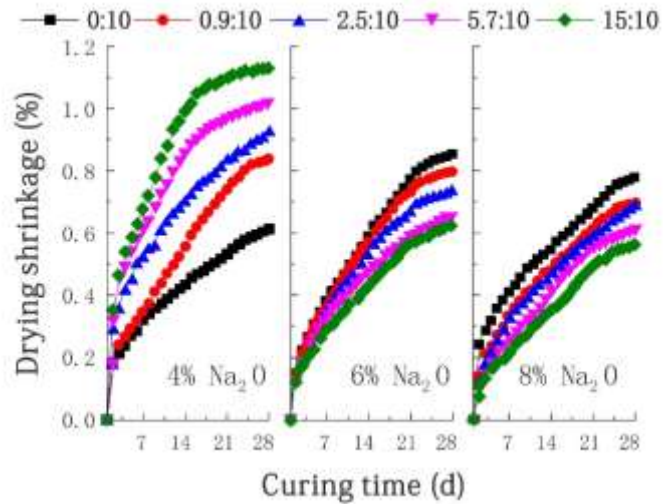


Figure 2-16. Effect of Na<sub>2</sub>CO<sub>3</sub> to NaOH mole ratios and Na<sub>2</sub>O dosages on the drying shrinkage of AAS pastes (Jiao et al. 2018).

With regard to the chemical additive, expanding admixtures (EA), Styrene-Butadiene Rubber (SBR), and Acrylic Ester (AE) were reported to decrease the shrinkage in AAMs (Thomas et al. 2017). The reduction of shrinkage is ascribed to the lower surface tension of the pore solution and the blocking of capillary pores with latex. The most effective curing regimes to mitigate shrinkage are long duration curing or thermal curing (El-Yamany et al. 2018). This is attributed to the improvement of volumetric stability and reduction of total porosity after curing.

The AAMs exhibit higher shrinkage than PC. In the same way, volume stability is a vital factor in HAC related to durability. Consulting the previous research, the shrinkage could be lowered by altering the dosage or composition of alkali activators or adding chemical admixtures. Furthermore, the high temperature curing is also regarded as an effective method to reduce the shrinkage. Hence the shrinkage behavior of HAC with various alkali activators under different curing conditions is a crucial problem in further research, particularly shrinkage behavior under steam curing conditions or high temperature sealed conditions.

## 2.7 Some hints on efflorescence

Efflorescence is essentially a set of physiochemical reactions consisting of surface carbonization, alkali release, and salts migration from cement or aggregates to dry

surfaces, which results in deposition of white salts on the outside surface of materials (Zhang et al. 2018). Škvára et al. (2009a and 2009b) stated that the leaching behavior of alkalis derived from the weak bond between the sodium ions and the aluminosilicate structure. Efflorescence is an unsolved drawback that may cause a step back in the development of alkali-activated cementitious materials. The mitigation of efflorescence has also been studied in recent years.

Firstly, the addition of alumina-rich admixtures could ameliorate the efflorescence rate. Najafi Kani et al. (2012) reported a FTIR analysis of geopolymer with and without Secar71 calcium aluminate cement (see Table 2-3). It has been shown that the wavenumber of Si-O- (Si, Al) asymmetric stretch peak increased with the addition of Secar71, which indicated an increase in gel connectivity. Then the mobility of alkalis was decreased due to the increased crosslinking in the binder, resulting in reduced efflorescence. This demonstrated that efflorescence of geopolymers could be mitigated by alumina-rich admixtures. Other researchers also found that the mobility of alkalis can be reduced significantly by using 8% calcium aluminate cement, which leads to minimum efflorescence (Abdollahnejad et al. 2014).

Table 2-3. Si-O-(Si, Al) asymmetric stretch peak positions in FTIR spectra of P2 and P9 (Najafi Kani et al. 2012).

Peak positions (cm <sup>-1</sup> )	Secar 71 content	
	0%	6%
P2	998	1007
P9	996	1004

Secondly, the hydrothermal curing is conducive and so reduces the efflorescence. According to Najafi Kani et al. (2012), the hydrothermal curing at a temperature more than 65 °C could decrease the efflorescence rate and improve the compressive strength of geopolymer binders (see Figure 2-17), which were derived from the regional reorganization and crystallization of N-A-S-H gels (Zhang et al. 2014b).

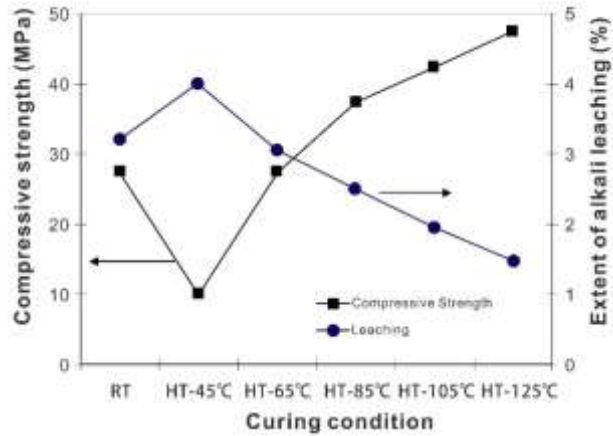


Figure 2-17. Effect of curing condition on alkali leach ability and compressive strength of the geopolymer binder (Najafi Kani et al. 2012).

Furthermore, the decreased pore sizes and porosities of AAMs due to the increment replacement of fly ash by slag could result in a much lower efflorescence rate. This situation corresponds to the research result from Krivenko et al. (2013). They stated that the higher concentration of calcium, the greater rate of bounded sodium in the matrix, which results in a lower rate of efflorescence. Therefore, how to bind alkalis in AAMs hydration products and prevent them from migrating with water vapor is a problem that needs to be solved at present.

Until now, very few studies have addressed efflorescence of HACs. Existing research reported that the efflorescence phenomenon of HACs was not obvious. It was assumed that HACs possess the ability to bind  $\text{Na}^+$  (Krivenko et al. 2013). Pore volume and permeability are also regarded as factors affecting efflorescence. HACs present a very compact and uniform ITZ, small pore volume and low permeability (Abdollahnejad et al. 2014), which could result in decreased efflorescence rate.

## 2.8 Perspectives for future research

The inclusion of OPC leads to rapid setting of HACs. To facilitate the application of HACs, controllable setting time must be guaranteed. Therefore, understanding and controlling the hydration kinetics of HAC has to be well understood. It is suggested to prolong the setting time of HAC by altering the proportion of precursors and changing the nature of alkali activators. Moreover, using a high dose of gypsum is also an

approach worth investigating.

Regarding the durability, there are a few issues that have been raised in concern. Although the permeability of HACs is usually lower than OPC, which means theoretically lower chloride transport rate, the susceptibility to carbonation is greater due to the high alkalinity. The carbonation mechanisms of HACs under different conditions are needed. The influences of the types and proportions of cementitious materials, the types and modulus of activator on the carbonization behavior of HACs needs to be further studied. In terms of eliminating efflorescence, the capability of HAC hydrates formed from different precursors and under different curing regimes to bind alkali cations must be studied, so a proper precursor selection and proportion can be justified.

It is also because of the higher concentration of alkalis, there are still doubts of ASR risk for engineering application, although the current studies in literature showing that expansion value of ASR in HACs is smaller than that of OPC. It is likely that the high amount of fly ash and metakaolin contain high concentration of Al, which low the reaction of ASR in HAC, and the quantitative relationship between these parameters, such as reactive Al, free alkalis and water access and status, should be studied in the future to further low the risk of ASR by better proportioning of raw materials, or improve the public confidence of using HAC.

Furthermore, it is worthy to conduct the quantitative analysis of CO<sub>2</sub> emissions in HACs manufacture, such as application of LCA (Life Cycle Assessment) methodology and comparison between OPC and HACs. In terms of precursors, seeking future SCMs that can replace fly ash and slag to prepare new HACs is also a vital topic for further research.

## **2.9 Conclusions**

The hydration mechanisms and some properties regarding durability of HACs can be summarized as follows:

- (1) The hydration behavior of HACs is similar to OPC hydration which includes two exothermic peaks. The rapid hydration of Portland cement in HAC accelerates

the reaction and shortens the setting time, which is unfavorable to industrial practice. The hydration kinetics of HACs has to be well understood to facilitate the control of setting time.

The microstructure of HACs is more homogeneous and denser than geopolymers and OPC, which could result in higher mechanical strength and excellent durability. Besides the HAC concrete presents a uniform and compact ITZ.

- (2) HACs possess excellent sulfate resistance due to the lack of  $\text{Ca}(\text{OH})_2$  and low permeability; the research conclusions of anti-chloride penetration of HACs are undefined at present though. HACs are more vulnerable to carbonation compared to OPC even though their microstructures are more compact. The conclusive carbonation mechanism of HAC has not yet been sufficiently understood.
- (3) HACs exhibit superior resistance of ASR compared with OPC. The basicity of pore solution is also the main factor controlling the ASR of HAC. Considerable research on ASR of HACs is still needed to facilitate the marketability and viability of applications.
- (4) The resistance to high temperature of HACs is between OPC and AAMs, i.e. better than OPC but worse than AAMs).
- (5) Up to now, much remains unknown regarding the shrinkage behavior of HAC concrete, especially the shrinkage behavior of HAC with various precursors and activators under steam curing or high temperature sealed conditions, which deserves future research.
- (6) The efflorescence of HACs is not heavy. How to bind more alkalis in HACs hydration products and prevent them from migrating is a critical problem that needs to be solved in further research.

## **CHAPTER 3: RESEARCH PLAN AND METHODOLOGY**

### **3.1 Introduction**

Although some research has been carried out on HAC, such as manufacturing processes, mechanical property and some aspects of durability, issues of hydration kinetics control and volume stability have not yet been well understood. Study of hydration kinetics is not only important to understand the hydration mechanism, but also useful to predict and improve the properties of HAC. On the other hand, volume stability is a vital factor for HAC related to durability. To facilitate the application, hydration kinetics of HACs and control, effect of precursors and activators on the shrinkage behavior of HACs must be understood and addressed.

This chapter will describe the research plan and methodology of this thesis. The solid materials refer to materials that exist in powder form, including Portland cement, slag, fly ash and gypsum. Alkali activators include liquid activator and solid activator.

### **3.2 Research Plan**

The objective of this research is to optimize the properties of HAC and apply it to pipe pile production so that the production cycle could be shortened due to the high early strength. The technical benchmark aim is that compressive strength of HAC concrete reaches 30 MPa in 24 h with steam curing or room temperature curing. The initial setting time should be about 1 h to facilitate the construction. It is well known that AAMs set too rapidly, which is unfavorable to industrial practice. Therefore, suitable setting time must be guaranteed. These technical requirements define the objectives of this study:

- To investigate the early hydration heat of HAC with different precursors and alkali activators; determine the reaction extent of raw materials
- To control the hydration kinetics of HAC by changing the type of alkali activator or mixing gypsum to binders, especially to prolong the initial setting time without compromising of early strength. Correlate the hydration products with the kinetics of reaction

- To learn the shrinkage behavior of HAC with different precursors and activators under steam curing and standard curing conditions, including autogenous shrinkage, drying shrinkage and carbonation shrinkage. Correlate the microstructure evolution with the shrinkage behavior under different conditions.
- To mitigate the shrinkage of HAC by optimizing curing regime and introducing applicative alkali activators and expansion agents.

### 3.3 Materials

#### 3.3.1 Solid materials

Grade S95 ground blast furnace slag (GBFS) (according to Chinese standard GB/T 18046-2017) with a specific surface area of 448 m<sup>2</sup>/kg and grade I fly ash (FA) (according to Chinese standard GB/T 1596-2017) with specific surface area of 420 m<sup>2</sup>/kg were used in this study. P II 52.5 ordinary Portland cement (OPC) (according to Chinese standard GB 175-2007) was also used. The technical index of Portland cement is shown in Table 3-1. The chemical compositions of OPC (ordinary Portland cement), GBFS (granulated blast furnace slag) and FA (fly ash) are shown in Table 3-2.

Table 3-1. Technical indexes of Portland cement

Type	Strength grade	3 d Compressive strength (MPa)	28 d Compressive strength (MPa)	Standard consistency
PII	52.5	36	60	27%

Table 3-2. Chemical compositions of OPC, GBFS and FA (wt.%)

Type	SiO <sub>2</sub>	Al <sub>2</sub> O <sub>3</sub>	Fe <sub>2</sub> O <sub>3</sub>	CaO	MgO	SO <sub>3</sub>	K <sub>2</sub> O	TiO <sub>2</sub>	Na <sub>2</sub> O	MnO	P <sub>2</sub> O <sub>5</sub>	Σ	LOI
OPC	20.99	5.36	3.81	61.36	1.38	2.4	0.65	0.27	0.13	0.1	0.14	96.59	2.71
GBFS	31.43	15.22	0.71	37.79	9.62	1.2	0.43	0.67	0.52	0.312	0.02	98.02	0.76
FA	54.78	24.61	5.20	3.16	0.84	0.62	2.22	1.09	0.66	0.067	0.19	93.42	5.96

The phase analysis of raw materials was conducted by X-ray Diffraction (XRD). The XRD patterns of OPC, GBFS and FA are shown in Figure.3-1.



sodium hydroxide was dissolved in water and then added to the mixture.

Table 3-3. Chemical composition of sodium silicate

Component	SiO <sub>2</sub>	Na <sub>2</sub> O	Al <sub>2</sub> O <sub>3</sub>	Fe <sub>2</sub> O <sub>3</sub>	CaO	K <sub>2</sub> O	SO <sub>3</sub>	P <sub>2</sub> O <sub>5</sub>	TiO <sub>2</sub>	Cl
m/m%	62.82	27.78	0.399	0.0561	0.0733	0.143	0.0236	0.0432	0.0203	0.0526

Solid alkali activator: Modulus is range from 1.0 to 1.5. It is made of solid sodium silicate ( $M_s=2$ ) and solid NaOH.

ISO standard sand was used as a fine aggregate to prepare HAC mortar.

### 3.3.3 Other materials and chemicals

The poly-carboxylic acid superplasticizer (SP) with a water-reducing rate of 35% was supplied by Subote new materials corporation in China. In addition, ISO standard sand was used as a fine aggregate.

## 3.4 Methodology

In this project, experimental studies and theoretical analysis would be conducted. The main HAC system of research is 75% ground blast furnace slag (GBFS) or GBFS and fly ash (FA), 25% OPC and 3-5% alkali activator (liquid or solid). Setting time, early hydration heat and shrinkage will be investigated. Mechanical properties will also be tested.

### 3.4.1 HAC hydration kinetics and control

#### *Setting time testing and control*

Pastes with normal consistency are prepared. The initial and final setting times are measured using a Vicat apparatus according to a Chinese standard GBT 1346-2011<Test methods for water requirement of normal consistency, setting time and soundness of the Portland cement>. Both liquid and solid alkali activator are used to control the setting time of HAC. Also the gypsum or retarder will be added in order to prolong the setting time.

#### *Early hydration heat characterization*

The early hydration heat (72 h) of HAC pastes are determined by isothermal conduction calorimetry on a THERMOMETRIC TAM air calorimeter. The HAC systems that studied included slag/cement blend and slag/fly ash/cement blend which

are hydrated with liquid alkali activator or solid alkali activator. The control system is 100% cement hydrated with water. Superplasticizer is excluded so as to obtain more accurate results. The weight of one test sample is about 5-10 gram. These pastes are stirred by a hand-mixer, then poured into the test bottle quickly and placed into the calorimeter. The test will be finished 72 h after mixing.

### ***Reaction extent***

The reaction extent of different HAC systems is monitored by XRD quantitative analysis, FTIR and BSEM-EDX at different ages. The ages studied are chosen on the basis of information that provided by the calorimetric curves, such as the peak, the lowest point, inflection point and so on.

### **3.4.2 HAC mortar shrinkage and strength**

ISO sand and HAC mentioned above were used to prepare HAC mortar. The specimens are cured under standard curing (at  $20 \pm 2$  °C and humidity higher than 95%) and steam curing (at 85°C for 2 hours) in order to determine the effect of curing temperature on the shrinkage and strength of HAC pastes and mortars.

### ***Autogenous shrinkage***

The corrugated pipe ( $\varnothing 25$  mm $\times$ 300 mm) and length comparator are used to test the autogenous shrinkage. The slurry is rapidly stirred for 3 minutes according to the set mix ratio, and then poured into the corrugated pipe (which is sealed on one end), vibrate and maintain the same amount of filling. Then the corrugated pipes are sealed and placed on V-shaped glass sheets and put into a curing chamber with temperature of  $20 \pm 2$  °C. The initial length is measured at 10min after initial setting. The length of the specimens is measured at different ages (6h,8h,10h,12h, 1 d, 2d, 3d,7 d, 14d and 28 d), and the autogenous shrinkage can be calculated according to Eq. (1).

$$\varepsilon_{as} = \frac{L_0 - L_t}{250} \quad (1)$$

where  $L_0$  is the initial length,  $L_t$  is the length at various ages.

### ***Drying shrinkage***

Three 40 mm  $\times$  40 mm  $\times$  160 mm HAC mortar prisms are prepared for the drying shrinkage test for each group. The length comparator is used to measure the length of

mortar prisms. The initial length is measured after 24h, and then the prisms are put into a drying room which temperature is  $20 \pm 2$  °C and relative humidity is about  $60 \pm 5\%$ . The length of the prisms is measured at different ages (2 d, 3 d, 7 d, 14 d, 28 d and 56 d), and the drying shrinkage will be calculated according to Eq.(2).

$$\epsilon_{ds} = \frac{L_0 - L_t}{160} \quad (2)$$

where  $L_0$  is the initial length,  $L_t$  is the length at various ages.

#### ***Carbonation shrinkage***

Three 40 mm × 40 mm × 160 mm HAC mortar prisms are prepared for the carbonation shrinkage test for each group. The length comparator is used to measure the length of mortar prisms. The initial length is measured after 24h, and then the prisms are put into a carbonation chamber which relative humidity is kept at 75% with a  $K_2CO_3$  solution to keep the  $CO_2$  saturated. The length of the prisms is measured at different ages (2 d, 3 d, 7 d, 14 d, 28 d and 56 d), and the carbonation shrinkage can be calculated by Eq. (3).

$$\epsilon_{cs} = \frac{L_0 - L_t}{160} \quad (3)$$

where  $L_0$  is the initial length,  $L_t$  is the length at various ages.

#### ***Compressive strength testing***

The strength of HAC mortar is tested with reference to the method specified in GB/T 17671-2005 (Method of testing cements-Determination of strength (ISO)).

### **3.4.3 Microscopic characterization of HAC**

#### ***XRD quantitative analysis***

To monitor the reaction extent, XRD quantitative analysis is used to determine the types and quantities of crystals in the reaction products. In addition, the XRD analysis is used to illustrate the effects of carbonation on phase assemblage of HAC.

#### ***BSEM-EDX and SEM-EDX analysis***

To determine the reaction extent of HAC with different activators, BSEM-EDX is used to monitor the microstructural evolution and phase composition of hydration products. It is reported that the area fraction of the phase on the two-dimensional plane can represent the volume fraction of the phase on the three-dimensional scale (Scrivener

et al. 2014a; Scrivener 2014b). The degree of reaction  $\alpha$  of HAC can be calculated by Eq. (4):

$$\alpha = 1 - \frac{V(t)}{V(0)} \times 100\% \quad (4)$$

Where  $V(t)$  is the volume fraction of unreacted particles at age  $t$  calculated based BSEM image analysis,  $V(0)$  is the initial volume fraction of HAC that before reaction.

In the shrinkage section, SEM-EDX is applied to investigate the effect of curing temperature, alkali activators and expansion agents on the microstructure of HAC.

#### ***NMR analysis***

To understand the polymerization of silicate anions when HAC is activated by different type of activators, the  $^{29}\text{Si}$ -NMR is used to detect the chemical shifts.

#### ***Thermogravimetric (TG) analysis***

TG analysis of the samples was carried out under  $\text{N}_2$ -atmosphere on a STA-409PC instrument heated from 25 °C to 1000 °C at a heating rate of 10 °C/min.

#### ***Mercury intrusion porosimetry (MIP) analysis***

The pore size distribution and total porosity of the HACs were characterized by MIP on an automatic mercury porosimeter (AutoPore Iv 9510) which could measure the pore diameters range from 5 to 340 000 nm. The surface tension of mercury was 485 dynes/cm and the contact angle was set to be 130°.

### **3.5 Conclusions**

This chapter gives the objectives, raw materials, methodology and characterization employed in this research. These materials and methods will be used for reference or directly in subsequent chapter.

# CHAPTER 4: EARLY HYDRATION KINETICS AND MICROSTRUCTURE DEVELOPMENT OF HAC AT ROOM TEMPERATURE

*Note: this chapter is based on the published paper entitled “Early hydration kinetic and microstructure development of HAC at room temperature”, by Lili Xue, Zuhua Zhang, Hao Wang, accepted for publication in **Cement and Concrete Composites**, 123(2021)104200.*

## 4.1 Introduction

HAC is a new promising cement alternative that comprises less than 30% Portland cement and more than 70% SCMs with a small dosage of activator (Palomo et al. 2007; Shi et al. 2011). Many investigations have been carried out on HACs, such as hydration process, mechanical properties and aspects of durability. García-Lodeiro et al. (2011 and 2013c) studied the hydration process of HACs and found that the mixed gels of C-A-S-H and (N, C)-A-S-H were the main hydration products. It is also suggested that HACs possess denser and more homogeneous microstructure than Portland cement and pure alkali activated cement due to more binding gels and coexisting of N-A-S-H and C-A-S-H, resulting in higher mechanical strength and lower permeability (Qu et al. 2016; Mejía et al. 2015). It is worth mentioning that the hydration heat of Portland cement accelerates the alkali activation reaction of SCMs. As a result, HACs could set and develop strength at room temperature rather than high temperature curing that required by alkali activated cement (García-Lodeiro et al. 2011; García-Lodeiro et al. 2013c). In the current stage, HACs can be acceptable by the cement and concrete industry when the fully adoption of alkali-activated cementitious materials remains in doubt (Yang 2018; Palomo et al. 2019). However, the issue of early hydration kinetics behavior which governs the workability, microstructure development (Cao et al. 2020) and mechanical properties of HACs is insufficiently understood. The effective method to explore hydration kinetics of cementitious materials is isothermal conduction calorimetry. García-Lodeiro et al. (2013b) studied the early hydration kinetics of the

HACs based on Portland cement and fly ash with two alkali activating solutions ( $\text{Na}_2\text{CO}_3$  and a mixture of  $\text{NaOH} + \text{Na}_2\text{SiO}_3$ ), concluding that the alkaline activator has an obvious impact on initial reaction kinetics. Angulo-Ramírez et al. (2017) reported that the HACs with Portland cement and slag showed slower rate of heat release and lower cumulative heat than that of 100% Portland cement. So far, the effect of alkali content on hydration kinetics of HACs has not been reported in literature. On the other hand, the effect of precursors and alkali content on the early microstructural evolution of HACs and relevant mechanisms are yet well understood. Some research reported the microstructure development and hydration products of high and low-Ca HACs, but there is very limited detailed quantitative analysis (Palomo et al. 2013; Askarian et al. 2018).

It is well known that alkali content is a critical parameter of alkali-activated materials (Escalante-Garcia et al. 2014). Hence the quantitative effect of alkali content on HAC hydration kinetics must be studied. Besides, the distinction of hydration kinetics of high calcium and low calcium HAC systems has not yet been studied systematically. And the early microstructural evolution and quantitative analysis of hydration products for HACs with different precursors and alkali contents are beneficial to control their macro properties precisely. To promote the application of HACs in the construction industry, it is essential to understand the early hydration kinetics and microstructure development of different HACs.

In this chapter, the early hydration kinetics and microstructural development of HACs with various precursors and alkali contents at room temperature were investigated systematically. The focus will be the comparison and quantitative analysis of the degree of early hydration reaction and microstructural evolution for various HAC systems. XRD and  $^{29}\text{Si}$  NMR deconvolution were used to performing quantitatively analyze the crystal and gel phases of hydration products.

## **4.2 Materials and methods**

### **4.2.1 Materials**

P II 52.5 Portland cement (according to Chinese standard GB 175-2007) and grade

S95 ground blast furnace slag and grade I fly ash (according to Chinese standard GB/T 18046-2017 and GB/T 1596-2017) were used as the prime materials in this study. The specific surface areas of the slag and fly ash are 448 and 420 m<sup>2</sup>/kg, and their specific gravity are 2.91 and 2.42, respectively. The chemical compositions of aforesaid raw materials were determined by X-ray fluorescence (XRF), and the result is given in Table 4-1.

The ISO standard sand was used as fine aggregate. The sodium water- glass with a modulus of 2.33 and concentration of 47% was mixed with solid sodium hydroxide and water to form liquid alkali activator which modulus is 1.5 and solid content (Na<sub>2</sub>O and SiO<sub>2</sub>) is 30%. The poly-carboxylic acid superplasticizer with water-reducing rate of 35% was provided by Sobute New Materials Co., Ltd.

Table 4-1. Chemical composition of Portland cement, GBFS and FA (wt.%)

Type	SiO <sub>2</sub>	Al <sub>2</sub> O <sub>3</sub>	Fe <sub>2</sub> O <sub>3</sub>	CaO	MgO	SO <sub>3</sub>	K <sub>2</sub> O	TiO <sub>2</sub>	Na <sub>2</sub> O	MnO	P <sub>2</sub> O <sub>5</sub>	Σ	LOI
Cement	20.99	5.36	3.81	61.36	1.38	2.4	0.65	0.27	0.13	0.1	0.14	96.59	2.71
GBFS	31.43	15.22	0.71	37.79	9.62	1.2	0.43	0.67	0.52	0.312	0.02	98.02	0.76
FA	54.78	24.61	5.20	3.16	0.84	0.62	2.22	1.09	0.66	0.067	0.19	93.42	5.96

The phase analysis of raw materials was conducted by X-ray Diffraction (XRD). The XRD patterns of OPC (ordinary Portland cement), GBFS (granulated blast furnace slag) and FA (fly ash) are shown in Figure 4-1.

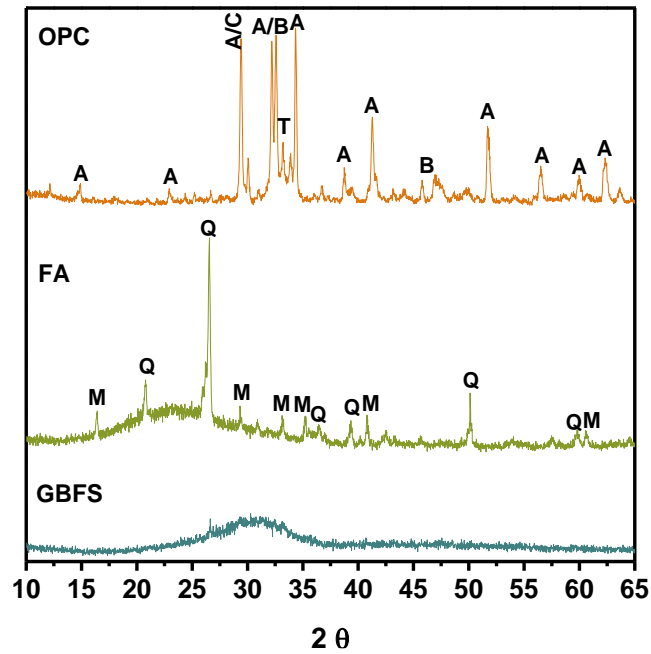


Figure 4-1. XRD patterns of OPC, GBFS and FA: A: Alite; B: Belite; C: Calcite; T: Tricalcium aluminate; Q: Quartz; M: Mullite

#### 4.2.2 Experimental method

The cementitious materials composition for HACs are presented in Table 4-2. The HAC systems studied include OPC-GBFS blend, OPC-FA blend and OPC-GBFS-FA blend hydrated with waterglass and NaOH. The control system is 100% OPC hydrated with water.

Table 4-2. Composition of various HAC systems (wt.%)

Group	OPC	GBFS	FA	Na <sub>2</sub> O	Activator (Ms =1.5)
OPC	100	-	-	-	-
HACS3	25	75	-	3	NaOH + waterglass
HACS4	25	75	-	4	NaOH + waterglass
HACS5/HACS	25	75	-	5	NaOH + waterglass
HACF	25	-	75	5	NaOH + waterglass
HACSF	25	50	25	5	NaOH + waterglass

#### *Setting time*

The initial setting times and the final setting times were measured by Vicat apparatus according to a Chinese standard GBT 1346-2011 (Test methods for water requirement of normal consistency, setting time and soundness of the Portland cement).

#### *Compressive strength*

ISO standard sand and HACs mentioned above were used to prepare HAC mortars. Three 40×40×40 mm mortar specimens were prepared as a parallel group, and then specimens were cured under standard curing (at  $20 \pm 2$  °C and RH > 95%) in accordance with ISO 1920-3-2004 (Li et al. 2019).

#### ***Early hydration heat***

The early hydration heat (72 h) of HAC pastes was determined by isothermal conduction calorimetry on a THERMOMETRIC TAM air calorimeter. Superplasticizer was excluded to obtain more accurate results. The weight of one test sample was approximately 5-10 grams. These pastes were stirred by a hand-mixer, then poured into the test bottle quickly and placed into the calorimeter. Besides, the test will be finished 72 hours after mixing.

#### ***Reaction extent and macrostructural evolution***

The reaction extent of different HAC systems was monitored by X-ray Diffraction (XRD) quantitative analysis, <sup>29</sup>Si NMR and BSEM-EDX at different ages. The ages studied were chosen on the basis of information, which was provided by the calorimetric curves, such as the lowest point and inflection point.

XRD patterns were measured using a 60-KV, 80-mA XRD-7000 diffractometer with Ceramic X-ray tube and Cu target, with scan speed of 2.5° /min in the range between 5 and 80° 2θ.

To determine the degree of polymerization of silicate in the hydration production of HACs, the <sup>29</sup>Si NMR studies were conducted by a BRUKER AVANCE-600M spectrometer. Samples were spined at 40 kHz with 3.5 μs pulse and 4 s relaxation period between scans. Repetition delay was 40 s, which was sufficient for complete relaxation. Up to 724 scans were collected for each sample. The software Peakfit was used to deconvolute the spectra. The minimum number of peaks was used to enable an accurate and meaningful interpretation of the spectra and peak full width at half height was restricted to 4 ppm.

To determine the reaction products of HACs with different precursors and alkali contents, BSEM-EDX was employed to monitor the microstructural evolution and

phase composition of hydration products. Some principles and testing conditions can be found else where (Scrivener et al. 2004a; Scrivener 2004b).

### 4.3 Results and discussion

#### 4.3.1 Setting time

The setting times of OPC and HACs are provided in Figure 4-2, demonstrating that HACs show much shorter setting times than those of OPC. With the increase of alkali content, the initial and final setting times reduce perceptibly, in a similar way to the behavior of alkali activated slag cement (Shi et al. 2006). The reason for this reduction is that the waterglass and NaOH increased with the increasing alkali dosage. The increased waterglass leads to a higher concentration of  $[\text{SiO}_4]^{4-}$  and then induces a higher reaction rate. Meanwhile, the higher concentration of NaOH promotes the dissolution of  $\text{Ca}^{2+}$  from slag, also increasing the reaction rate (Chang et al. 2003). In terms of precursors, the HACS present the shortest initial setting. The initial setting of HACF is longer than HACS but shorter than that of HACSF, implying that the incorporation of fly ash could slightly prolong the initial setting time of HACs due to its low reactivity. However, the final setting time of HACSF is longer than HACS and HACF, indicating that the final setting time of HACs could be retarded effectively when slag is combined with fly ash.

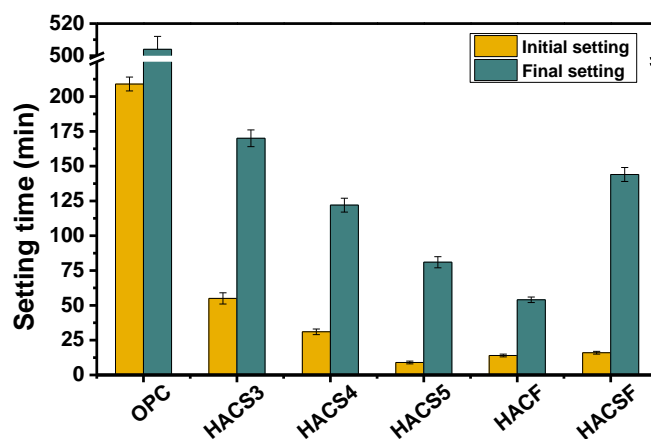
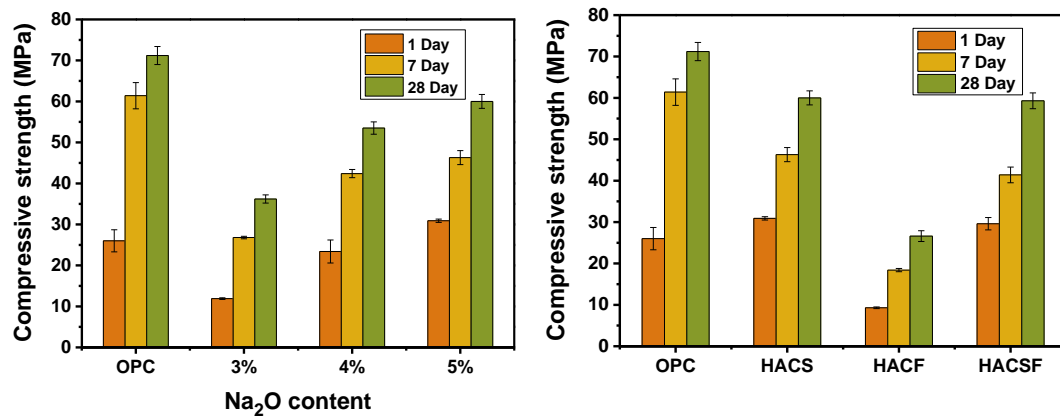


Figure 4-2. Initial setting time and final setting time of OPC and HACs.

### 4.3.2 Compressive strength



(a) OPC and HACS with different Na<sub>2</sub>O contents (b) OPC and HACs with different precursors

Figure 4-3. Compressive strengths of OPC and HACs.

Figure 4-3 shows the compressive strengths of OPC and HACs with different Na<sub>2</sub>O contents and precursors. As shown in Figure 4-3(a), the compressive strengths of HACs increase gradually with the increment of Na<sub>2</sub>O content. This can be explained using pozzolanic reaction. The pH of the aqueous solution is raised due to the increase of Na<sub>2</sub>O content and thus accelerates the slag dissolution, contributing to substantially higher reactivity. Although HACs show lower 28-day compressive strengths than 52.5 OPC, the 1-day compressive strengths of HACS with more than 4% Na<sub>2</sub>O are comparable to or even higher than P II 52.5 OPC. Observably, HACs exhibit high early strength. As for the precursors, HACF shows the lowest compressive strength at all curing ages, as presented in Figure 4-3(b). The incorporation of fly ash reduces the strength of HACs due to its lower reactivity. Additionally, the HACF and HACSF exhibit comparable strength. This indicates that the compressive strengths of HACs would not be affected when some amount of slag is replaced by fly ash.

### 4.3.3 Hydration heat

#### 3.3.1 Effect of Na<sub>2</sub>O content

The profiles of heat flow and cumulative heat vs time for OPC and HACS pastes with different Na<sub>2</sub>O contents are presented in Figure 4-4. The heat flow profile for OPC follows the typical characteristic of Portland cement hydration, involving stages of pre-induction, induction, acceleration, deceleration, and steady-state diffusion. The

calorimetric curve for HACS has two peaks as the curve of OPC. The first one is associated with the rapid dissolution of calcium aluminates, calcium silicate and alkali activator, and the second one is attributed to the formation of hydration products (García-Lodeiro et al. 2013b; Angulo-Ramírez et al. 2017). However, the intensity of the peaks is higher than that of OPC, and the second peaks appears earlier. With the increase of Na<sub>2</sub>O content, the second peaks of HACS curves are delayed although the peaks are about the same intensity. The reason for these reactions is that the increment of alkali content inhibits the CaO content in the system, which can thus impede the formation of hydration products, finally delaying the emergence of the accelerated reaction peak (Yang 2018; Yuan 1996; Taylor 1997). In delineating the aspect of cumulative heat, in the first 12 h, HACS have higher heat than OPC, while the trend reverses after 18h. As the Na<sub>2</sub>O content increased, the total heat of HACS decreases at first, but the trend reverses after 8 h.

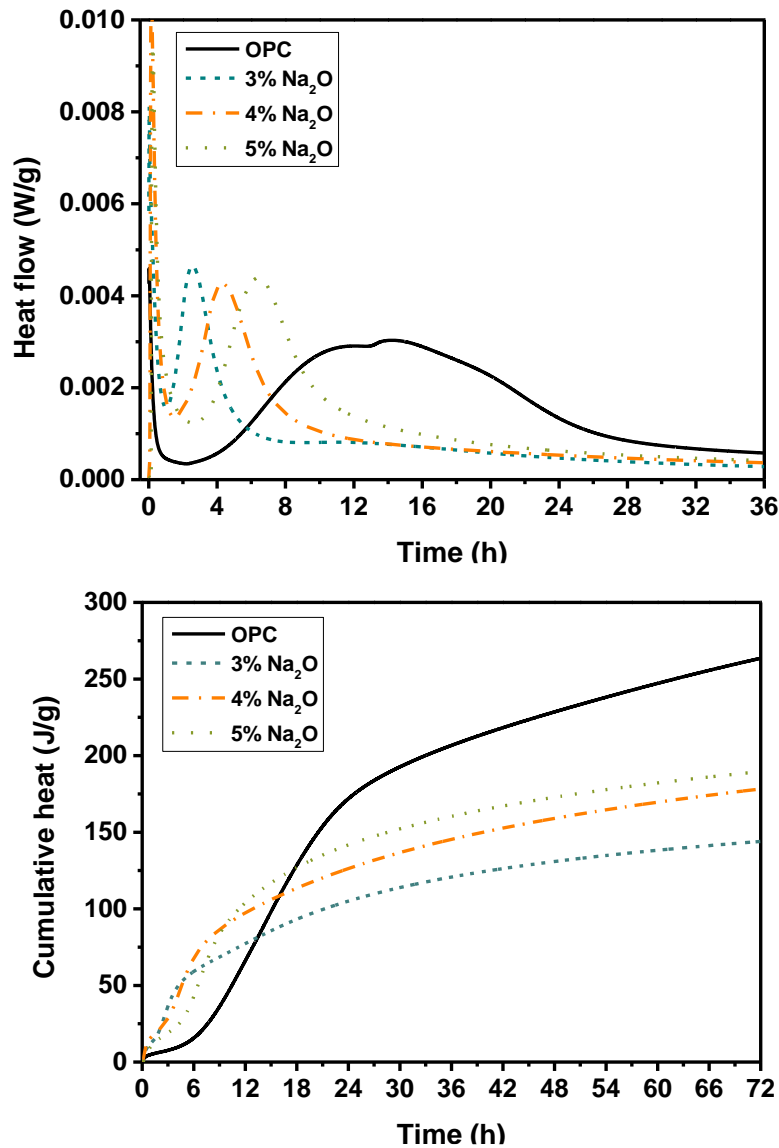


Figure 4-4. Heat flow and cumulative heat of OPC and HACS with different Na<sub>2</sub>O contents.

### 3.3.2 Effect of precursor type

Figure 4-5 shows the heat flow and cumulative heat of OPC and HACs with various precursors. The general shape of the calorimetric curves for HACs are similar, with narrower initial peaks and wider acceleration peaks. The HACS has the strongest acceleration peak, whereas the HACF presents the weakest acceleration peak which is about a quarter of the former. The acceleration peak for HACSF is lower than that of HACS but higher than HACF, indicating that the reaction rate of HACS is faster than that of HACF, and the reaction rate becomes slower when some slag is replaced by fly

ash. The cumulative heat of HACs is higher than that of Portland cement at the beginning of reaction, but the latter exceeds the former after 18 h. In terms of precursors, HACS always shows the maximum heat release, while the HACF shows the minimum cumulative heat, and the total heat of HACSF is between the previous two because the activity of slag is higher than that of fly ash.

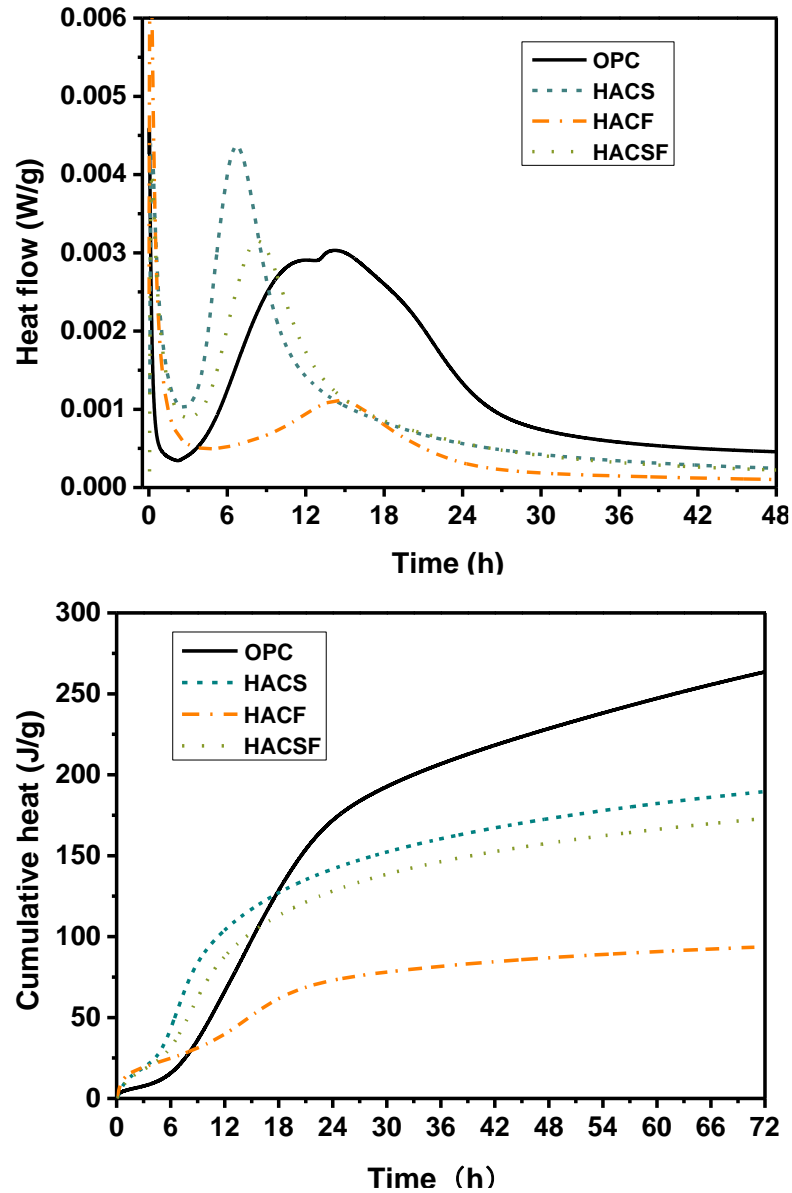


Figure 4-5. Heat flow and cumulative heat of OPC and HACs with different precursors.

#### 4.3.4 Mineralogical analyses of hydration products

XRD qualitative and quantitative analyses were carried out on all of the pastes. The XRD full spectrum fitting method was employed in quantitative analysis.

### 3.4.1 Effect of Na<sub>2</sub>O content

Figure 4-6 plots the XRD patterns for HACS with diverse Na<sub>2</sub>O contents at the curing age of 1 and 7 days.

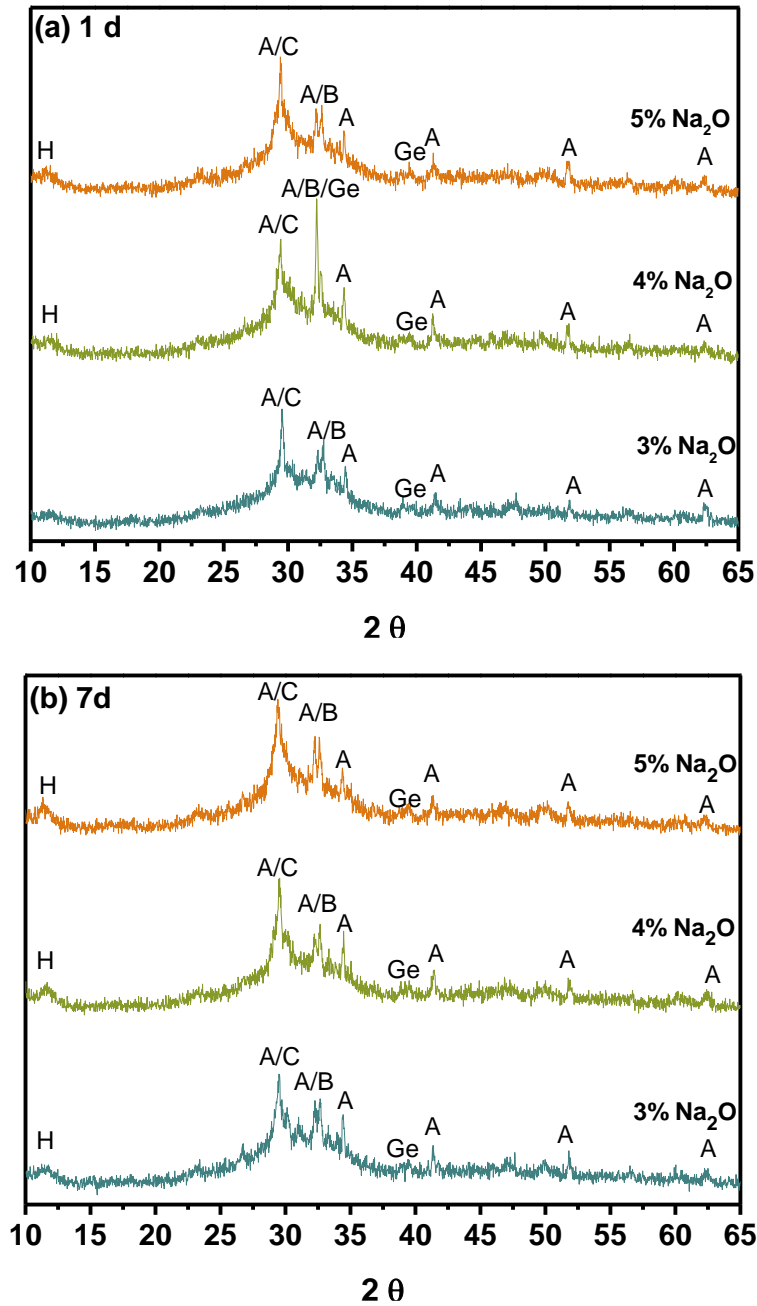


Figure 4-6. XRD patterns of HACS with different Na<sub>2</sub>O contents for 1-day and 7-day of curing. A: Alite; B: Belite; C: Calcite; H: Hydrocalumite ( $\text{Mg}_6\text{Al}_2(\text{CO}_3(\text{OH})_{16} \cdot 4\text{H}_2\text{O})$ ); Ge: hydrated Gehlenite ( $\text{C}_2\text{ASH}_8$ ).

As shown in the XRD patterns, the crystalline phases observed are calcite, hydrated gehlenite and hydrocalumite. Portlandite and ettringite, which are the main crystalline

hydration products of OPC, are not detected either in the very early age or in the 7-day diffractograms for the HACs with slag pastes. This is consistent with previous research (Angulo-Ramírez et al. 2017; Elahi et al. 2012), which is mainly caused by the lower amount of OPC in HACs and the retardance or inhibition of the hydration reaction in OPC due to the high alkalinity of the HACs solution (Puertas et al. 2011). The diffraction peak appearing at about 11.58 degree ( $2\theta$ ) is possibly hydrocalumite which belongs to a kind of layered double hydroxides (LDH) with well-ordered Ca and Al located in the hydroxide layers. It tends to appear in alkali activated materials with high Ca and Al contents (Qiu et al. 2015). Moreover, the hydrocalumite cannot be detected at a very early stage when the  $\text{Na}_2\text{O}$  content is 3%. Hydrated gehlenite ( $\text{C}_2\text{ASH}_8$ ) is a hydration product of GBFS activated by  $\text{Na}_2\text{SiO}_3$  and  $\text{NaOH}$  (Shi et al. 2006), which also shows a connection with the absence of  $\text{Ca}(\text{OH})_2$  (Torres et al. 2008). The formation of calcite of which the peak usually appears at  $29.5^\circ 2\theta$  has been attributed to the carbonation of Portlandite, because the high alkalinity environment tends to lead to carbonation (García-Lodeiro et al. 2013b, Cao et al. 2021). Unreacted Portland cement clinkers such as  $\text{C}_3\text{S}$  and  $\text{C}_2\text{S}$  are identified in all of the samples although their peak intensity varied with curing age and  $\text{Na}_2\text{O}$  content. A broad diffuse halo appearing at the value of  $2\theta$  ranging from  $25^\circ$  to  $40^\circ$  is generally considered to be a large quantity of amorphous products or non-crystalline gels (García-Lodeiro et al. 2013b; Angulo-Ramírez et al. 2017; Nath et al. 2015). The quantitative analysis of the above crystal phase is provided in Table 4-3.

Table 4-3. XRD quantitative analysis of hydration products for HACs with different  $\text{Na}_2\text{O}$  contents at 1 and 7 days age.

Type	$\text{C}_3\text{S}$ (%)	$\text{C}_2\text{S}$ (%)	Calcite (%)	Gehlenite (%)	Hydrocalumite (%)
HACS3-1d	59.9	14.2	23.9	2	0
HACS3-7d	39.1	6.4	30.5	19.8	4.2
HACS4-1d	44.2	14.8	19.1	18.8	3.1
HACS4-7d	34.4	10.1	34.7	14.0	6.8
HACS5-1d	42.4	12.9	26.6	13.2	5
HACS5-7d	34.1	7.1	40.8	9.4	8.7

The table shows that proportion of  $C_3S$  and  $C_2S$  in the total crystal volume is reduced gradually with increasing curing age and  $Na_2O$  content in HACS. Meanwhile, the proportion of crystalline hydration products such as calcite, hydrated gehlenite and hydrocalumite also increase indicating that the reaction degree of HACS increases when  $Na_2O$  content increases. This may explain the compressive strength development and hydration heat release trend for HACS with different  $Na_2O$  contents within a 7-day curing age. As mentioned above, higher alkaline environment is more prone to carbonization, and thus the generation of calcite increases with increasing alkali content. It has been found that when the  $Na_2O$  content is over 3%, the proportions of gehlendite decreases due to the increase of alkali content and curing age. The reason may be that the formation of calcite reduces the availability of calcium ions in the solution (Duchesne and Reardon 1995), contributing to the reduction of gehlendite. The gradual increase of hydrocalumite is associated with curing age and  $Na_2O$  content. Furthermore, the reduction of  $C_3S$  and  $C_2S$  decrease with increasing  $Na_2O$  content which may be explained by the slow reaction of Portland cement, which is delayed in a high alkaline environment (García-Lodeiro et al. 2013b; Martinez-Ramirez and Palomo 2001). Both the C-S-H gel (the main hydration product of OPC) and C-A-S-H gel (the main alkali activated GBFS product) are XRD amorphous. Their presence in the HACs will be identified with SSNMR and BSEM.

#### *3.4.2 Effect of precursor type*

Figure 4-7 shows the XRD patterns for HACs with different precursors at various curing periods which are chosen on the basis of the calorimetric profiles. At the end of the induction period, the first age is relatively short. The second age is chosen at the end of deceleration and 7-day is the third age of the study.

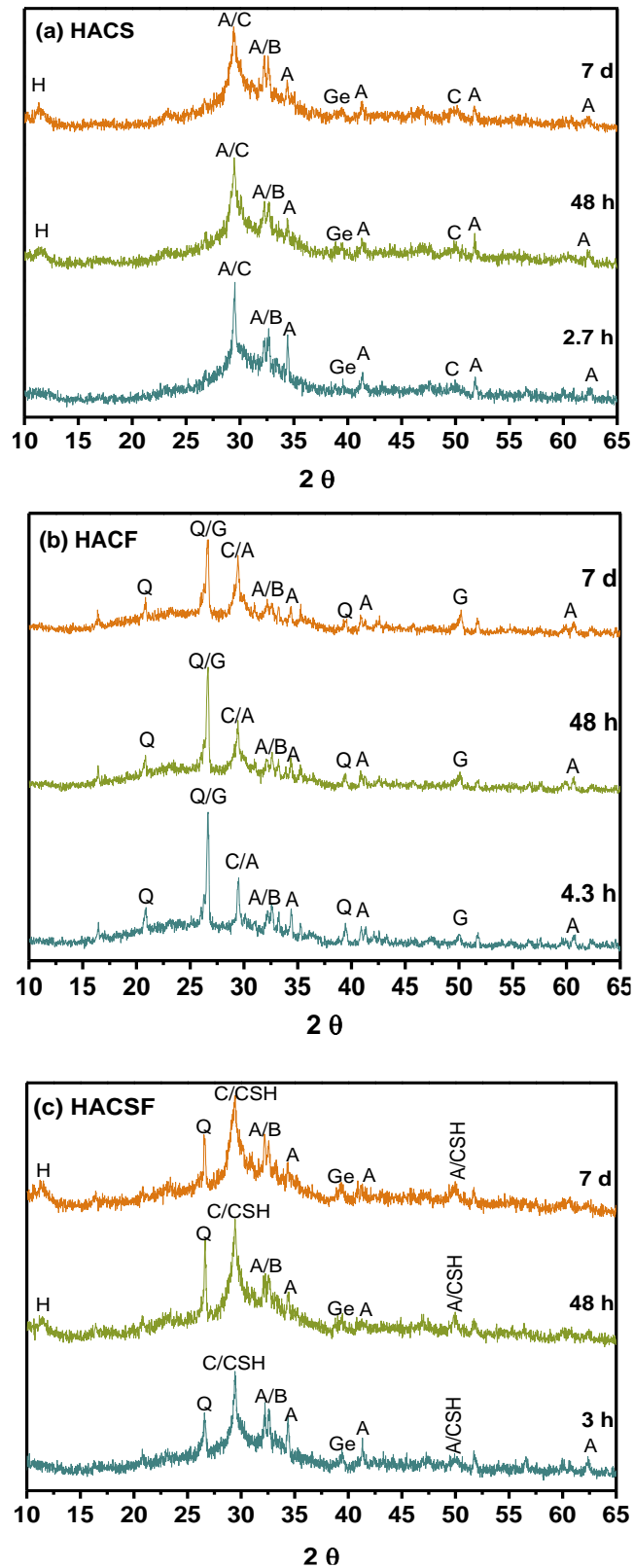


Figure 4-7. XRD patterns of HACs with different precursors at an early time, 2-day and 7-day of curing. A: Alite; B: Belite; C: Calcite; Q: Quartz; H: Hydrocalumite ( $\text{Mg}_6\text{Al}_2(\text{CO}_3(\text{OH}))_{16} \cdot 4\text{H}_2\text{O}$ ); Ge: hydrated Gehlenite ( $\text{C}_2\text{ASH}_8$ ); G: Gismondine; CSH: crystalline Calcium Silicate Hydrate.

In Figure 4-7, the diffraction peaks of  $C_3S$  and  $C_2S$  are shown in the XRD patterns for all the HAC systems. The crystalline phases in original fly ash such as quartz naturally exists in the hydration system due to the incomplete reaction. The hydration products of HACs with different precursors depend on the composition of precursors. In the HACS system (Figure 4-7a), the calcite, hydrated gehlenite and hydrocalumite are the main crystalline products, while the gismondine and calcite could be observed in the HACF system (Figure 4-7b). The absence of hydrated gehlenite and hydrocalumite may be due to the low calcium content of fly ash. When slag and fly ash coexist in the hybrid cement system, the diffractograms contain a series of signals associated with crystalline CSH in addition to calcite, hydrated gehlenite and hydrocalumite (Figure 4-7c). These signals could be explained by the formation of crystalline CSH which is controlled by the  $OH^-$  concentration and composition as reported in previous studies (Palomo et al. 2007; Askarian et al. 2018). The hump at  $20-40^\circ 2\theta$  is likewise attributed to amorphous products. The difference is that the hump at XRD pattern for HACF is broader and lower than that of HACS and HACSF systems, indicating a relatively small amount of amorphous products. The quantitative analysis of HACs with various precursors is shown in Table 4-4.

Table 4-4. XRD quantitative analysis of HACs with different precursors at different ages.

System	$C_3S$ (%)	$C_2S$ (%)	Quartz (%)	Calcite (%)	Gehlenite (%)	Gismondine (%)	C-S-H (%)	Hydrocalumite (%)
HACS- 2.7h	57.0	8.9	0	12.3	21.7	0	0	0
HACS- 48h	42.0	8.2	0	28.5	18.5	0	0	2.8
HACS-7d	34.1	7.1	0	40.8	9.4	0	0	8.7
HACF- 4.3h	12.3	15.7	38.7	32.8	0	0.5	0	0
HACF- 48h	8.4	11.6	30.4	21.4	0	18.7	0	0
HACF-7d	9.3	10	28.7	29.5	0	22.6	0	0
HACSF-3h	29.9	16	6.6	25.9	21.3	0	0.4	0
HACSF- 48h	20.1	11.4	6.3	15.8	31.6	0	12.3	2.5
HACSF- 7d	16.5	10.5	5.6	16.9	13.2	0	33.2	3.9

The amount of unreacted  $C_2S$  and  $C_3S$  in every HACs system reduces with the age, while the total amount of crystalline products simultaneously increase, especially

within 48 h. In the HACS system, the generation of calcite and hydrocalumite increase and the gehlenite reduce due to the increased curing age. This situation was explained in the previous section. It is of note that the proportion of unreacted quartz derived from fly ash in HACSF is much less than that in HACF. One reason could be the lower content of fly ash in HACSF. Additionally, it implies that the combination of fly ash and slag generates a synergistic effect which accelerates the reaction of fly ash. The amount of crystalline CSH only forms in the HACSF system also increases with the age. Obviously, the clinker reduction and the hydration products formation rate of the HACF system are both lower than that of the other two systems, suggesting that the extent of the reaction is lower. Therefore, the early compressive strength of HACF system develops more slowly than HACS and HACFS. The proportion of unreacted  $C_2S$  and  $C_3S$  observes in HACF is less than the other two systems. This is caused by the larger amount of crystals in fly ash than that in slag rather than the higher reaction degree. No significant difference exists in the extent of the reaction between the HACS and HACSF systems, as seen in the above table. As mentioned above, the gel products in HACs such as C-S-H, N-A-S-H and C-A-S-H are amorphous to XRD, and these will be identified by SSNMR and BSEM.

#### **4.3.5 Microstructural development**

$^{29}Si$  NMR and BSEM-EDX analyses were performed to explore the gel composition and the microstructure evolution of the HACs which were studied.

##### *3.5.1 $^{29}Si$ NMR analysis*

The  $^{29}Si$  NMR spectra for anhydrous starting materials and HACS with different dosages of activator can be found in Figure 4-8(a). The narrow signal at around -71.1 ppm and a shoulder at -72.9 ppm on the spectrum for OPC, denoted by  $Q^0$ , are attributed to the presence of  $C_3S$  and  $C_2S$  in the clinker (Palomo et al. 2007; Qu et al. 2016). The symmetrical signal centre over -73.5 ppm observed in the GBFS spectrum is associated with the Si tetrahedra ( $Q^1$ ) in unreacted GBFS (Palomo et al. 2013; Walkley and Provis 2019). The intensity of the two signals is observed to decline in all HACS, indicating that the OPC and GBFS are reacting. Moreover, the decline

degree increases with the increase of Na<sub>2</sub>O content, suggesting that the reaction degree of HACS improves with the increment of alkali dosage. This is consistent with the XRD quantitative analysis results. Meanwhile, two new signals located at around -79 ppm and -81.2 ppm are respectively assigned to Q<sup>1</sup> in C-S-H gel and Q<sup>2</sup> (1Al) in C-(A)-S-H (García-Lodeiro et al. 2011; Walkley and Provis 2019), and the intensity of the signals rises with the increment of alkali content. The intensity of signal relates to Q<sup>2</sup> (1Al) in C-(A)-S-H gradually exceeds that of Q<sup>1</sup> in C-S-H when the Na<sub>2</sub>O cement is over 4% in HACS. In addition, shoulder exists at -84 ppm generated by Q<sup>2</sup> in C-S-H gel in the spectrum for HACS5. These transformations imply that the degree of polymerization of HACS gelatinous products increase with the increment of alkali content. This also explains why the compressive strengths of HACS increases with alkalinity.

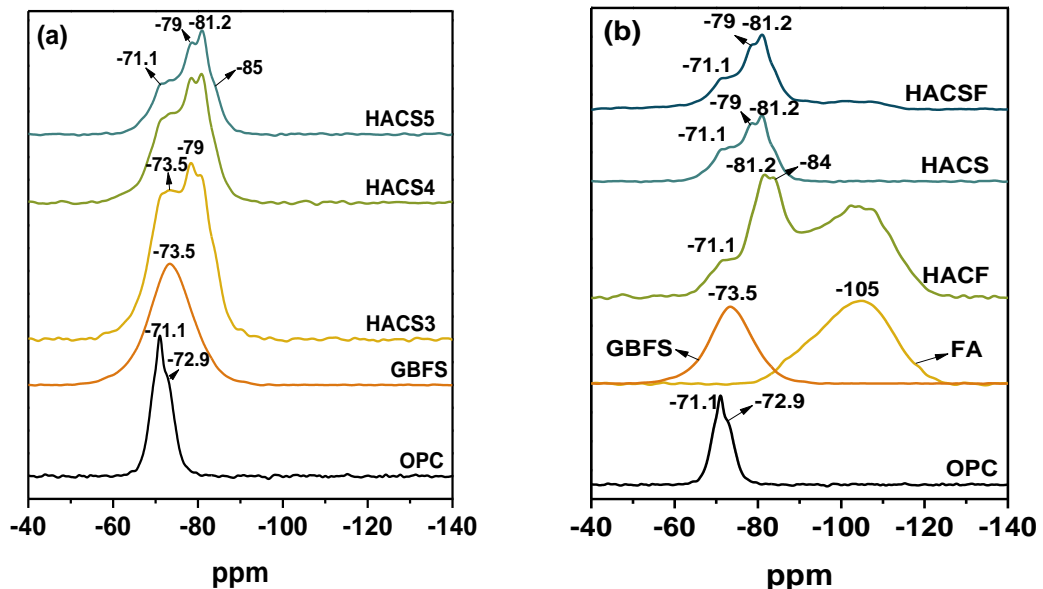


Figure 4-8. <sup>29</sup>Si NMR spectra of anhydrous OPC, GBFS, FA and 7-day cured HACS (a)with different Na<sub>2</sub>O contents;(b) with different precursors.

Figure 4-8 (b) shows the <sup>29</sup>Si NMR spectra for the anhydrous raw materials and 7-day cured HACs with different precursors. The spectra for OPC and GBFS were analyzed in the preceding section, and thus the analysis would not be repeated. The signal appearing from about -90 to -105 ppm in the <sup>29</sup>Si NMR spectrum of FA is associated with Q<sup>4</sup> (mAl, m=0-4) in the fly ash. The signal at -71.1 ppm denoted as C<sub>3</sub>S and C<sub>2</sub>S is observed in the NMR spectra of all HACs systems, confirming that the OPC has not

reacted completely. On the HACF spectrum, the high intensity signal appeared in the -90 to -108 ppm range associated with unreacted fly ash indicates the presence of a large amount of remnant fly ash, which could also explain the low compressive strength for the current system. The new resonances at approximately -81.2 ppm and -84 ppm on the HACF spectrum are respectively attributed to  $Q^2(1Al)$  in C-(A)-S-H and  $Q^2$  in C-S-H gel (Walkley and Provis 2019). The  $^{29}Si$  NMR spectra for HACS and HACSF both exhibit signals at around -79 ppm and -81.2 ppm, which are assigned to  $Q^1$  in C-S-H gel and  $Q^2(1Al)$  in C-(A)-S-H respectively. However, due to the incorporation of fly ash, the intensity of signal positioned around -81.2 ppm on the HACSF spectrum is higher than that of HACS. Compared with the spectrum for HACF, the resonance signal from -90 to -105 ppm (generated by unreacted fly ash) of HACSF is too weak to be observed, revealing the sufficient reaction of fly ash in this HAC system. It is in accordance with the results of XRD analysis. Therefore, the HACSF exhibits higher compressive strength than HACF. In addition, the signal at -79 ppm associated with  $Q^1$  in C-S-H gel is not observed in the HACF spectrum.

In order to obtain quantitative information about phase evolution, microstructure changes and chain lengths of the HAC reaction products, the deconvolution of the obtained spectra was carried out by PeakFit software. The spectra for the remnant unreacted raw materials were subtracted during deconvolution to provide accurate results (Provis et al. 2015; Gao et al. 2017; Le Saoût et al. 2011), as the spectra of the solid reactants and reaction products overlapped to a certain extent, especially fly ash (Lee and Lee 2015; Bernal et al. 2013). Figure 4-9 depicts the decomposition of  $^{29}Si$  NMR spectra of HACs hydration products and unreacted raw materials. The Si sites in the gel products of HACSs include  $Q^0$ ,  $Q^1$ ,  $Q^2(1Al)$ ,  $Q^2$ . Obviously, increasing  $Na_2O$  % results in a higher proportion of  $Q^2(1Al)$  and a lower proportion of  $Q^0$ , which indicates the higher degree of polymerization of HACSs products with high alkaline content. When the fly ash is used in HACs, the  $Q^4(mAl)$  groups which in association with N-A-S-H appear in the gel product, in addition to  $Q^1$ ,  $Q^2(1Al)$ ,  $Q^2$ . However,  $Q^1$  and  $Q^2$  groups account for a large proportion in HACSF product gel compared with

HACF.

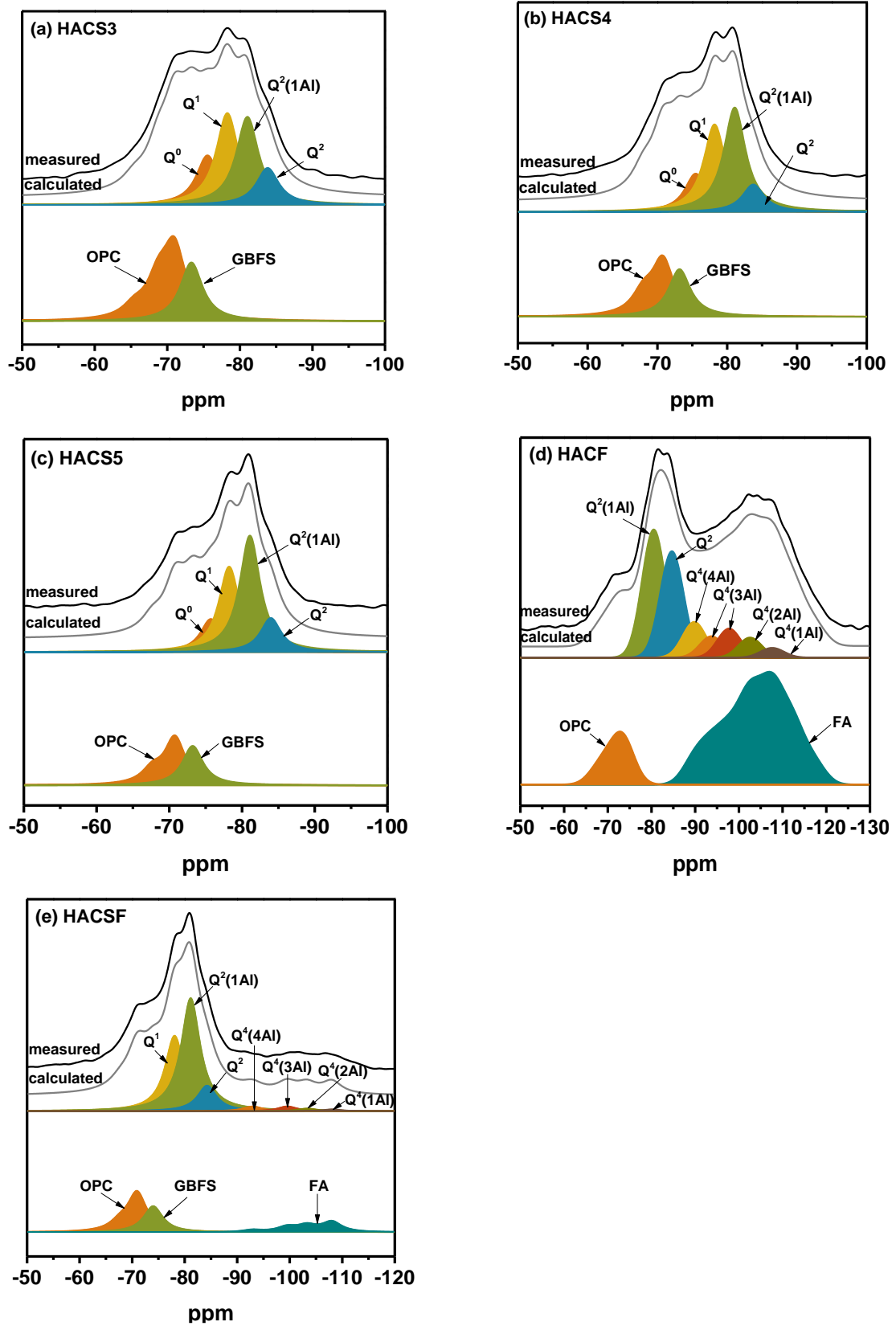


Figure 4-9. Decomposition of the  $^{29}\text{Si}$  NMR spectra of 7-day HACs pastes after subtraction of the signal from unreacted raw materials.

The deconvolution results and the calculation of mean chain length (MCL) and Si/Al of C-(A)-S-H and N-A-S-H in the hydration products are summarized in Table 4-5.

The MCL and Si/Al of gels were calculated as follows (Gao et al. 2017):

$$\text{MCL} = \frac{Q_1 + \frac{3}{2}Q_2(1Al) + Q_2}{\frac{1}{2}Q_1} \quad (1)$$

$$\text{Si/Al}_{\text{CASH}} = \frac{Q_1 + Q_2 + Q_2(1Al)}{\frac{1}{2}Q_2(1Al)} \quad (2)$$

$$\text{Si/Al}_{\text{NASH}} = \frac{\sum_{n=0}^4 Q^n(nAl)}{\sum_{n=0}^4 \frac{n}{4} Q^n(nAl)} \quad (3)$$

Table 4-5. Deconvolution results of <sup>29</sup>Si NMR spectra for 7-day HACs pastes after subtraction of the unreacted starting materials

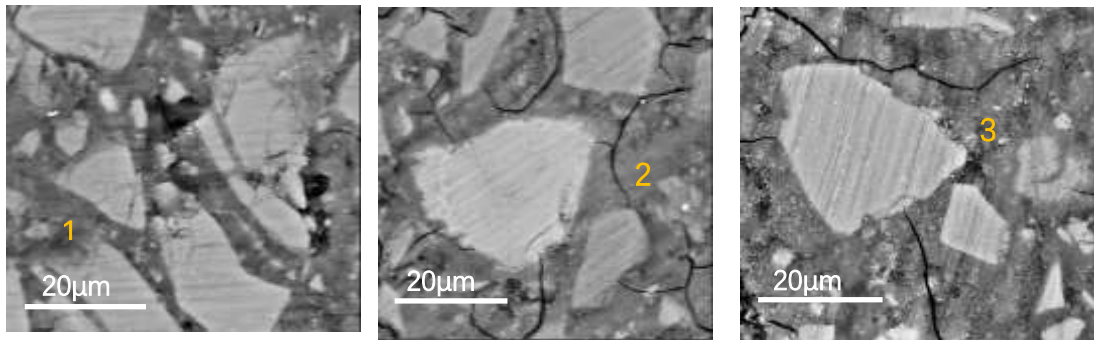
Group		Q <sup>0</sup>	Q <sup>1</sup>	Q <sup>2</sup> (1Al)	Q <sup>2</sup>	Q <sup>4</sup> (4Al)	Q <sup>4</sup> (3Al)	Q <sup>4</sup> (2Al)	Q <sup>4</sup> (1Al)	MCL	Si/Al
HACS3	Pos.(ppm)	-75.61	-78.27	-81.04	-83.82	-	-	-			
	Integration (%)	18.61	34.44	33.06	13.89	-	-	-		5.68	4.92
HACS4	Pos.(ppm)	-75.48	-78.18	-81.07	-83.74	-	-	-			
	Integration (%)	14.89	33.95	40.49	10.67	-	-	-		6.18	4.20
HACS (5)	Pos.(ppm)	-75.7	-78.22	-81.08	-83.96	-	-	-			
	Integration (%)	12.34	31.90	43.49	12.74	-	-	-		6.89	4.05
HACF	Pos.(ppm)	-	-	-80.51	-84.27	-90.0	-97.77	-102.55	-107.7		
	Integration (%)	-	-	35.00	33.97	9.66	13.29	5.42	2.64	-	1.35*
HACSF	Pos.(ppm)	-	-78.1	-81.1	-84.3	-92.9	-99.6	-103.4	-108.1		
	Integration (%)	-	33.00	49.42	11.21	2.14	2.16	1.22	0.85	7.17	3.79/ 1.37*

\*Means Si/Al in N-A-S-H, otherwise, it is Si/Al in C-(A)-S-H.

In the HACS system, the results demonstrate that the MCL of the generated C-(A)-S-H gel is increased with a faintly reduced Si/Al with increasing Na<sub>2</sub>O%. The long MCL and reduced Si/Al suggest a more polymerization and crosslinking in the C-(A)-S-H gel, resulting in higher compressive strengths. In the case of HACSF, the formed C-(A)-S-H gel exhibits longer MCL and lower Si/Al compared with HACSs, which is in accordance with previous research (Gao et al. 2017). This is derived from an interaction between the precursors. Due to the absence of Q<sup>1</sup> in gel, the MCL cannot be calculated in the HACF system. In terms of Si/Al in N-A-S-H gel, there is a slight reduction in HACF than in HACSF.

### 3.5.2 BSEM-EDX analysis

The BSEM-EDX analysis was carried out to determine the microstructural development and elemental composition of HACS with various alkali dosages (see in Figure 4-10). In the BSEM micrographs, the OPC particles generally show a brighter and uneven grey shade, while the slag particles are relatively dark and remain uniform in color (Nath et al. 2015). The gelation matrix has the darkest grey shade. It can be observed from the BSEM micrographs that a denser and less porous microstructure is formed by increasing the  $\text{Na}_2\text{O}$  content in HACS in spite of some small cracks (black regions) due to high drying shrinkage. Additionally, the inner product shells around the unreacted particles also become more obvious due to the increase of alkali content.



(a) 3%  $\text{Na}_2\text{O}$

(b) 4%  $\text{Na}_2\text{O}$

(c) 5%  $\text{Na}_2\text{O}$

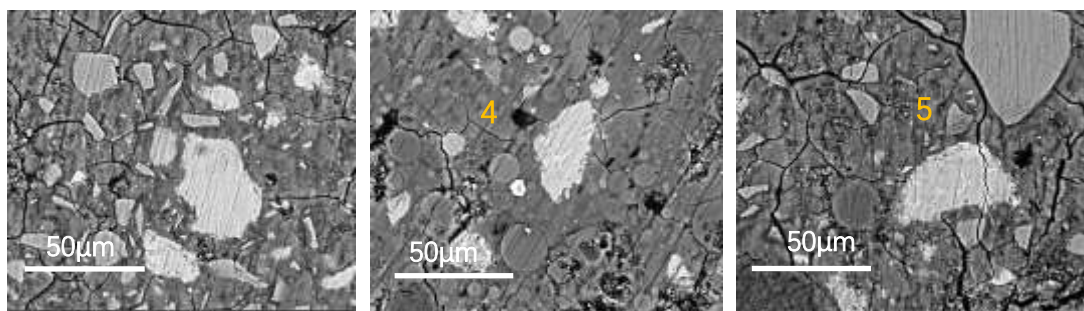
Figure 4-10. BESM images of HACS with different  $\text{Na}_2\text{O}$  contents for 7 days of curing.

According to the EDX analyses, the hydration product compositions of HACS are similar for all systems apart from a slightly increased concentration of Na and Al due to increased  $\text{Na}_2\text{O}$  content. The primary product compositions are Si and Ca with a small amount of Na, Al, and Mg, which could be attributed to the mix of C-S-H and C-(A)-S-H gels (Gebregziabiher et al. 2015). This is consistent with the NMR analysis. Table 4-6 summarizes the elemental atomic ratios of these hydration products. The Ca/Si and Si/Al decrease with the  $\text{Na}_2\text{O}$  content (point 1,2,3), indicating higher polymerization and crosslinking in the product gel. The Na/Si is also reduced with an increased concentration of alkali.

Table 4-6. Elemental ratios of HACs hydration products.

Point	Ca/Si	Na/Si	Si/Al
1	1.35	0.59	4.62
2	1.25	0.46	3.57
3	0.94	0.43	3.32
4	0.65	0.41	4.21
5	1.19	0.24	3.04

The BSEM-EDX analysis was used to further determine the gelation components and microstructure of HACs with different precursors. Figure 4-11 presents the microstructure images of HACs after 7 days of hydration. As presented in the BSEM graphs, HACS exhibits a more compact microstructure compared to HACF and HACSF, and HACF shows a relatively loose structure than HACSF. A large amount of unreacted fly ash exists in the HACF, which is also obvious in the XRD quantitative analysis and  $^{29}\text{Si}$  NMR spectra. The loose microstructure due to less formation of amorphous gels indicates the lower hydration reaction degree of HACF, leading to reduced compressive strength. Besides, the remnant fly ash grains embedded in matrix in HACSF are significantly less than those in HACF, which is in line with the XRD and  $^{29}\text{Si}$  NMR measurements.



(a) HACS

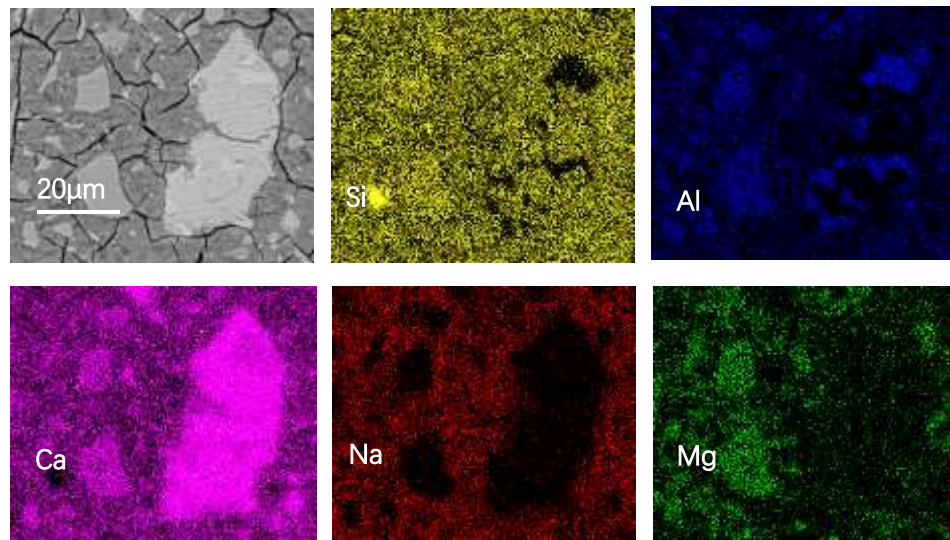
(b) HACF

(c) HACSF

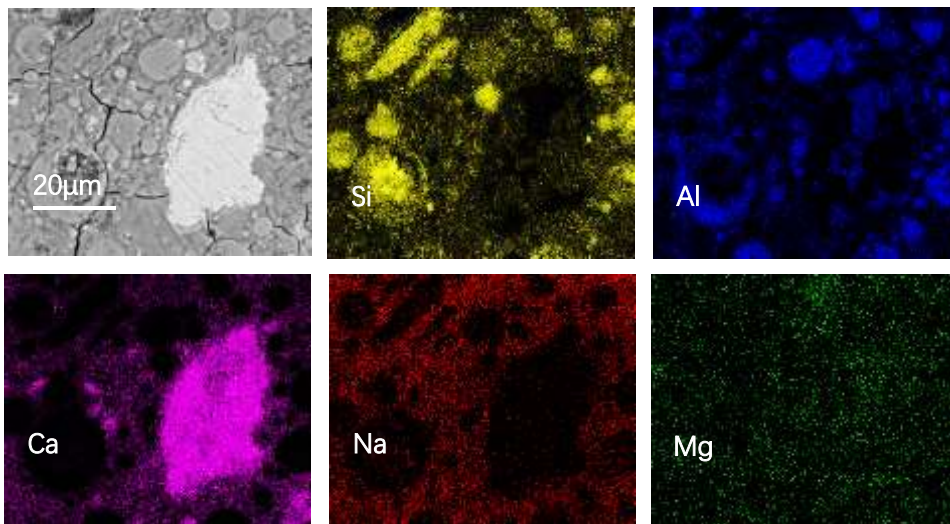
Figure 4-11. BSEM images of HACs with diverse precursors on 7 days of curing

The EDX analyses show that the chemical composition of the gel product in HACS is similar to that of the product in HACSF except for a relatively lower concentration of Al. The main gelation product could be C-S-H and C-(A)-S-H gel. However, the elemental composition for HACF is significantly different from that of the two

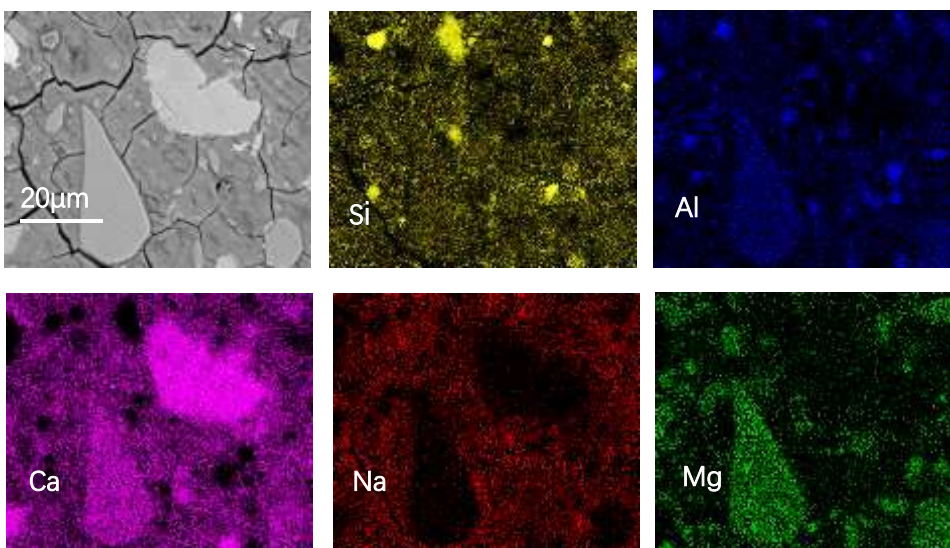
previous systems, which is richer in Na and Al but poorer in Ca. This could be N-A-S-H gel or (N, C)-A-S-H gel (Donatello et al. 2014b). Table 6 presents the hydration product of HACF, showing the lowest Ca/Si (point 4) due to the low Ca content in the raw materials. The elemental atomic ratios of HACSF (point 5) are akin to the HACS (point 3) except for a lower Na/Si. In the BSEM images, neither HAC systems shows the extremely obvious inner product ring around the unreacted grains, indicating that the main process of product formation is through the precipitation of ions from the solution, generally known as ‘through solution’ precipitation (Gruskovnjak et al. 2006). Electron-mapping under EDX was performed on the 7-day hydrated HACs with various precursors to further analyze the elemental composition and hydration degree (see Figure 4-12). The visual degree of diffusion of Na into the unreacted grains and the dissociation of Ca into the outer matrix can be observed in electron maps. The distribution of Na for different HAC systems do not show a significant difference. In terms of Ca ions, the abundance of Ca in the matrix means adequate dissociation of grains into the pore solution, suggesting the improved hydration degree due to the creation of plenty of nucleation sites (Hubler et al. 2011), as HACS and HACSF systems. However, the matrix of HACF shows less Ca which results in a reduced degree of hydration.



(a) HACs



(b) HACF



(c) HACSF

Figure 4-12. Elemental distribution mapping of 7-day cured HACs with various

precursors.

#### 4. 4 Conclusions

HACs have much more complex hydration mechanisms compared to normal Portland cement. Through this study the following conclusions can be drawn:

- Setting times of HACs decrease with the increment of Na<sub>2</sub>O content. The HACS that contains 75% slag, 25% OPC and 5% activator shows the shortest initial setting time. The inclusion of fly ash could delay setting time slightly but will significantly reduce compressive strength. Increasing Na<sub>2</sub>O content leads to increased compressive strength at all testing ages.
- HACs have short induction but long acceleration periods. The increment of Na<sub>2</sub>O content leads to the delayed onset of acceleration and increased cumulative heat. The HACF, which is HAC with fly ash, is found to have the lowest acceleration and total heat.
- Increasing Na<sub>2</sub>O content could improve the reaction degree of HACs and the dense of microstructure. HACF exhibits the minimum reaction extent and a relatively porous microstructure with a large amount of unreacted fly ash grains. The HACS and HACSF systems show a similar degree of reaction. Portlandite and ettringite are not detectable in all of the HAC samples.
- The early gels of HACS are mainly C-S-H and C-(A)-S-H, and the gelation component proportion varies with the alkali content, while the early gel composition for HACF is principally C-(A)-S-H and N-A-S-H. When fly ash and slag are blended in HAC, the gels are C-S-H, C-(A)-S-H and N-A-S-H. According to deconvolution results of <sup>29</sup>Si NMR spectra, the increased alkali content results in a more polymerization and crosslinking in the C-(A)-S-H gel in HACs. When fly ash and slag are both applied in HAC, the formed gels seem to have an increased degree of polymerization.

## **CHAPTER 5: HYDRATION CONTROL-THE RETARDING MECHANISM OF GYPSUM FOR HACs**

*Note: this chapter is based on the manuscript entitled “Early hydration kinetic and microstructure development of HAC at room temperature”, by Lili Xue, Zuhua Zhang, Hongfei Liu, Yuanhai Jiang and Hao Wang, submitted for publication in **Construction and Building Materials**,2022.*

### **5.1 Introduction**

HACs combine the advantages of alkali activated materials and Portland cement and exhibit excellent mechanical properties and durability (García-Lodeiro et al. 2013c; Xue et al. 2021; Donatello et al. 2014a). However, HAC with high alkali content has been handicapped by several difficulties: such as setting rapidly, especially when activated by water glass, which is unfavorable to construction, while the commercial retarder for Portland cement does not present an obvious retarding effect on HACs (Li et al. 2019). Therefore, developing a novel method of HAC retarding is vital to facilitate its application. It is well known that gypsum is used as retarder in Portland cement production. The mechanism is that calcium sulfate reacts with tricalcium aluminate ( $C_3A$ ) (which is the cause of rapid setting) to form ettringite (AFt), which covers the surface of  $C_3A$ , thus preventing the hydration reaction and delaying the setting time of Portland cement (Jelenic et al. 1977; Tang and Gartner 1988). Some industrial by-product gypsums, such as flue gas desulfurization gypsum has been reported and these could be used for prolonging the setting of slag cement (Shi and Liu 2008). Using the industrial by-product gypsum to delay the setting will further reduce the carbon footprint of HACs and this can be considered to be a sustainable approach.

The retarder mechanism of cementitious materials is generally illuminated as follows: complexes formed due to retarder hinder the process of crystal nucleation and growth, or the formation of products such as ettringite covers the surface of unreacted particles and thus prevents the reaction (Li et al. 2018; Guo et al. 2019). In terms of alkali

activated materials, barium chloride was reported to be used to lengthen the setting time of alkali activated slag cementitious materials. It is attributed to the formation of a relatively dense layer on the surface of slag grain derived from the reaction between barium chloride and water glass, which hinders the reaction (Dan et al. 2014). The malic acid and calcium hydroxide show a good retarding effect on alkali activated slag cement with water glass activated (Yu et al. 2005; Brough et al. 2000). The retarding research of HAC and the effect of gypsum on the setting of HAC have been rarely investigated. It can be assumed that ettringite or AFm generated due to the reaction between gypsum and Portland cement clinker in HAC, then covering the surface of the slag particles, which leads to the reaction slowing down.

In this chapter, an industrial by-product gypsum was used as retarder of slag based HAC (75% slag +25% Portland cement +5% water glass) in various proportions. The effect of gypsum on setting time, hydration products and microstructure evolution of HAC were investigated via isothermal calorimetric analysis, XRD, TG analysis and SEM-EDS analysis and the retarding mechanism of gypsum on HACs was revealed.

## 5.2 Materials and methods

### 5.2.1 Materials

The main starting materials used in this study were P II 52.5 (according to Chinese standard GB175-2007) Portland cement (OPC) and grade S95 (according to Chinese standard GB/T 18046-2017) ground blast furnace slag (GBFS). The specific surface area of the slag is 448 m<sup>2</sup>/kg, and its specific gravity is 2.91. The chemical compositions of OPC and GBFS were determined by X-ray fluorescence (XRF), and the results are given in Table 5-1. The X-ray Diffraction (XRD) analysis of raw materials is shown in Figure 5-1.

Table 5-1. Chemical composition of Portland cement and GBFS (wt.%)

Type	SiO <sub>2</sub>	Al <sub>2</sub> O <sub>3</sub>	Fe <sub>2</sub> O <sub>3</sub>	CaO	MgO	SO <sub>3</sub>	K <sub>2</sub> O	TiO <sub>2</sub>	Na <sub>2</sub> O	MnO	P <sub>2</sub> O <sub>5</sub>	Σ	LOI
Cement	20.99	5.36	3.81	61.36	1.38	2.4	0.65	0.27	0.13	0.1	0.14	96.59	2.71
GBFS	31.43	15.22	0.71	37.79	9.62	1.2	0.43	0.67	0.52	0.312	0.02	98.02	-0.76

The alkali activator with a modulus of 1.5 and solid content of 30% was prepared by

water glass with a modulus of 2.33 and solid sodium hydroxide. The poly-carboxylic acid superplasticizer (SP) with a water-reducing rate of 35% was used.

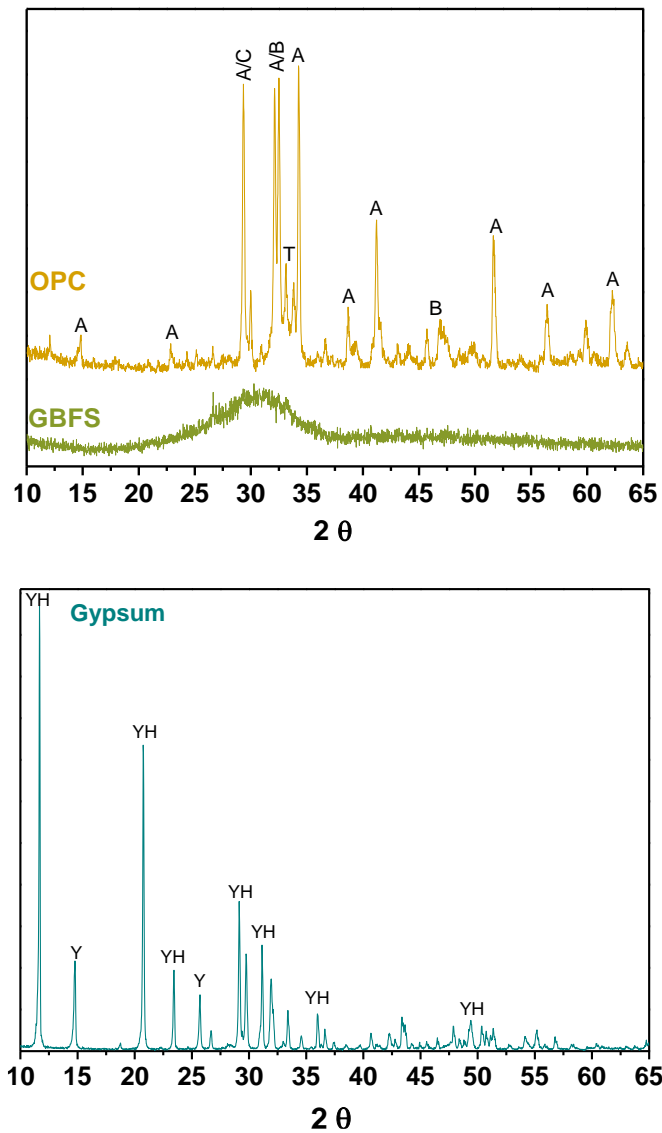


Figure 5-1. XRD patterns of OPC, GBFS and Gypsum. A: Alite; B: Belite; C: Calcite; T: Tricalcium aluminate; YH:  $\text{CaSO}_4 \cdot 2\text{H}_2\text{O}$ ; Y:  $\text{CaSO}_4$ .

## 5.2.2 Mixture proportions and specimen preparation

### *Mixture proportions*

The composition of cementitious materials is presented in Table 5-2, including OPC and HACs with and without gypsum. The control system was 100% OPC hydrated with water and HAC without gypsum.

Table 5-2. Proportions of HAC systems (wt.%)

Group	Cement	Slag	Gypsum	Na <sub>2</sub> O (%)	W/C	Alkali activator	SP (%)
OPC	100	0	0	0	0.27	0	0
HAC	25	75	0	5	0.32	42.6	0.5
HAC5	25	75	5	5	0.33	42.6	0.5
HAC10	25	75	10	5	0.39	42.6	0.5
HAC15	25	75	15	5	0.43	42.6	0.5
HAC20	25	75	20	5	0.45	42.6	0.5
HAC25	25	75	25	5	0.40	42.6	0.5
HAC30	25	75	30	5	0.41	42.6	0.5
HAC35	25	75	35	5	0.42	42.6	0.5

*Specimen preparation*

Hydration of test pastes at different ages was terminated with ethanol and then broken into small pieces. The 5-8 mm pieces were selected and vacuum dried for SEM-EDS analysis. The pieces less than 5mm were vacuum dried and ground into powder for XRD and TGA testing.

**5.2.3 Experimental methods**

*Setting time*

Pastes with normal consistency were prepared. The initial and final setting times were tested using a Vicat apparatus in accordance with Chinese standard GBT 1346-2011< Test methods for water requirement of normal consistency, setting time and soundness of the Portland cement >.

*Early hydration heat*

The early hydration heat of the binders was conducted via isothermal conduction calorimetry on a TAM Air Calorimeter at 20±0.5 °C. In order to eliminate interference, the superplasticizer was excluded. Sample components for each group about 5 grams were stirred using a hand-mixer and poured into an ampoule bottle quickly, then placed into the calorimeter. The measurement ended after 72 hours.

*XRD analysis*

XRD patterns of powdered samples were obtained on a 60-KV, 80-mA XRD-7000 diffractometer with Ceramic X-ray tube and Cu target. The scan speed is 2.5°/min, with  $2\theta$  in the 5 - 80° range.

#### *Thermogravimetric (TG) analysis*

TG analysis of the samples was carried out under N<sub>2</sub>-atmosphere on a STA-409PC instrument heated from 25 °C to 1000 °C at a heating rate of 10 °C/min.

#### *Scanning electron microscopy and energy dispersive spectroscopy (SEM-EDS) analysis*

The morphology of hydration products for OPC and HACs were recorded on a Zeiss Sigma 300 with an accelerating voltage of 15 kV. The spot scan and elemental analysis were performed on a Zeiss Smart EDX Energy Disperse Spectroscopy.

## **5.3 Results and discussion**

### **5.3.1 Setting time**

The setting time of OPC and HACs are given in Figure 5-2. It is observed that the setting time of OPC is much longer than that of HACs. In HAC systems, the setting times are prolonged with the addition and increment of gypsum. The setting time of HAC incorporating 20% gypsum achieves a maximum, with 89 min initial setting and 185 min final setting. However, both the initial and final setting time of HACs with more than 20% gypsum begin to decrease. The reason for the prolonged setting time may be that the ettringite (AFt) formed due to gypsum precipitates the surface of the unreacted particles and prevents the reaction. In terms of the decrease in setting time, it can be assumed that the massive formation of ettringite inside the layer and then breaks the coating, thus the unreacted particles begin to be exposed to the solution and react again, resulting in a shortened setting time. It is also possible that a substantial amount of ettringite is formed in the matrix and cross-linked with C-S-H, which leads to the decreased setting. Another possibility for accelerated setting of HACs is that the formation amount of ettringite changes or some new product generates as the increase of gypsum. For instance, SO<sub>4</sub><sup>2-</sup> ions from gypsum have been reported to hasten the

early hydration of alite, which would generate more  $\text{Ca}(\text{OH})_2$  and then improve the solution PH of HACs (Donatello et al. 2013a), whilst the AFt could keep stable only in the PH range of 10.5-13.4 (Shimada and Young 2004; Damidot and Glasser 1993), so the excess gypsum limits the formation of AFt, resulting in a shortened setting time again. On the other hand, the gypsum may cause changes in the ion dissolution rate, thus prolonging or shortening the setting time of hybrid alkaline cement. Hence the veritable mechanism that gypsum influences the setting of HACs needs to be determined via the following calorimetric analysis and microscopic analysis such as XRD, TG and SEM-EDS analyses. Based on the setting time results, the OPC, HAC, HAC10, HAC20, HAC30 pastes were selected for further microscopic analysis.

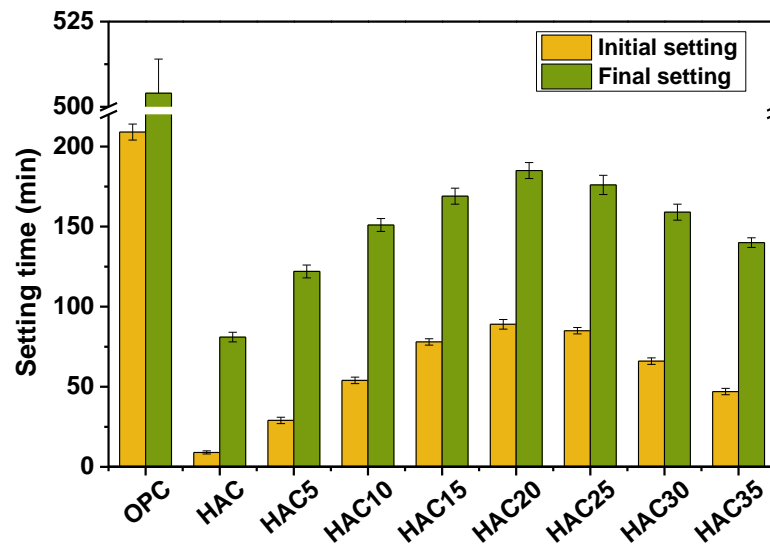


Figure 5-2. Initial setting time and final setting time of OPC and HACs.

### 5.3.2 Hydration heat characterization

The calorimetric curves for HACs with and without gypsum are shown in Figure 5-3. All heat flow curves include two exothermic peaks, one sharp exothermic peak appears for a very short time at first, another main acceleration peak appears later for a long time. The two peaks are attributed to rapid dissolution of raw materials and formation of hydration products respectively (Angulo-Ramírez et al. 2017; García-Lodeiro et al. 2013b). In the enlarged version of sharp exothermic peak of heat flow curves, it can be seen that the incorporation of gypsum decreases the heat release rate of HACs, and the HAC20 shows the lowest exothermic rate. This is consistent with the trend of

setting time, which can explain the effect of gypsum on the setting of HAC. However, the acceleration peaks of HAC with gypsum appear earlier than those without gypsum, and the acceleration peak of HAC20 appears earliest. The formation of hydration products can be impeded by the reduction of CaO content in the system caused by high alkali content (Yang 2018; Yuan 1996; Taylor 1997). It can be inferred that the incorporation of gypsum alters the alkali content of the HAC system and thus affects the setting time. Further to the total heat curves, the HACs with gypsum released more heat at first, but the final cumulative heat of HACs was lower than that of HAC without gypsum after 6 hours. It was reported that the total cumulative heat could be an indicator of the amount of hydration products because the heat of hydration was generated from the formation of hydration products, and thus the total heat of hydration could be used to reflect the hydration degree (Li et al. 2018; Scrivener et al. 2015). Therefore, it can be deduced from the cumulative heat curve that the introduction of gypsum reduced the production of HAC, and HAC 20 is the least productive. The hydration products and microstructure of HAC with and without gypsum need to be investigated to further explore the retarding mechanism.

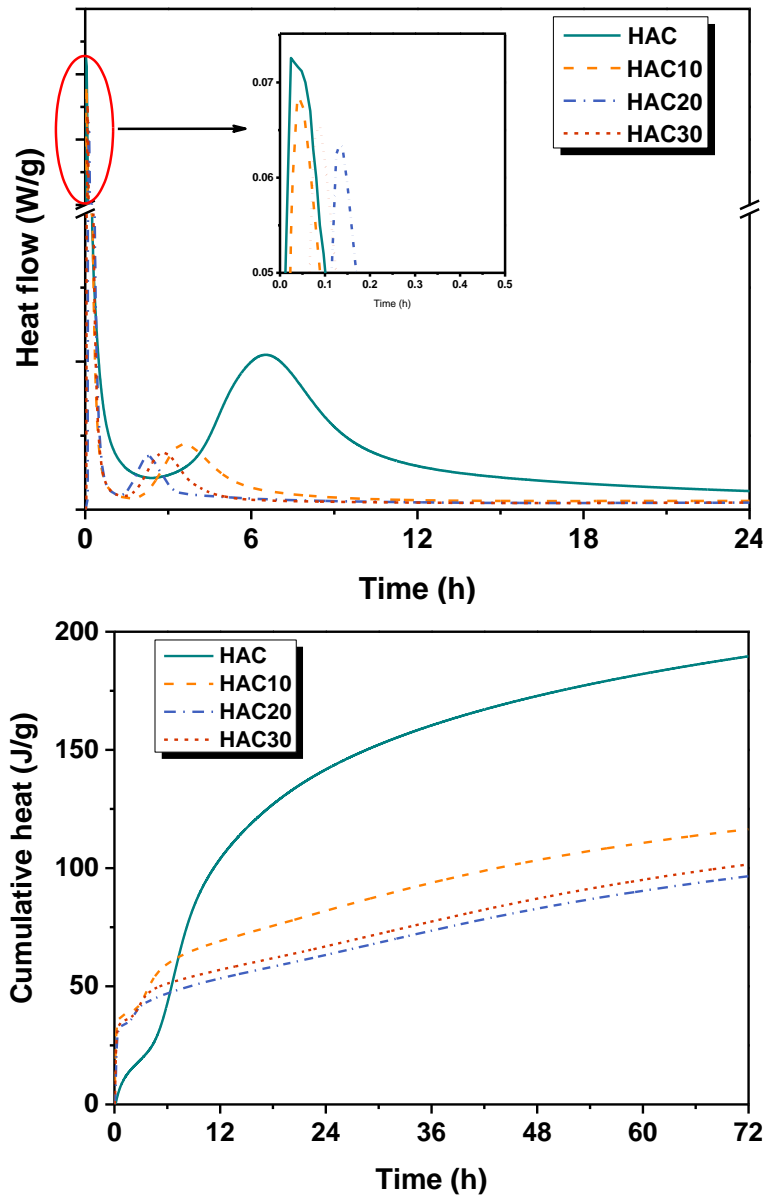


Figure 5-3. Heat flow and cumulative heat of HACs with and without Gypsum

On the ground of calorimetric profiles, initial setting times and 24 hours were chosen as the OPC and HACs sample ages for XRD, TG and SEM-EDS analyses.

### 5.3.3 XRD analyses of hydration products

Figure 5-4 depicts the XRD patterns of OPC and HACs incorporating 0-30% gypsum. The diffraction patterns for these pastes at initial setting time are shown in Figure 5-4 (a). The main crystal phases found in OPC were alite and belite, together with small amounts of calcite, ettringite, gypsum, Portlandite and CSH. The few hydration products indicated that the hydration rate of OPC was slow during the initial setting time, which led to long initial setting time. In terms of HAC systems, the unreacted

gypsum was also the main phase in addition to alite and belite. However, signals associated with Portlandite and ettringite precipitation were weak or unobservable, especially in HAC and HAC20, results that were in accord with previous research (Angulo-Ramírez et al. 2017; Elahi et al. 2012). It is considered that the stability of ettringite depends on the system PH which ranges from 10.5 to 13.4 (Donatello et al. 2013a; Shimada and Young 2004; Damidot and Glasser 1993). Some less crystalline phases that are not easily detected via XRD may be formed beyond this range, such as Phase U, monosulfate and thaumasite. In this study, the alkali content (5% Na<sub>2</sub>O) of the HAC systems was high. Meanwhile, the monosulphoaluminate and thaumasite are present in HACs with gypsum. Therefore, the ettringite is deemed to be converted into other forms. In addition, gismondine and strätlingite were detected in HACs with gypsum. The increasing gypsum in HACs results in increased generation of thaumasite, monosulphoaluminate and strätlingite. As for gismondine, the maximum amount is obtained when the gypsum dosage is 20%. Peaks associated with C-S-H become more intense with the increase of gypsum, which is likely to indicate an increased amount of C-S-H.

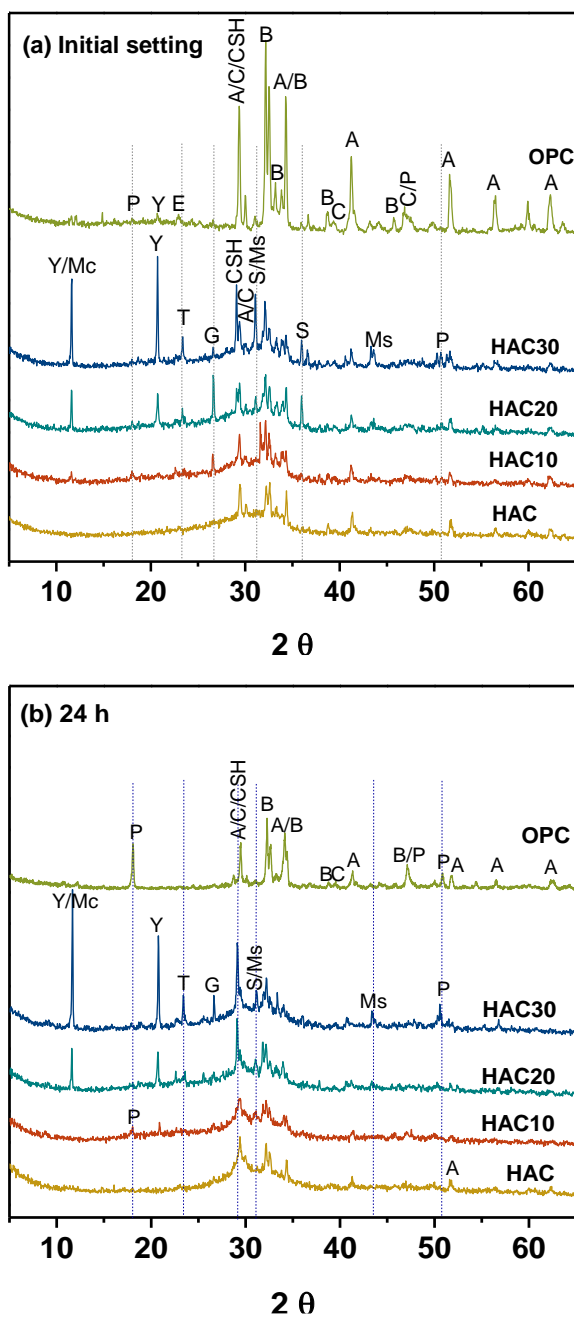


Figure 5-4. XRD spectra of OPC and HACs with and without Gypsum for initial setting and 24 h curing. A: Alite; B: Belite; C: Calcite; CSH: Calcium Silicate Hydrate; E: Ettringite; G: Gismondine ( $\text{CaAl}_2\text{Si}_2\text{O}_8(\text{H}_2\text{O})_4$ ); P: Portlandite; T: Thaumasite ( $\text{Ca}_3\text{Si}(\text{OH})_6(\text{CO}_3)(\text{SO}_4)(\text{H}_2\text{O})_{26}$ ); S: Strätlingite ( $\text{Ca}_2\text{Al}((\text{AlSi})_{1.11}\text{O}_2)(\text{OH})_{12}(\text{H}_2\text{O})_{2.25}$ ); Y: Gypsum; Ms: Monosulphoaluminate ( $\text{Ca}_4\text{Al}_2(\text{OH})_{12}(\text{SO}_4)(\text{H}_2\text{O})_6$ ); Mc: Monocarbonate.

The 24 h XRD patterns for OPC and HAC system were revealed in Figure 5-4 (b). Compared with the initial setting period paste, the main distinction of OPC

diffraction pattern is the increased Portlandite and decreased alite and belite. The C-S-H phase is difficult to detect due to its amorphous and overlapped peak with calcite and alite, which needs to be confirmed by TG analysis. There is still unreacted gypsum and cement mineral composition in the HAC system after 24 h hydration. The peak intensity of Portlandite in HACs is the same as that of the initial setting time. The ettringite is still absent, replaced by thaumasite and monosulphoaluminate. The intensity of the signals generated by thaumasite, monosulphoaluminate and gismondine reach the maximum in HACs incorporating 30% gypsum. The halos appeared at 25-40° 2θ on the spectra for HACs are normally due to the precipitation of amorphous products (García-Lodeiro et al. 2013b).

According to the results of XRD analysis, crystalline phases such as thaumasite, gismondine and monosulfate were formed rather than ettringite when gypsum was added into HACs. The reason could be that the changes of PH value in the matrix cause instability of ettringite (Donatello et al. 2013a). Combining the assumptions mentioned in section 3.1, the mechanism by which gypsum influences the setting of HACs may be the formation of crystalline products covering the surface of unreacted particles and thus delaying the setting of HACs. When the dosage of gypsum was more than 20%, more crystalline products were cross-linked with the gel and formed a condensed structure or the large amount of products formed inside the coating and broke it, accelerating the setting of HACs. The amount of gel production which was difficult to detect via XRD needs to be further determined via TG and DTG analysis. In addition, some phase diffraction peaks overlapped, TG analysis should be combined to determine the type and quantity of phases, such as gypsum and monocarbonate, strätlingite and monosulfate, and so on.

#### **5.3.4 TG analysis of hydration products**

Figure 5-5 depicts the thermogravimetric (TG) and derivative thermogravimetric (DTG) analysis of the HACs pastes at their initial setting time. The mass loss of OPC from 25°C to 1000 °C is nearly 4%, which is less than HACs with a total mass loss of about 6%-11% (Figure 5-5a). The incorporation of gypsum increases the mass loss of

HACs. It can be observed that all samples show a quick decline of weight between 110 °C and 130 °C, which is mainly attributed to evaporation of free water in reaction products or hydration products (Kong and Sanjayan 2010). Then these binders exhibit a gentle mass loss until 650 °C. In the HAC system, there is a second rapid decline of weight around 900 °C.

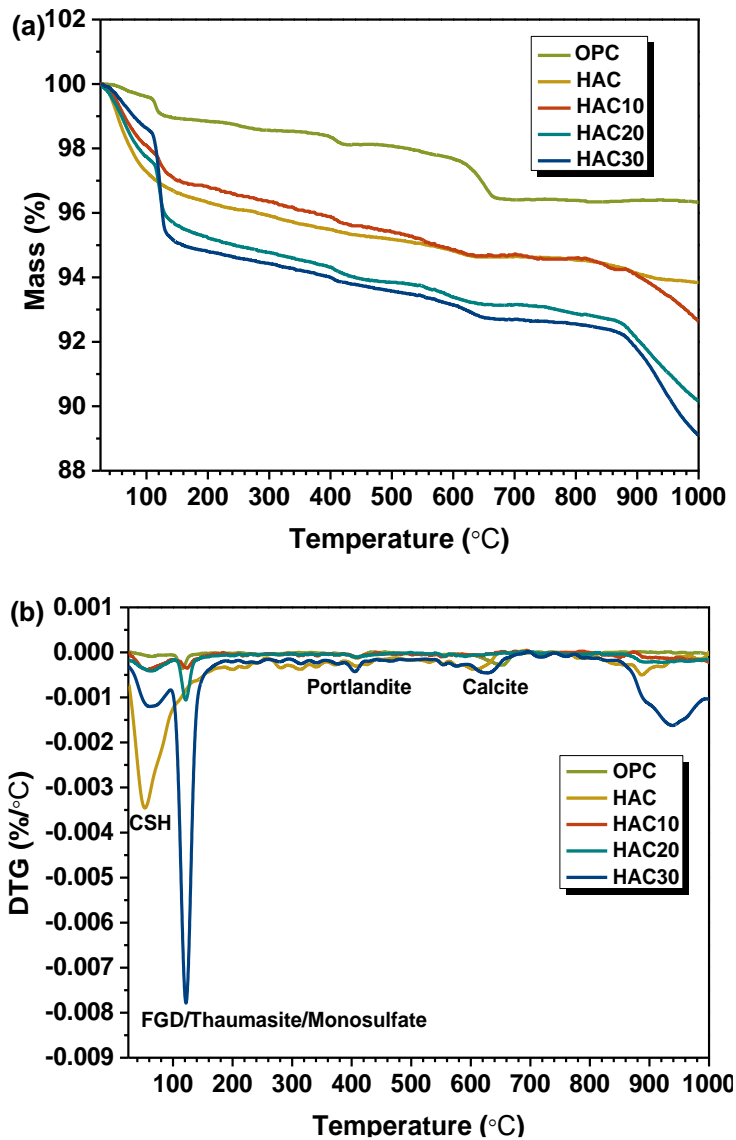


Figure 5-5. TG and DTG analysis of hydrated OPC and HACs pastes at initial setting time (a)TG and (b)DTG.

Figure 5-5b reveals the DTG analysis of OPC and HACs pastes at initial setting time. Three distinct endothermic peaks are found in the OPC curve. The first peak located about 110 °C is due to the removal of bound water within ettringite or gypsum

(Alahrache et al. 2016). The peak around 400 °C is attributed to the decomposition of Portlandite (Alarcon-Ruiz et al. 2005). The third peak, which appears at 650 °C, can be related to the calcite decomposition (Kaja et al. 2018). The HAC system displays another two characteristic endothermic peaks at approximately 60 °C and higher than 850 °C in addition to the three peaks mentioned above. It is reported that the C-S-H phases would lose water from 50 °C to 400 °C (Kaja et al. 2018; García-Lodeiro et al. 2011), so the peak located around 60 °C indicates the generation of C-S-H gel in HACs at a very early age. In addition, the C-S-H gel in HAC is more than HACs with gypsum. This implies that the gypsum delayed the generation of gel, resulting in longer initial setting. The mass loss peak which appears beyond 850 °C is attributed to other structure forms of carbonates and release of CO<sub>2</sub> (Angulo-Ramírez et al. 2017; Deschner et al. 2012). It is worth discussing the exothermic peak around 125 °C on DTG curves of HACs with gypsum, which is normally due to the water loss of ettringite or gypsum or gel. However, the ettringite phase is not detected in XRD patterns, instead of other forms of AFt phases, such as thaumasite and monosulfate. Moreover, the thaumasite which possess a structure similar to ettringite usually loses water at around 130 °C (Scrivener et al. 2016), and the monosulfate may lose water at around 120°C (Scrivener et al. 2016; Durdzinski 2016), whereas the monocarbonate does not lose water until about 125 °C. Therefore, the exothermic peak of 125 °C located on the DTG curves of HACs with FGD could be an indication of the gypsum, thaumasite and monosulfate, and the monocarbonate could be excluded (Gruskovnjak et al. 2008). Increasing the gypsum leads to increased generation of thaumasite and monosulfate, which is consistent with the results of XRD analysis. The results of TG and DTG analysis for OPC and HACs after 24 hours curing are shown in Figure 5-6.

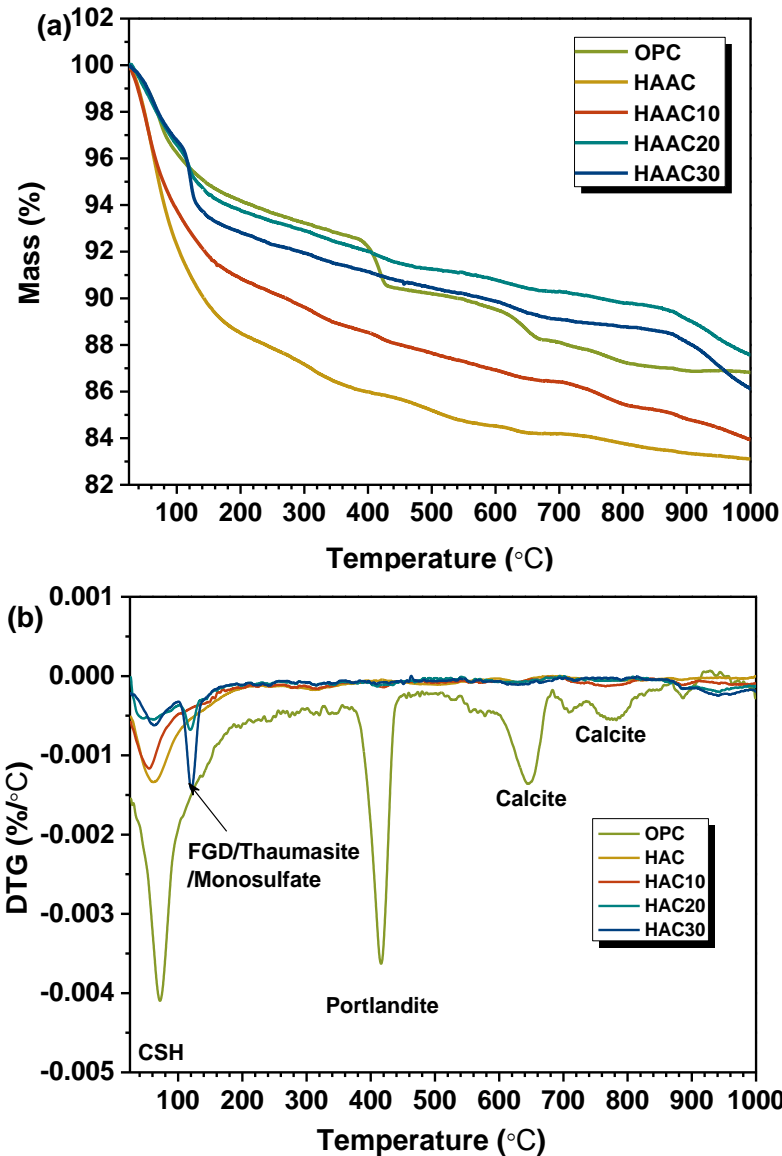


Figure 5-6. TG and DTG analysis of hydrated OPC and HACs paste after 24 h, (a)TG and (b)DTG.

The total weight loss of OPC is slightly higher than that of HACs except for HAC20 (Figure 5-6a). The abrupt decline of mass between 110 °C and 130 °C is also noted on the TG curves of OPC and HACs. Beyond 200 °C, the HACs show slight mass loss until 850 °C, while OPC displays several notable mass declines on TG curves. The finding suggests that OPC generates more hydration products after 24 h curing. In DTG graphs (see Figure 5-6b), there are six obvious peaks in the OPC curve which are associated with the dehydration or decomposition of C-S-H, portlandite and calcite respectively. Compared with the DTG analysis at initial time, the exothermic peaks on

the OPC curves are more distinct, indicating more generation of products, whereas the peak related to ettringite is imperceptibly like an XRD analysis. The characteristic exothermic peak due to C-S-H around 60 °C is still found in the HAC system, but the peak intensity is less than that of OPC. As can be seen in the DTG curves, the HACs with gypsum presents a weaker peak of C-S-H than HAC, which indicates a smaller amount of gel. Only HAC20 and HAC30 show an exothermic peak at 120 °C which indicates the presence of thaumasite and monosulfate, and that the HAC30 exhibits more of these products than HAC20. These results are in line with XRD analysis. The microstructure and products composition for HACs should be confirmed by SEM-EDS to further determine the retarding mechanism of gypsum, and the dissolution rate of ions such as Ca, Si, Al and so on also needs to be investigated.

### **5.3.5 SEM-EDX analyses of hydration products**

SEM-EDX was performed to study the microstructure evolution and products composition of OPC and HACs at different curing stages. Figure 5-7 shows the micromorphology of OPC and HACs in the initial setting time. It can be seen that very little product gel is generated in OPC, and the unreacted cement particles are bonded into a loose structure by the small amount of gel. However, more gels were produced in the initial setting time of HACs, resulting in a relatively small microstructure, especially HAC. When gypsum is added into hybrid alkaline cement, the hydration products are obviously reduced and the microstructure is relatively loose. It is worth noting that the hydration products in HACs with 20% gypsum are few and the microstructure is also loose. According to the previous hypothesis of coverage theory, the HAC20 should have more hydration products covering the surface in comparison to HAC10 and HAC30. Nonetheless, there are also fewer gel products on the surface of unreacted particles. Therefore, the coverage theory is not likely to be valid, pending further analysis.

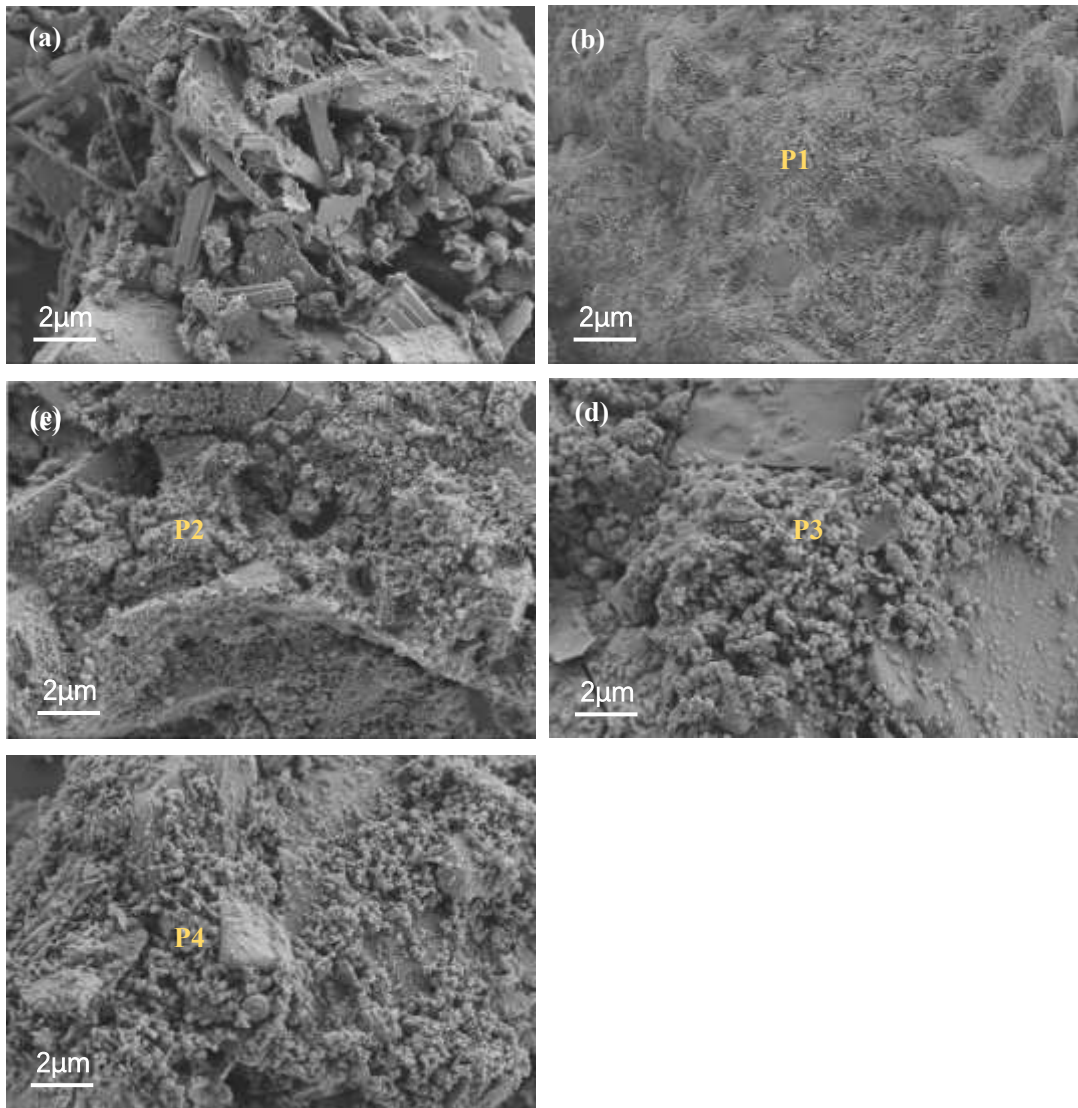


Figure 5-7. SEM images of OPC and HACs pastes at initial setting (a)OPC, (b)HAC, (c)HAC10, (d)HAC20, (e)HAC30.

The micromorphology of OPC and HACs after hydration for 24 hours is shown in Figure 5-8. The hydration products of OPC such as  $\text{Ca(OH)}_2$  and C-S-H gels are cross-linked with each other to form a microstructure and the unreacted particles are almost invisible. The HAC systems also exhibit more hydration products than that of the initial time. The microstructure of HAC without gypsum is so dense that raw materials particles are not visible. The incorporation of gypsum also leads to a loose and porous structure as in the initial setting state. The microstructure of HAC20 is looser and the gel particles are larger than those in HAC10 and HAC30. This is consistent with the result of SEM analysis of HACs at initial setting time.

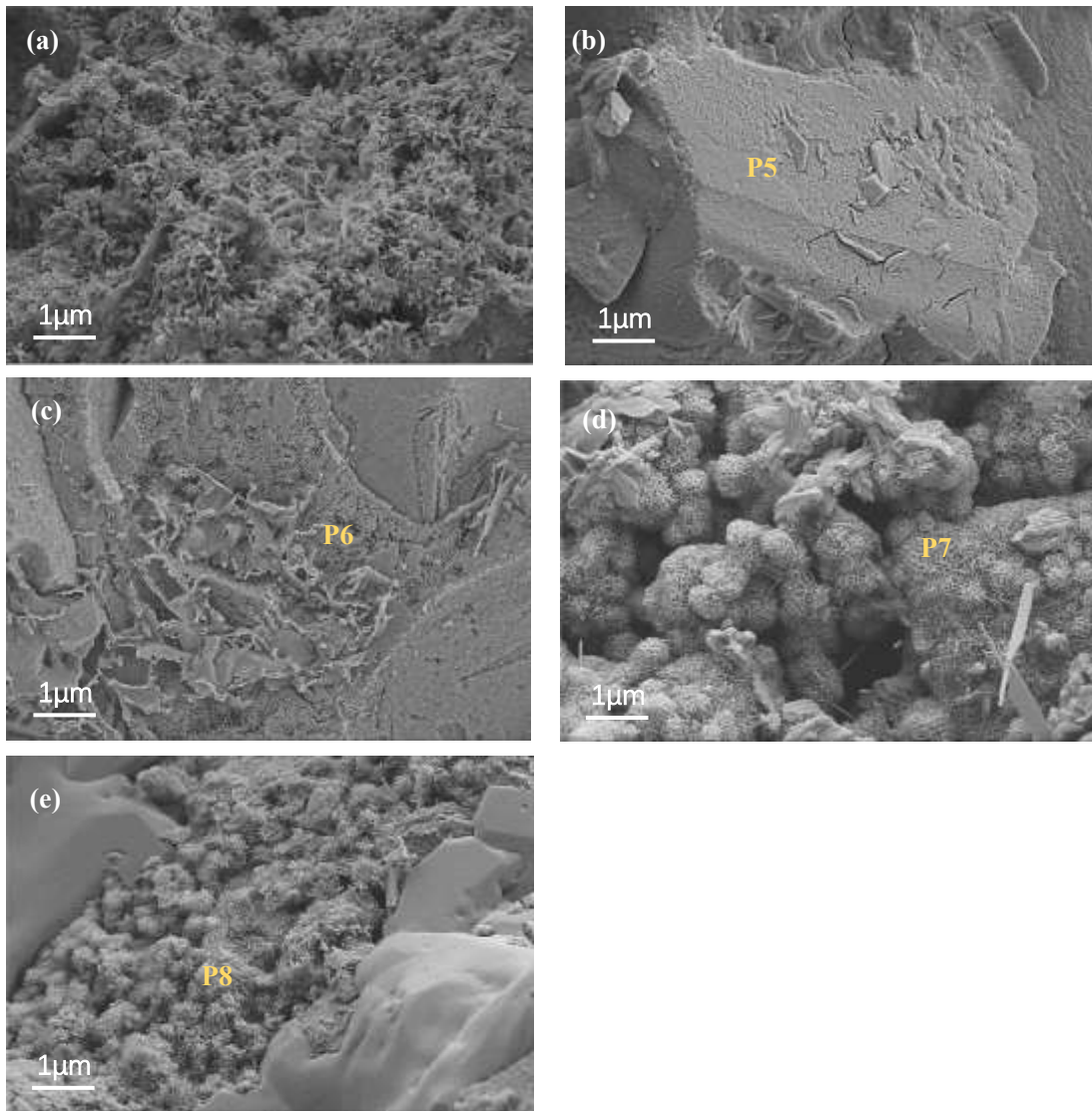


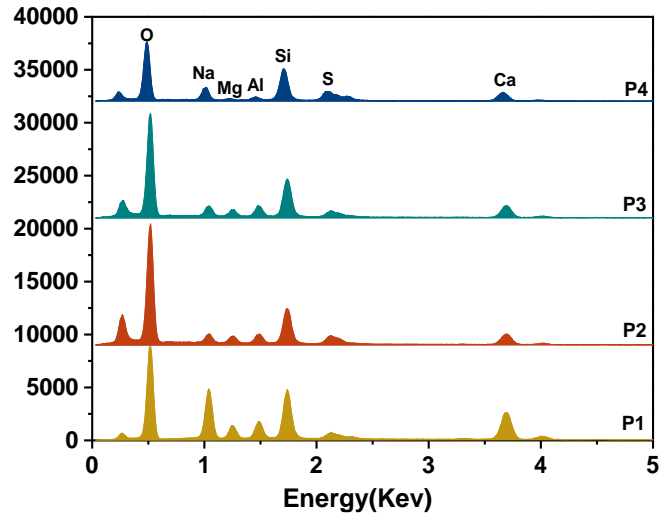
Figure 5-8. SEM micrographs of OPC and HACs pastes for 24 hours curing (a)OPC, (b)HAC, (c)HAC10, (d)HAC20, (e)HAC30

As can be seen from SEM micrographs, the distinction of microstructure and hydration products between OPC and HACs is obvious. It is evident that gypsum alters the microstructure of HAC. A comparison of Figure 5-8(b) and Figure 5-8(c) shows that the intervention of gypsum leads to the loosening of the compact microstructure of the HAC, and the original dense contours are dimly visible except for some unreacted particles. Increasing gypsum causes fewer reaction products and more porous structure. However, no coating layer is observed on the surface of the unreacted grains of HACs with gypsum at the two study stages. Therefore, the preceding assumption that the gypsum caused ettringite or other products to cover the surface of unreacted particles

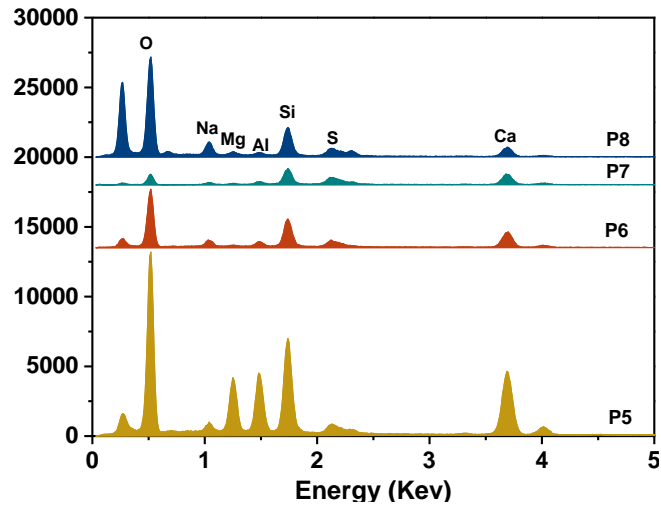
and thus delay the setting time is untenable. The amount and size of hydration products could be the main cause for the variation of HACs setting time, while the reason for the changes of hydration products is usually considered to be the changes of ions' dissolution rate.

The SEM-EDS was employed to explore the distribution of elements of HACs with and without gypsum. Figure 5-9 depicts the EDS results in the matrix of HACs. It can be seen that the Ca in HAC is more than that in HAC with gypsum at the initial setting time and 24 hours curing. The more Ca in HAC matrix indicates that more Ca ions are dissolved from the raw material particles, which leads to more hydration products and denser microstructure and thus results in rapid setting.

In terms of HACs with gypsum, the Ca and Si concentrations in HACs that are provided by the slag and OPC decrease with the increase of gypsum, indicating that the initial dissolution of the slag and cement particles were delayed (Gebregziabiher et al. 2015). Moreover, the distribution of Na element in the matrix shows significant differences. The HAC20 matrix has the lowest Na cation at initial setting time and 24 hours curing, and the Na cations in the solution are related to the alkali dosage which could accelerate the rate of hydration (Donatello et al. 2013a). This can explain why HAC with 20% gypsum shows the longest setting time. The reduced Na element may be attributed to the reaction with  $\text{SO}_4^{2-}$  in gypsum to generate  $\text{Na}_2\text{SO}_4$ .



(a) Initial setting time



(b) 24 hours

Figure 5-9. Element distribution in matrix of HACs.

### 5.3.6 Retarding mechanism

Based on the analysis results in the previous section, the retardation mechanism of gypsum for HAC can be inferred and discussed as follows. On the one hand, Na ions from the activator are consumed by reacting with  $\text{SO}_4^{2-}$  provided by gypsum to generate  $\text{Na}_2\text{SO}_4$ , which reduces the basicity of the HAC system and thus delays the hydration reaction of HAC (Ríos et al. 2020; Jia et al. 2018). On the other hand, the dissolution rate of cations such as Ca and Al provided by the slag and Portland cement is slowed down due to the gypsum. And the SEM results show that the unreacted particles are not covered with dense products, indicating that the formation of hydration products is controlled by nucleation rather than diffusion. Hence having

fewer Ca cations in the matrix of HACs with gypsum leads to a decrease in nucleation sites, resulting in a reduction of hydration products and ultimately delayed setting time. As for the effect of gypsum dosage on setting time of HACs, it can be interpreted as follows. When the gypsum content in the HAC system is less than 20%, the dissolution rate of Ca cation from the raw material slows down with the increase of gypsum production. Meanwhile, the Na cation in the alkali activator decreases due to the reaction with  $\text{SO}_4^{2-}$  from gypsum, which reduces the reaction rate of the HAC system and then leads to the decrease of gel quantity, resulting in prolongation of setting time. Therefore, HAC incorporating 20% gypsum shows the longest setting time. As  $\text{SO}_4^{2-}$  in gypsum gradually participates in the formation reaction of thaumasite and monosulphate, Na ions in the solution are no longer consumed, and the Ca cation dissolution rate is accelerated simultaneously with the decrease in the concentration of Ca in the solution caused by the consumption of Ca in the crystal formation reaction, so the reaction starts to accelerate again in HAC with more than 20% gypsum. On the other hand, more crystal products generated in HAC incorporating gypsum are cross-linked with the gel to form a dense structure, which ultimately leads to a shorter setting time.

## 5.4 Conclusions

This study aims to explore the retarding mechanism of gypsum on the setting of HACs. Based on the results presented, the following main conclusions can be drawn:

- The gypsum could prolong the initial and final setting times of HACs. Increasing the dosage of gypsum results in a longer setting time of HACs, and both initial and final setting time reach the maximum value when the gypsum content is 20%. The calorimetric analysis indicates that the incorporation of gypsum leads to the decrease of reaction rate and reaction products of HAC, and changes the basicity of the system.
- No ettringite was formed when gypsum was mixed with HAC. Instead, products such as thaumasite, monosulphate and gismondine were detected, presumably because the higher alkali content in HACs is not suitable for ettringite.

- The HACs with gypsum exhibits a relative loose microstructure due to the reduction in the number of cations in the matrix and HAC with 20% gypsum shows the loosest microstructure. The SEM-EDS analysis confirmed that the retarding mechanism of gypsum on HACs is the decreased ions dissolution rate rather than coverage theory.
- The retardation mechanism of gypsum on hybrid cement can be attributed to two aspects: the basicity of the system is reduced due to the decrease in the concentration of Na ions reacting with  $\text{SO}_4^{2-}$ ; the dissolution rates of Ca and Al ions are decreased, induced by gypsum.

# CHAPTER 6: SHRINKAGE BEHAVIOR OF HAC MORTARS

*Note: this chapter is based on the manuscript entitled “Drying shrinkage behavior of hybrid alkali activated cements (HACs) mortars”, by Lili Xue, Zuhua Zhang, Hongfei Liu, Yuanhai Jiang and Hao Wang, submitted for publication in **Construction and Building Materials**, 2022.*

## 6.1 introduction

HAC can absorb vast industrial by-products and possesses the advantages of alkali activated cementitious materials and Portland cement (García-Lodeiro et al. 2013a; Al-Kutti et al. 2018). It can be used as a transitional material for small-scale projects when the complete use of alkali activated cementitious materials is still in doubt (Palomo et al. 2019). The volume stability of cementitious materials plays a key role in engineering applications. Shrinkage is a vital property affecting the durability of cementitious materials, especially alkali activated cement. Cracks derived from shrinkage could lead to infiltration of water and corrosive liquid and thus destroy the structure ultimately (Bissonnette et al. 1999). So far, there are few reports on the shrinkage properties of hybrid cement. As a novel alkali activated cementitious material, the shrinkage behavior of HAC has not been systematically studied. Janotka et al. (2014) showed that the shrinkage rate of HAC (20-30% Portland cement + 70-80% steel slag +5%Na<sub>2</sub>SO<sub>4</sub>) concrete was lower than that of Portland cement, but the shrinkage mechanism was not clarified. The Palomo team presented a keynote lecture on hybrid alkaline cement at the 15<sup>th</sup> International Conference on Cement Chemistry (ICCC 2019). Relevant data indicated that HAC showed a lower shrinkage value than Portland cement (Martauz et al. 2019; Martauz et al. 2016). However, neither the specific influence mechanism nor the shrinkage mechanism had been studied. These two mechanisms should be studied, together with other factors that influence the shrinkage properties, to facilitate the application of HAC in practical engineering. The shrinkage behavior and control measure of AAM have been well-documented.

AAM shows excessive shrinkage compared to Portland cement. The primary reason is high capillary force caused by the refinement of pore size in the material due to alkali activator (Molo Neto et al. 2008; Collins and Sanjayan 2000). In terms of drying shrinkage, more free water in the AAM exists in the internal pores of the gel rather than combined with hydration products, then loss of this part water leads to obvious drying shrinkage (Singh and Siddique 2014; Mastali et al. 2018). In addition, the main hydration products such as C-A-S-H and N-A-S-H exhibit higher amorphous morphology than C-S-H gels due to the lower Ca/Si ratio, resulting in greater autogenous shrinkage (Tennis and Jennings 2000; Matalakah et al. 2019; Yang 2018). The crystal-gel ratio is also a vital factor. It has been reported that the main hydration products of AAMs were gels, and thus the crystal-gel ratio of AAMs was too low, which makes the gel have a large "free path" of shrinkage in the mesoscopic space, resulting in a large shrinkage (Gu and Fang 2012). Ye et al. (2016) believed that dry shrinkage of alkali activated slag was due to the structural combination of base cations in C-A-S-H, which reduced the superposition law of the C-A-S-H layer, leading to C-A-S-H collapse and redistribution more easily. Research shows that the nature of precursors and activators, relative humidity and curing temperature all have effects on the shrinkage of AAM. Moreover, the hydration products and pore structure are important factors to determine the shrinkage of cementitious materials (Atis et al. 2009; Ye et al. 2017; Jia et al. 2018; Thomas et al. 2017; El-Yamany et al. 2018; Lee et al. 2014; Partha Sarathi Deb et al. 2015). To promote the application in large precast concrete members with high early strength and durability requirements, shrinkage behavior and the mechanism of HAAC composed of AAM and Portland cement need to be explored urgently (Xue et al. 2021).

In this chapter, the drying shrinkage behavior of HACs with different precursors, curing regimes and activator states were investigated, while the drying shrinkage behavior of HACs was compared to Portland cement and alkali activated cement (AAC). XRD, MIP, and SEM-EDS analyses were employed to study the chemical composition, pore structure and microstructure of hydration products. The analysis of

total porosity and pore structure is the key to shrinkage of hybrid alkali activated cement. The focus is to characterize the drying shrinkage behavior of HACs.

## 6.2 Experimental programs

### 2.1. Raw materials

Grade S95 ground blast furnace slag (GBFS) (according to Chinese standard GB/T 18046-2017) with a specific surface area of 448 m<sup>2</sup>/kg and grade I fly ash (FA) (according to Chinese standard GB/T 1596-2017) with specific surface area of 420 m<sup>2</sup>/kg were used in this study. P II 52.5 ordinary Portland cement (OPC) (according to Chinese standard GB 175-2007) was also used. The chemical compositions of these raw materials are shown in Table 6-1, which were determined by X-ray Diffraction (XRD) analysis. The X-ray Diffraction (XRD) patterns of GBFS, FA and OPC are given in Figure 6-1.

Table 6-1 Table 1 Chemical composition of Portland cement, GBFS and FA (wt.%)

Type	SiO <sub>2</sub>	Al <sub>2</sub> O <sub>3</sub>	Fe <sub>2</sub> O <sub>3</sub>	CaO	MgO	SO <sub>3</sub>	K <sub>2</sub> O	TiO <sub>2</sub>	Na <sub>2</sub> O	MnO	P <sub>2</sub> O <sub>5</sub>	Σ	LOI
Cement	20.99	5.36	3.81	61.36	1.38	2.4	0.65	0.27	0.13	0.1	0.14	96.59	2.71
GBFS	31.43	15.22	0.71	37.79	9.62	1.2	0.43	0.67	0.52	0.312	0.02	98.02	0.76
FA	54.78	24.61	5.20	3.16	0.84	0.62	2.22	1.09	0.66	0.067	0.19	93.42	5.96

Liquid activator with a modulus of 1.5 and concentration of 30% was prepared from liquid water glass, reagent sodium hydroxide pellets and water. Powered sodium silicate with a modulus of 2 was used as solid-state activator. To adjust the modulus of the solid activator to 1.5, sodium hydroxide was dissolved in water and then added to the mixture. The poly-carboxylic acid superplasticizer (SP) with a water-reducing rate of 35% was supplied by Subote new materials corporation in China. In addition, ISO standard sand was used as a fine aggregate.

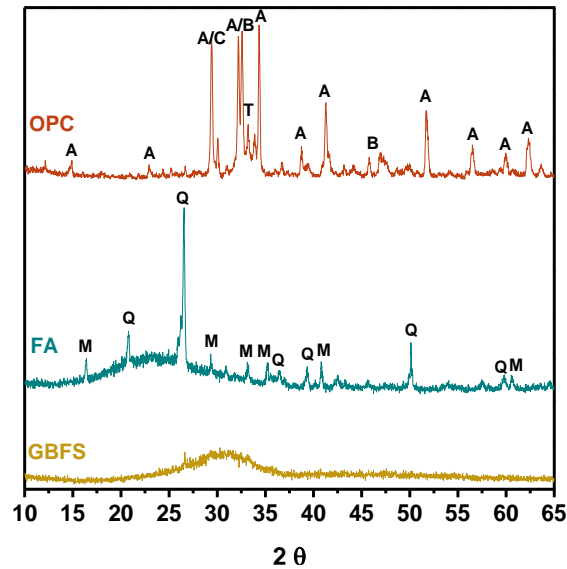


Figure 6-1. XRD patterns of OPC, GBFS and FA: A: Alite; B: Belite; C: Calcite; T: Tricalcium aluminate; Q: Quartz; M: Mullite.

## 2.2 Experimental method

The composition for AAC and HACs is summarized in Table 6-2.

Table 6-2. Composition of AAC and various HAC systems (wt.%).

Group	OPC	GBFS	FA	Na <sub>2</sub> O	Activator (Ms =1.5)
AAC	0	300	-	5	NaOH + waterglass
HACS	25	75	-	5	NaOH + waterglass
HACS*	25	75	-	5	NaOH + waterglass
HACF	25	-	75	5	NaOH + waterglass
HACSF	25	50	25	5	NaOH + waterglass
HACS''	25	75	0	5	NaOH + solid Na <sub>2</sub> SiO <sub>3</sub>

**HACS\* means HACS under steam curing; HACS'' means HACS with solid activator.**

ISO sand and HACs pastes were used to prepare HAC mortar. The specimens were cured under standard curing (at  $20 \pm 2$  °C and humidity higher than 95%) (Li et al. 2019) and steam curing (at 85°C for 2 hours) in order to determine the effect of curing temperature on the drying shrinkage and strength of HAC mortars. The HACs paste specimens were terminated by hydrating with anhydrous ethanol, and then broken into small pieces or ground into powders for microscopic analysis.

### *Compressive strength testing*

The strength of HAC mortar is tested in accordance with the method specified in ISO

1920-3-2004.

#### *Drying shrinkage and water loss*

Three 40 mm × 40 mm × 160 mm HAC mortar prisms are prepared for the drying shrinkage test and mass change for each group. The length comparator is used to measure the length of mortar prisms. The initial length is measured after 24h, and then the prisms are put into a drying room where the temperature is 20 ± 2 °C and relative humidity is about 60 ± 5%. The length of the prisms is measured at different ages (2 d, 3 d, 7 d, 14 d, 28 d and 56 d), and the drying shrinkage ( $\epsilon_{ds}$ ) is calculated according to Eq. (1)

$$\epsilon_{ds} = \frac{L_0 - L_t}{160} \quad (1)$$

where  $L_0$  is the initial length,  $L_t$  is the length at various ages.

The mass change of specimens was measured daily for the first week, and then at 14, 21, 28, 56 d. The water loss ( $M_{wl}$ ) is calculated according to Eq. (2).

$$M_{wl} = \frac{M_0 - M_t}{M_0} \times 100\% \quad (2)$$

where  $M_0$  is the initial mass,  $M_t$  is the mass of various ages.

#### *XRD analysis*

To detect the types and quantities of crystals in the reaction products of HACs, XRD qualitative analysis is performed on a 60-KV, 80-mA XRD-7000 diffractometer with Ceramic X-ray tube and Cu target. The scanning speed is 2.5°/min, with 2θ ranging from 5 to 80°.

#### *Scanning electron microscopy with energy-dispersive spectrometry (SEM-EDS)*

SEM-EDS is implemented to investigate the morphology and chemical composition of hydration products of HACs. The spot scan and elemental analysis were conducted on a Zeiss Smart EDX Energy Disperse Spectroscopy.

#### *Mercury intrusion porosimetry (MIP) analysis*

The pore size distribution and total porosity of the HACs were characterized by MIP on an automatic mercury porosimeter (AutoPore Iv 9510) which could measure the pore diameters range from 5 to 340 000 nm. The surface tension of mercury was 485 dynes/cm and the contact angle was set to be 130°.

## 6.3 Results and discussion

### 6.3.1 Compressive strength

Compressive strength development of OPC and HACs mortars at various curing ages are given in Figure 6-2. The AAC mortar exhibits the highest compressive strength at each age. Both AAC and HAC mortars show higher early strength than OPC mortar, but the later strength of HAC mortar is inferior to that of OPC mortar. In HAC systems, the compressive strength decreases when the fly ash is used as a precursor, and the substitution of fly ash for partly slag has little effect on the HAC compressive strength. The steam curing could improve the early strength of HAC. In addition, HAC with liquid activator could develop higher compressive strength than that of solid activator, which may be related to the lower reaction rate.

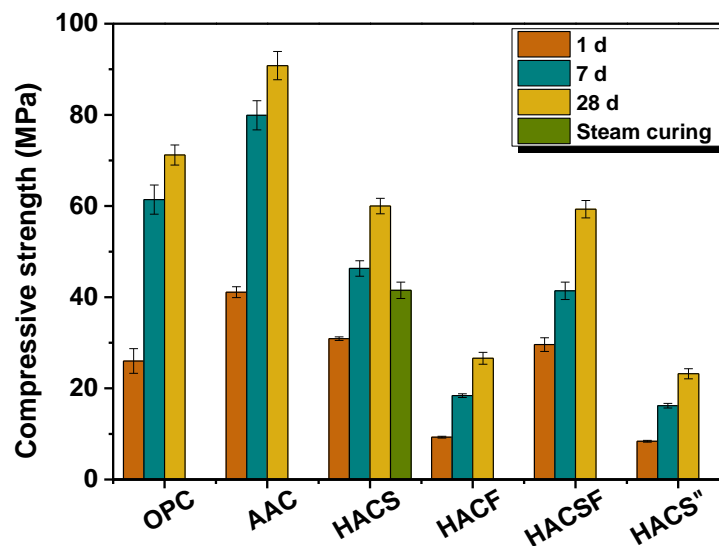


Figure 6-2. Compressive strengths of OPC and HACs at different curing ages.

### 6.3.2 Drying shrinkage and water loss

The autogenous shrinkage caused by capillary stress and the drying shrinkage due to moisture change were included in the drying shrinkage investigated in this research (Jia et al. 2018). Figure 6-3 shows the influence of the precursors, activator state and curing regime on the drying shrinkage for HACs. Figure 6-3(a) compares the values of drying shrinkage for OPC, AAC and HACS mortars versus time. The drying shrinkage value of HACS is much lower than AAC and comparable to OPC throughout

the curing age. In Figure 6-3(b), it can be found that the drying shrinkage of HACF is the lowest during the HACs system. There is no significant distinction in drying shrinkage between HACS and HACSF.

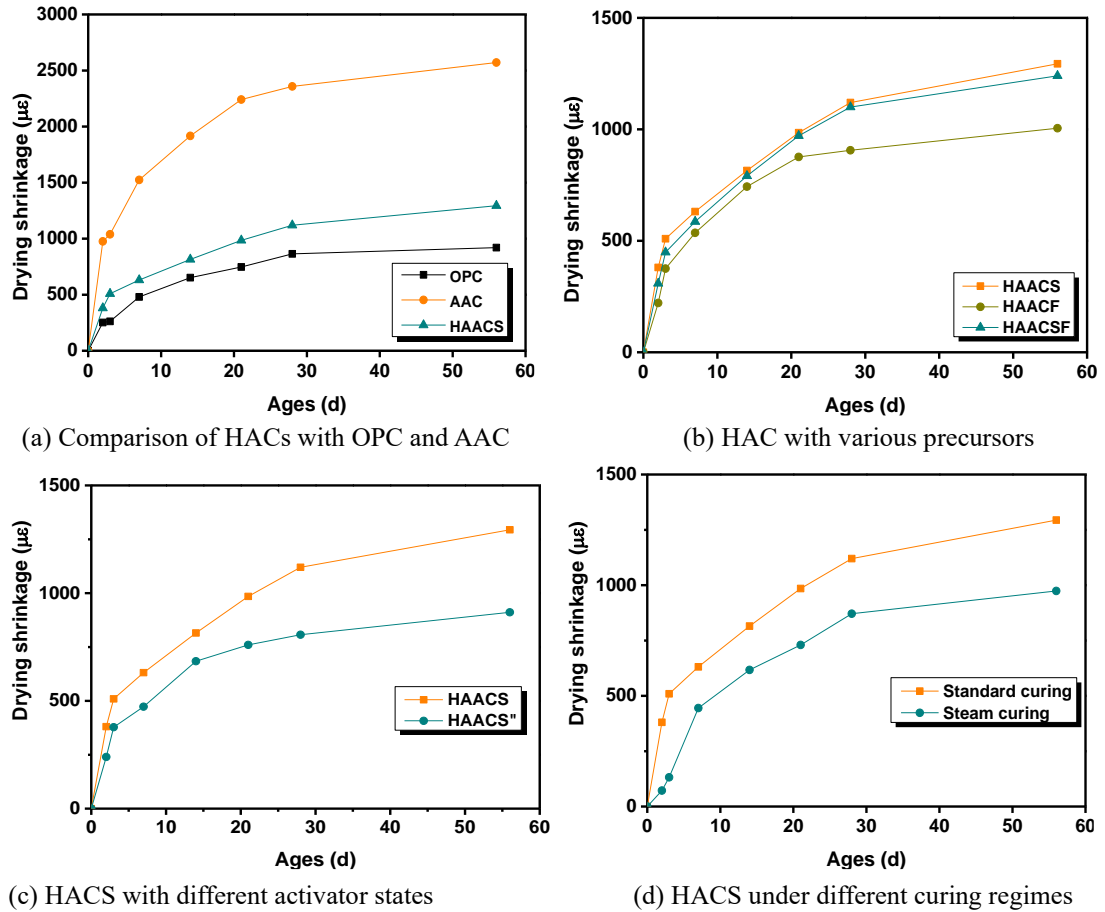
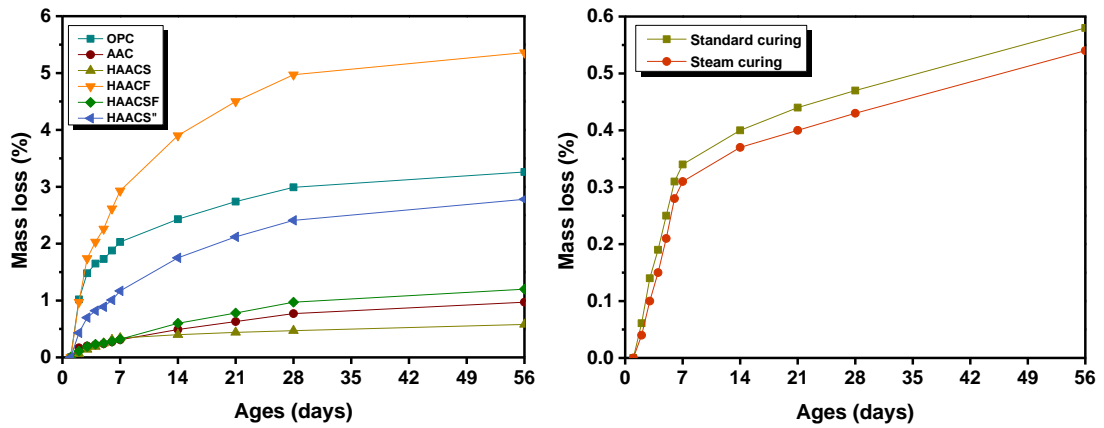


Figure 6-3. Time-dependent drying shrinkage of OPC, AAC and HACs mortars.

HACS mortar activated by a solid activator exhibits lower drying shrinkage than that activated by a liquid activator (see Figure 6-3(c)). The steam curing could reduce the drying shrinkage of HACS mortar noticeably.

The magnitude of shrinkage of cementitious materials is generally correlated to water loss (Bažant 2001), so the water loss in specimens was measured and the results are plotted in Figure 6-4. The OPC mortar shows a higher water loss than that of AAC and HACS, although the magnitude of drying shrinkage strain in OPC is the least among the three type binders (see Figure 6-4(a)). In terms of precursors, HACF mortar exhibits the largest water loss, approximately 6% by mass, followed by HACSF mortar, and the water loss rate of HACS mortar is the lowest. This water loss trend is the

opposite of the drying shrinkage change. The HACS mortar with liquid activator shows less water loss than that with solid activator. In Figure 6-4(b), it can be found that steam curing leads to less water loss than drying curing. In conclusion, it seems that the water loss rate of the studied specimens is negatively correlated with the drying shrinkage rather than positively. This counter-intuitive conclusion needs to be explained via further investigation such as pore structure analysis, hydration products composition and microstructure.



(a) OPC, AAC and HACS mortars

(b) HACS mortars under different curing regimes

Figure 6-4. Water loss of OPC, AAC and HACS mortars.

### 6.3.3 Pore structure analysis

Pore structure affects the transport and transfer of water in cementitious materials which are closely related to shrinkage, thus understanding the changes of pore structure in the hydration and curing process is vital to study the shrinkage behavior of HACS. The total porosity and pore structure of OPC, AAC and HACS pastes at 28-day via mercury intrusion analysis is demonstrated in Figure 6-5. The OPC exhibits the highest total porosity of 19.13%, followed by HACF and HACS'', the HACS has the lowest total porosity of 4.85% (see Figure 6-5(a)). The steam curing leads to higher porosity than that of standard curing. Higher porosity usually leads to higher water loss, hence the total porosity results of specimens could explain their variation trend of mass loss. Materials with lower porosity theoretically possess better volume stability and higher compressive strength. It is obvious that the compressive strength of AAC and HACS mortar is well correlated to their total porosity (see Figure 6-2 and

Figure 6-5(a)). However, there is a negative correction between total porosity and drying shrinkage in this study, which needs to be elucidated via the analysis of pore size distribution (Collins and Sanjayan 2000). According to previous references (Mehta and Monteiro 2006; Zeng et al. 2012), the pore structure in cementitious materials is usually divided into four types: large pores (>100 nm), capillary pore (50-100 nm), meso-pores (10-50 nm), and gel micro-pore and meso-pore (<10 nm). In Figure 6-5(b), AAC and HACs pastes exhibit a finer pore structure than that of OPC paste due to a considerable proportion of gel micro-pore and meso-pore (<10 nm). Meanwhile, the capillary pore (50-100 nm) in OPC is more than in AAC and HACs. It is reported that refined pore structure may be correlated to the shrinkage behavior, which can explain the higher drying shrinkage of AAC and HACs (Gao et al. 2016). Compared to AAC, the proportion of capillary pores in HACs is lower. The steam curing could increase the proportions of gel micro-pore and meso-pore despite the increase in total porosity. The HACs with solid activator has less gel micro-pore and meso-pore but more meso-pores. The correction between pore distribution and drying shrinkage is discussed as follows.

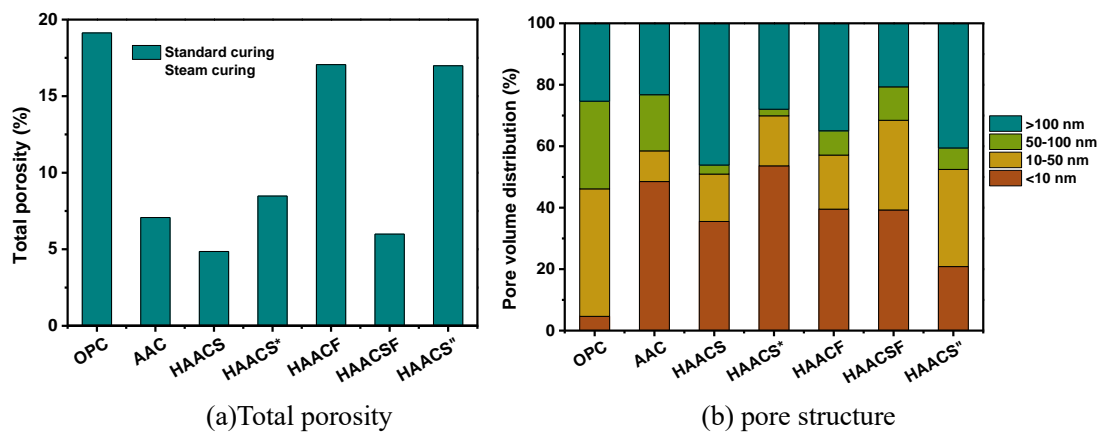


Figure 6-5. Total porosity and pore structure of OPC, AAC and HACs.

The pore distribution of specimens in the present study is plotted in Figure 6-6.

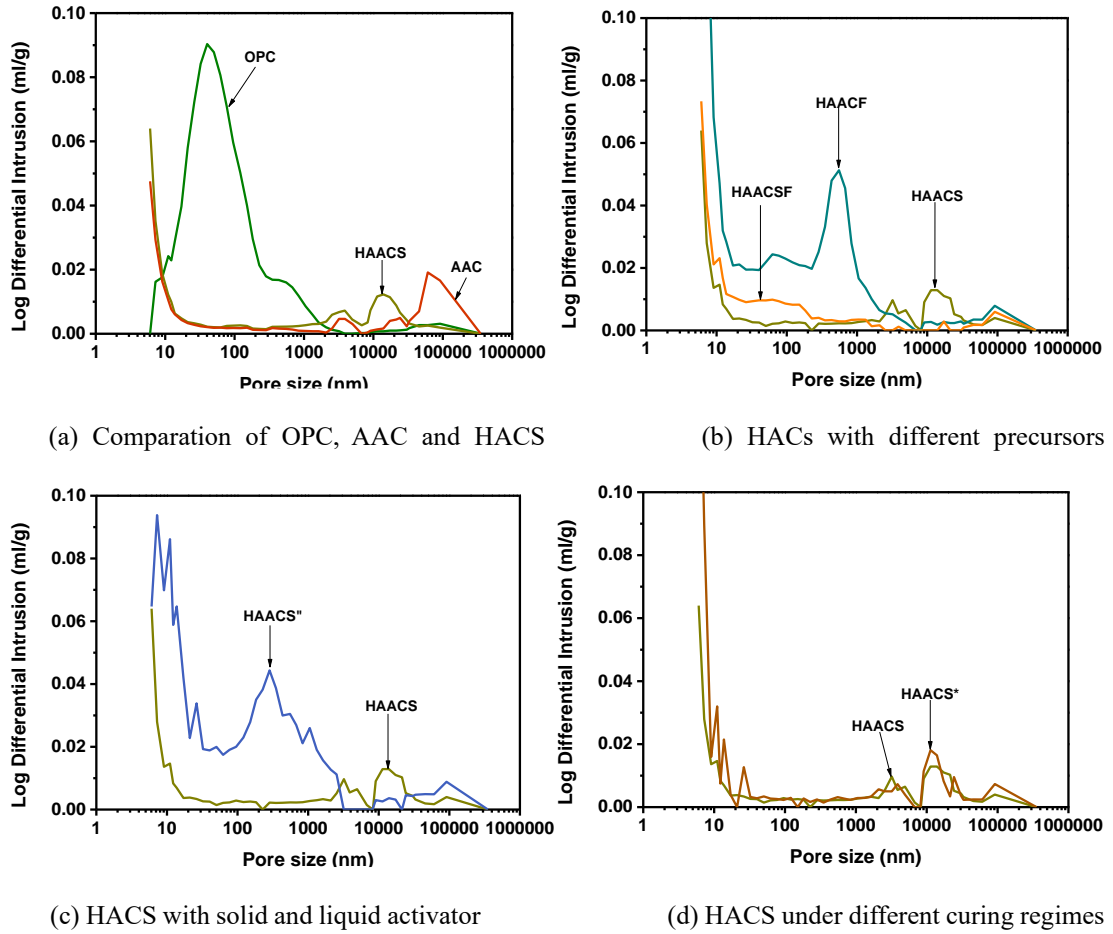


Figure 6-6. Pore distribution of OPC, AAC and HACs pastes after 28 days curing

There are three well-known dominant mechanisms of drying shrinkage: surface energy, capillary stress and disjoining pressure (Thomas et al. 2017). Surface energy plays a significant role when the relative humidity (RH) is less than 45%, while capillary stresses are significant only above 45% RH is derived from the instability of menisci below 45% RH (Mehta and Monteiro 1993). The RH in this study is approximately 60%, so capillary stress is the major contributing factor. The capillary pressure  $P_{cap}$  is related to surface tension  $\gamma$  and pore radius  $r$  based on the Kelvin Laplace equation as shown in Eq. (3) (Thomas et al. 2017; Slowik et al. 2008).

$$P_{cap} = \frac{2\gamma}{r} \quad (3)$$

The surface tension of alkali activated material pore solution is apt to be similar to or stronger than that of OPC (Ye et al. 2017). Hence, larger pore radius results in lower capillary pressure and then in lower shrinkage magnitude. According to the pore

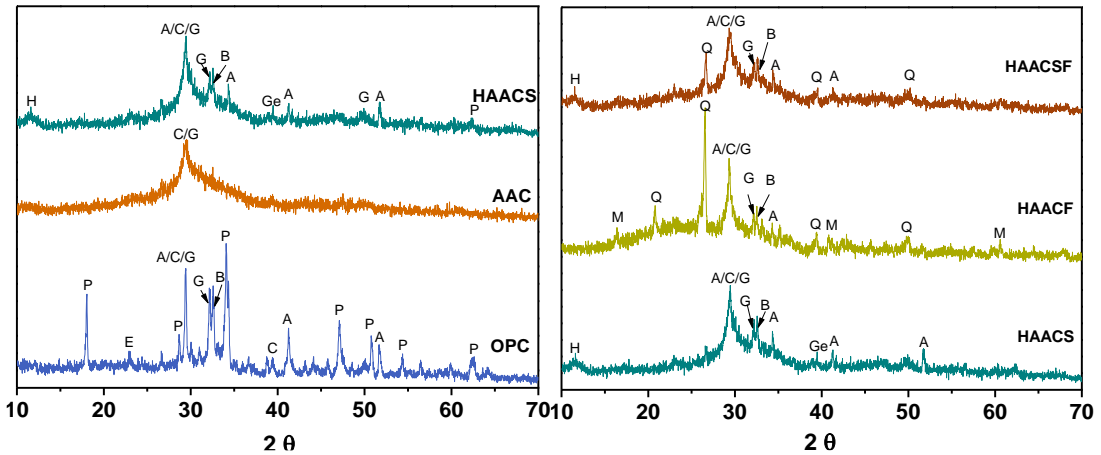
structure results, the capillary pore radius of OPC is larger than that of AAC and HACs, thus resulting in lower drying shrinkage. Compared with HACs, more refined pores (< 50 nm) that could lead to higher capillary stress are found in HACs, which could explain the lower drying shrinkage of HACS mortar compared to AAC mortar. In terms of the precursors, the pore distribution is likely to have little change in addition to larger large pore size in HACS. The larger proportion of capillary pores seems to be able to account for the low shrinkage of HACF according to Laplace equation. However, some research has reported that the mesopore volumes (< 50 nm) could cause higher drying shrinkage which seems to contradict the result that the mesopore volume of HACF is the largest during the HAC systems, but the drying shrinkage is the lowest in this study. This result remains to be clarified by further analysis of hydration products. The HACS activated by solid activator has a larger proportion of capillary pores, meanwhile, the pore size is larger than that activated by liquid activator, which could result in reduced drying shrinkage. In case of a curing regime, steam curing improves the total porosity of HACS, but refines the pore radius (increases the proportion of pores less than 10 nm and reduces the large pores proportion). The lower magnitude of drying shrinkage by steam curing may be attributed to the stiffer and denser microstructure than that of curing under standard condition (Thomas et al. 2017).

It is well known that the factors influencing the drying shrinkage behavior of cementitious materials include many aspects, thus drying shrinkage of specimens in this study is not merely dependent on the total porosity and pore structure distribution, but also the composition of hydration products and microstructure. The mineralogical and morphological analysis were conducted via XRD and SEM-EDS to determine the phase composition, microstructure and elemental composition of hydration products.

#### **6.3.4 Mineralogical and morphological analysis**

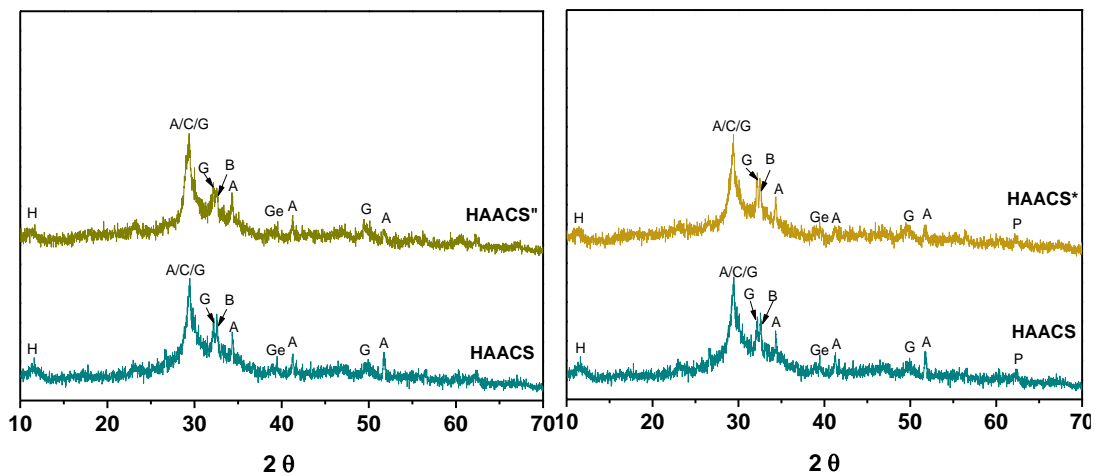
Figure 6-7 depicts the XRD patterns of OPC, AAC and HACs pastes dried for 28 days. Figure 6-7(a) compares the phase composition of OPC, AAC and HACS pastes. It is obvious that more crystalline products such as portlandite, ettringite and calcite

generate in OPC than in AAC and HACS. The broad halo occurring between  $25^\circ$  and  $35^\circ$  indicates that the AAC and HACS pastes contain a mass of amorphous phases. The high peak at around  $29\text{-}30^\circ 2\theta$  is associated with poorly crystalline C-S-H or calcite and a residue of alite (Ismail et al. 2014). Compared with AAC, the products of HACS have more crystal phase, including calcite, hydrocalumite and poorly crystalline C-S-H. Moreover, the peak at  $29\text{-}30^\circ 2\theta$  in HACS diffraction pattern is more intense and sharper than in the AAC pattern. The more crystalline phase logically predicts greater dimensional stability (Thomas et al. 2017). This can explain the difference in the drying shrinkage behavior of OPC, AAC and HACS. The XRD patterns of HAC with various precursors are shown in Figure 6-7(b). A broad hump appeared in every diffraction pattern, but in a different  $2\theta$  degrees. The mutual crystalline products of HACs are crystalline C-S-H, calcite and unreacted alite and belite. The peaks corresponding to quartz and mullite were observed in HACF and HACSF pastes as fly ash contains such crystalline phases (Cao et al. 2020; Cao et al. 2021). A small quantity of hydrocalumite (at around  $11.58^\circ 2\theta$ ) which belongs to a kind of layered double hydroxides (LDH) with well-ordered Ca and Al was also detected in HACS and HACSF, and it was reported that hydrocalumite was more likely to occur in alkali activated materials rich in Ca and Al (Qiu et al. 2015). The more inert crystalline phase in fly ash results in more crystalline phases in HACF and HACSF, and thus ultimately tempered the magnitude of drying shrinkage.



(a) Comparison of HACs with OPC and AAC

(b) HAC with various precursors



(c) HACs with different activator states

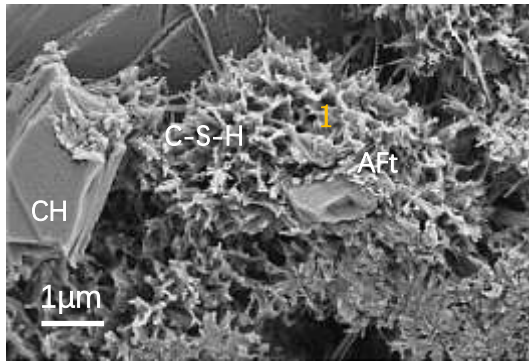
(d) HACs under different curing regimes

Figure 6-7. XRD patterns for OPC, AAC and HACs pastes after 28 days of curing. A: Alite; B: Belite; C: Calcite; P: Portlandite; E: Ettringite; G: calcium silicate hydrate; Q: Quartz; H: Hydrocalumite ( $Mg_6Al_2(OH)_{16}CO_3 \cdot 4H_2O$ ); Ge: hydrated Gehlenite ( $C_2ASH_8$ ).

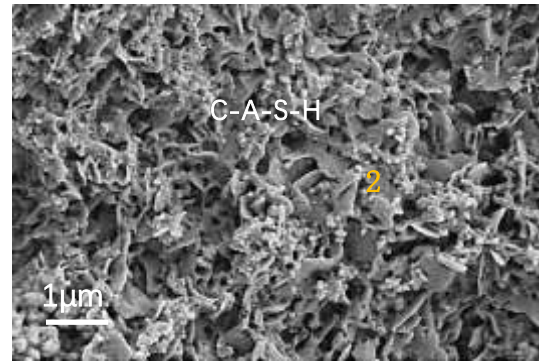
As can be seen from Figure 6-7(c), the change of the alkali activator state of HACs does not influence the type and quantity of the reaction products, but it may affect the composition of these products. Similarly, there is no significant distinction with the hydration products of HACs between standard curing and steam curing different curing regimes as shown in Figure 6-7(d). The composition of hydration products for specimens, especially that the gel which cannot be detected by XRD, needs to be further determined by SEM energy spectrum.

Figure 6-8 displays the microscopic morphology of OPC, AAC and HACs pastes after

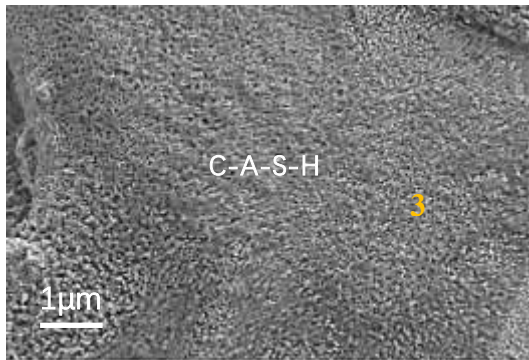
28 days curing. Amorphous calcium silicate hydrate (C-S-H) gel, crystalline Portlandite (CH) and some ettringite (AFt) could be identified in the hydrated OPC paste as reported in previous research (Matalkah et al. 2019). The obvious pores, together with the aforesaid products, constitute a porous matrix of OPC. In AAC paste, a relatively dense alkali aluminosilicate hydrate (C-A-S-H) gel is cross-linked with a small amount of unreacted slag to form a homogeneous matrix with few pores. In the case of HACs, all pastes exhibit a denser microstructure than OPC and AAC in addition to HACF, so that it is impossible to distinguish the gel product from the unreacted particles. Reticular gels and unreacted fly ash (FA) spheres are observed in the test areas of HACF, and the matrix is not uniform and dense, which is attributed to the low reactivity of fly ash (García-Lodeiro et al. 2013b). The gel generated in HACF can be concluded to be N-C-A-S-H which is a hybrid gel of C-S-H from OPC and N - A-S-H from geopolymer. The HACS under steam curing and standard curing display a similar dense microstructure. As for the alkali activator state, the HACS with solid activator has the same homogeneous matrix as that of the liquid activator in addition to some crystalline products on the surface due to an early slow reaction (Fernández-Jiménez et al. 2019). The micromorphology analysis results of specimens correspond to those of the pore structure. The denser microstructure does not result in a lower magnitude of shrinkage, so the composition of hydration products is required for more accurate characterization of the drying shrinkage behavior of OPC, AAC and HACs mortar, especially the Ca/Si ratio of gels.



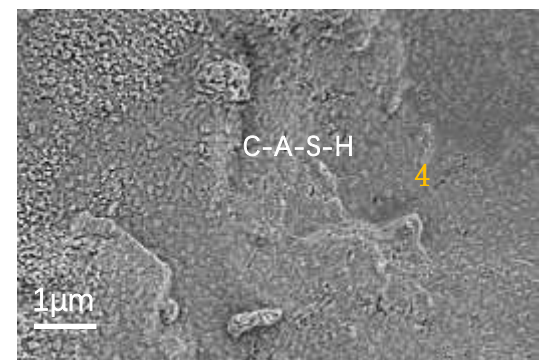
(a) OPC



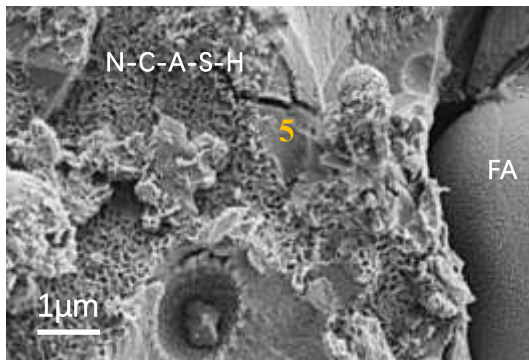
(b) AAC



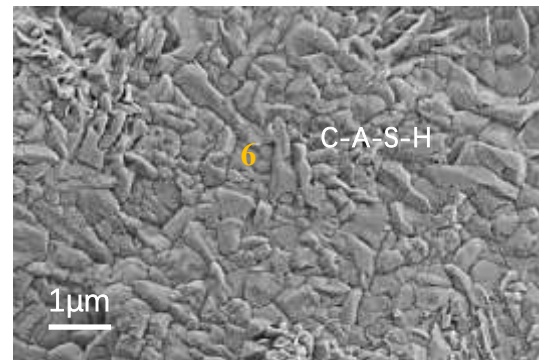
(c) HACS



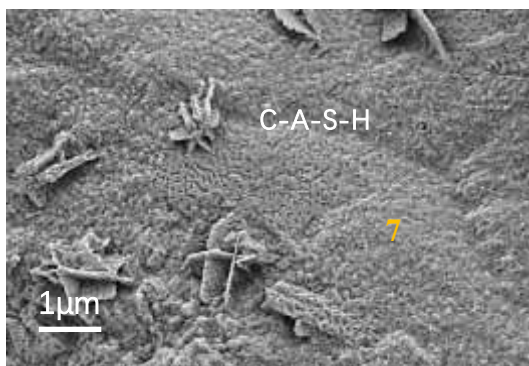
(d) HACS\*



(e) HACF



(f) HACSF



(g) HACS''

Figure 6-8. Microtopography of OPC, AAC and HACs pastes cured for 28 days.

Table 6-3 shows the Ca/Si ratio, Na/Si ratio and Al/Si ratio of specimen reaction

products derived from EDS point analysis which is marked in yellow in Figure 6-8. The Ca/Si ratio of C-S-H gel in Portland cement is reported to range from 1.2 to 2.3 (Yip and Van Deventer 2003), whereas the main hydration product of AAC is C-S-H gel with low Ca/Si ratio (Lecomte et al. 2006). It can be seen in Table 3 that the Ca/Si ratio in OPC is the highest (1.71), whereas the Ca/Si ratio in AAC is much lower (0.85), and the HACS has an intermediate Ca/Si ratio. It can be deduced that the product gel in HAC is a hybrid type phase of C-S-H generated by OPC and C-A-S-H from AAC. The HAC with fly ash generates gels with a lower Ca/Si ratio than that with slag, which is attributed to the lower Ca/Si ratio gel N-A-S-H generated in activated fly ash. The steam curing and solid activator both lead to higher Ca/Si ratio gel in HACS. The Ca helps to form an ordered structure, while Si helps to increase the amorphous structure, hence product gel with a higher Ca/Si ratio could temper the shrinkage of cementitious materials. The Ca/Si ratio of gel is well correlated with the drying shrinkage performance in this study. There is no certain regularity in the Na/Si ratio of the studied product gel except that the HAC containing this gel has a higher Na/Si ratio. The reason is likely to be that the higher reaction rate in this type of HAC leads to the more Na cations from the activator form part of the product gel. In terms of Al/Si ratio, AAC and HACS under steam curing generate a lower Al/Si ratio hydration gel, while HAC with fly ash and activated by a solid activator produces a larger Al/Si ratio gel. The higher Al/Si ratio gel suggests more polymerization and crosslinking in the C-(A)-S-H gel, resulting in denser microstructure and higher compressive strengths (Gao et al. 2017). The Ca/Si molar ratio has the highest effects on the drying shrinkage of alkali activated materials, followed by the Al/Si ratio, and the Na/Si ratio is the lowest impactor (Mastali et al. 2018). Therefore, the Ca/Si molar ratio is considered to be the main influence impacting on drying shrinkage in this study.

Table 6-3. Elemental ratios of OPC, AAC and HACs hydration gel.

Point	Ca/Si	Na/Si	Al/Si
1	1.71	-	0.26
2	0.85	0.86	0.32
3	1.14	1.19	0.34
4	1.51	0.84	0.36
5	0.79	0.76	0.36
6	1.12	1.40	0.35
7	1.4	0.87	0.29

#### 6.4. Conclusions

The drying shrinkage behavior of HAC mortars was evaluated, including the effect of precursors, curing regimes and activator states. Meanwhile, the shrinkage characteristics of HAC mortars were compared with those of OPC and AAC mortars. Several conclusions were derived from the experiment as follows.

- AAC mortar exhibits the largest magnitude of drying shrinkage, followed by HAC mortar, while the shrinkage value of OPC mortar is the lowest. The more capillary pressure caused by refined pores, the more amorphous hydration products and low Ca/Si ratio gel of HAC lead to a larger magnitude of drying shrinkage than that of OPC. Compared to AAC, relatively large size pores, more crystalline phase and higher Ca/Si product gel of HAC paste tempers the drying shrinkage of HAC mortar.
- Slag-based HAC mortar shows the highest drying shrinkage. The incorporation of fly ash could temper the magnitude of drying shrinkage. The drying shrinkage of HACs is not concerned with water loss. The larger capillary pores size is likely to explain the lower shrinkage of fly ash -based HAC mortar according to Laplace equation. The main reason lies in the more crystalline phase in fly ash-based HAC due to the more inert crystalline phase in fly ash.
- The drying shrinkage of slag-based HAC mortar was lower in magnitude under steam curing compared to standard curing. The types and composition of

hydration products under the two curing regimes are similar except for differences in Ca/Si ratio in gel. The lower drying shrinkage with steam curing could be attributed to the stiffer and denser microstructure and higher Ca/Si ratio gel than that curing under standard conditions.

- The magnitude of drying shrinkage for slag-based HAC mortar decreased when a solid activator was used instead of liquid, whereas, the alkali activator state did not affect the type and quantify of the reaction products in addition to the higher Ca/Si ratio hydration gel with solid activator. The reason may be attributed to a larger proportion of capillary pores and a larger pore size which could decrease the capillary stress, ultimately resulting in lower drying shrinkage.

# CHAPTER 7: CARBON DIOXIDE EMISSIONS FOR HACS

## 7.1 Introduction

Ordinary Portland cement (OPC) manufacturing is a high-energy industry, and thus the emissions of carbon dioxide account for approximately 5-7% of global CO<sub>2</sub> emissions (McLellan et al. 2011). The proposal of carbon neutrality at the 75<sup>th</sup> United Nations Conference has promoted the transformation and upgrading of the cement industry. Researchers are working on low-carbon approaches, including adjusting the balance of ingredients used in cement production, using carbon capture and storage technology to eliminate emissions, and removing cement from concrete altogether. While HAC in this study is proposed mainly for its potential lower carbon footprint (Palomo et al. 2019). However, the quantitative study of carbon dioxide emission of HACs has not been reported yet. Obviously, it is unscientific to assume that HAC has a low carbon footprint without previously having carried out accurate calculation of carbon emissions. The carbon dioxide equivalent (CO<sub>2</sub>-e) is commonly used to compare the emissions of various greenhouse gases based on their global warming potential (Turner and Collins 2013). In this chapter, the CO<sub>2</sub>-e of HACs is analyzed and compared with that of geopolymers and Portland cement. In addition, the comparison of CO<sub>2</sub> emission of HACs, geopolymers, alkali activated cement (AAC) and Portland cement is vital and significant to perform. The impact of Global Warming Potential (GWP) will be the focus.

## 7.2 Materials and methodology

### 7.2.1 Materials

P II 52.5 Portland cement (according to Chinese standard GB 175-2007), grade S95 (according to Chinese standard GB/T 18046-2017) ground blast furnace slag (GBFS) and grade I (according to Chinese standard GB/T 1596-2017) fly ash (FA) were used as main materials. The chemical compositions of aforesaid raw materials were determined by X-ray fluorescence (XRF), and the result is given in Table 3-2. The alkali

activator with a modulus of 1.5 was prepared by liquid sodium silicate and solid hydroxide pellets.

The river sand with fineness modulus of 1.5 was used as fine aggregate and gravel of particle size 5 was used as coarse aggregate.

### **7.2.2 Methodology**

In this study, the HAC cementitious system is composed of 25% ordinary Portland cement (OPC), 75% GBFS or FA and 3-5% alkali activator. The geopolymer is composed of FA and 5% alkali activator. The carbon dioxide equivalent (CO<sub>2</sub>-e) emissions of 1m<sup>3</sup> concrete with various binders were examined. The design and mixture proportions of the concrete were determined by combining with Zhejiang Longding company's practical production and the method described in the Chinese specification JGJ 55-2011. Table 7-1 shows the mix proportions for these concretes. The amount of cementitious materials per cubic meter of concrete is 420 kg. The HACs with 5% Na<sub>2</sub>O are chosen to make a comparative analysis of CO<sub>2</sub> emission with OPC and geopolymer.

Table 7-1. Mix proportions for concretes (kg/m<sup>3</sup>).

Type	Cement	GBFS	FA	Sand	Gravel	NaOH	Water glass	Sodium silicate	Water
OPC	420	0	0	714	1320	0	0	0	118
Geopolymer	0	0	420	652	1280	9.7	93.6	0	90
AAC	0	420	0	700	1300	9.7	93.6	0	92
HACF									
3% Na <sub>2</sub> O	105	0	315	663	1290	5.8	56.2	0	86
4% Na <sub>2</sub> O	105	0	315	663	1290	7.7	74.9	0	87
5% Na <sub>2</sub> O	105	0	315	663	1290	9.7	93.6	0	89
HACS (WG)									
3% Na <sub>2</sub> O	105	315	0	700	1300	5.8	56.2	0	95
4% Na <sub>2</sub> O	105	315	0	700	1300	7.7	74.9	0	90
5% Na <sub>2</sub> O	105	315	0	700	1300	9.7	93.6	0	89
HACSF									
3% Na <sub>2</sub> O	105	210	105	690	1300	5.8	56.2	0	93
4% Na <sub>2</sub> O	105	210	105	690	1300	7.7	74.9	0	89
5% Na <sub>2</sub> O	105	210	105	690	1300	9.7	93.6	0	87
HACS (SS)									
5% Na <sub>2</sub> O	105	315	0	700	1300	6.8	0	46.2	99
HACS (NH)									
5% Na <sub>2</sub> O	105	315	0	700	1300	27.1	0	0	90
HACS									
(One part) 5% Na <sub>2</sub> O	105	315	0	700	1300	0		61.7	96

### 7.3 Results and discussion

The present study evaluates the Global Warming Potential (GWP) impact which is expressed as kg·CO<sub>2</sub>·eq. The GWP category is a metric of the cumulative effect of different greenhouse gas emissions, including short and long lifetime gases that may alter the average atmospheric temperature in the next 20 to 500 years (Robayo-Salazar et al.2018). The GWP data was mainly extracted from the Ecoinvent 3.2 database which was developed by the Swiss Centre for Life Cycle Inventories and also from references. For the curing regime of geopolymer, the elevated temperature curing of concrete (approximately 16 h overnight) at an average temperature of 50 °C, which

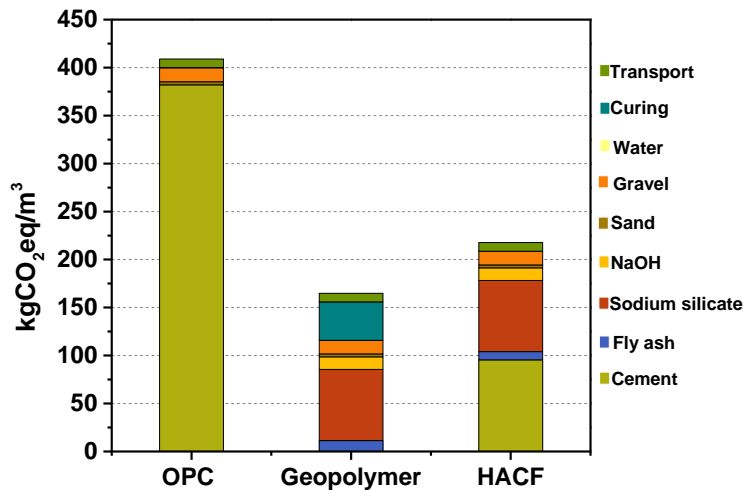
was extrapolated to 24 h for our calculations (plus approximately 9 h gradual heating/cooling time). The calculated emission for elevated temperature curing was  $39.97 \text{ kg} \cdot \text{CO}_2\text{-eq} / \text{m}^3$  (Turner and Collins 2013). Moreover, the carbon footprint of transporting raw materials from the source to the cement and concrete factory was also considered. GWP100 (GWP environmental impact projected to 100 years) associated with the raw materials and curing conditioning of OPC concrete, geopolymer concrete and HAC concrete are given in Table 7-2.

Table 7-2. Inventory data and impacts associated with the raw materials, curing regime of OPC, geopolymer and HAC concretes.

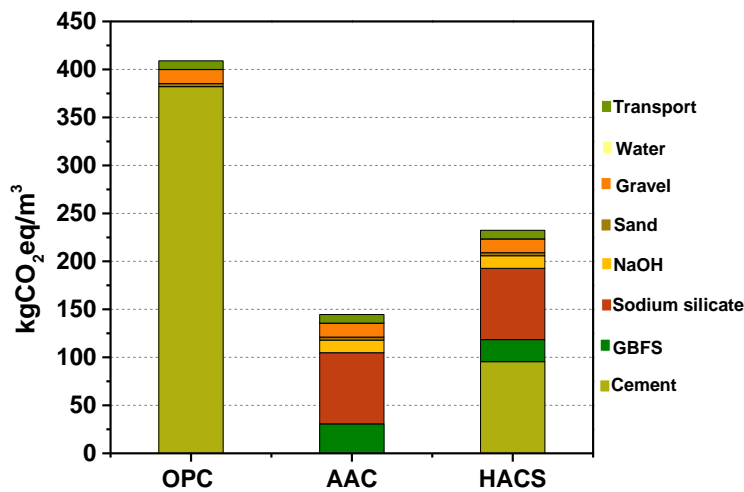
Raw materials/curing	Items	Input mass(kg)	GWP100 ( $\text{kg} \cdot \text{CO}_2\text{-eq}$ )	Reference
Cementitious material/precursors	OPC	105/420	$9.097 \times 10^{-1}$	(Boesch and Hellweg 2010)
	GBFS	315/420	$7.73 \times 10^{-2}$	Ecoinvent
	FA	315/420	$2.700 \times 10^{-2}$	(Turner and Collins 2013)
Alkali activators	NaOH	5.8/7.7/9.7	$1.359 \times 10^0$	(Althaus et al. 2007)
	Sodium silicate	46.6/61.7	$1.0 \times 10^0$	(Duxson et al. 2007)
	Waterglass	56.2/74.9/93. 6	$7.925 \times 10^{-1}$	(Zah et al. 2007)
Water	Water	86-118	$4.288 \times 10^{-4}$	Ecoinvent
Aggregates	Sand	714	$4.473 \times 10^{-3}$	(Kellenberger et al. 2004)
	Gravel	1320	$1.108 \times 10^{-2}$	(Kellenberger et al. 2004)
Curing	Heat curing	-	39.97	(Turner and Collins 2013)
Transport	-	-	9	(Stengel et al. 2009)

### 7.3.1 Comparison of HACs, OPC, geopolymer and AAC concretes

The GWP for the studied concretes were calculated based on the mix proportions (Table 7-1) and GWP 100 shown in Table 7-2. Figure 7-1 presents the GWP100 for each component of  $1 \text{ m}^3$  concrete with binders of OPC, geopolymer, AAC and HACs respectively.



(a) The comparison of GWP 100 for OPC, geopolymer and HACF concrete



(b) The comparison of GWP 100 for OPC, AAC and HACS concrete

Figure 7-1. A comparison of OPC, geopolymer, AAC and HAC binders on the impact of GWP of their concrete mixtures.

Figure 7-1(a) compares the GWP 100 for OPC concrete to the low-Ca alkali activated binder geopolymer and HACF. As can be seen that OPC concrete is the most significant contributor to carbon emissions, followed by HACF and geopolymer concretes. It is obvious that Portland cement shows the largest CO<sub>2</sub>·eq for OPC concrete, accounting for about 93%. In geopolymer concrete, sodium silicate and curing are the main carbon footprint contributors. The total carbon emission from geopolymer concrete is less than half of that of OPC concrete, which is primarily due to the absence of OPC. HACF shows less carbon emission than that of OPC, but a little higher than geopolymer due to the incorporation of Portland cement. Figure 7-1(b)

shows the GWP 100 for OPC concrete to the high-Ca alkali activated binder AAC and HACs. The GWP 100 of OPC concrete is still the largest one. AAC concrete exhibits the lowest carbon emission. Similarly, HACS concrete exhibits less carbon emission than that of OPC concrete, and OPC and activator remain a major contributor to carbon emissions. HACF shows less carbon footprint than HACS because the carbon emission of fly ash is much lower than GBFS (The et al. 2017). In summary, HAC can be considered as a low carbon cementitious material due to its lower carbon footprint compared to OPC.

### **7.3.2 Comparative analysis of HACs with different precursors and alkali contents**

The alkali activator and precursors are the major carbon emission contributors of HAC (see Figure 7-1), so the influence of alkali content on carbon emission is necessary for analysis (Mejía-Arcila et al. 2020). The GWP100 of HAC concrete with different precursors and alkali contents are summarized in Figure 7-2. The carbon emission of HAC decreases when the fly ash is substituted for slag. It is evident that increasing the alkali contents results in an increase in carbon emissions in all HAC concretes. The GWP value of HACS concrete increases from 197.5 to 214.9 kg·CO<sub>2</sub>·eq/m<sup>3</sup> when the Na<sub>2</sub>O content increases from 3% to 5%. As for HACF, the GWP value increases from 182.7 to 217.7 kg·CO<sub>2</sub>·eq/m<sup>3</sup>. When the fly ash partially replaces slag (HACSF system), the GWP value is somewhere between HACS and HACSF. Therefore, the alkali content should be reduced as far as possible under the premise of meeting the requirements to reduce the impact on the environment, meanwhile, the fly ash is suggested to add fly ash into HAC without affecting the compressive strength of concrete to reduce carbon emissions.

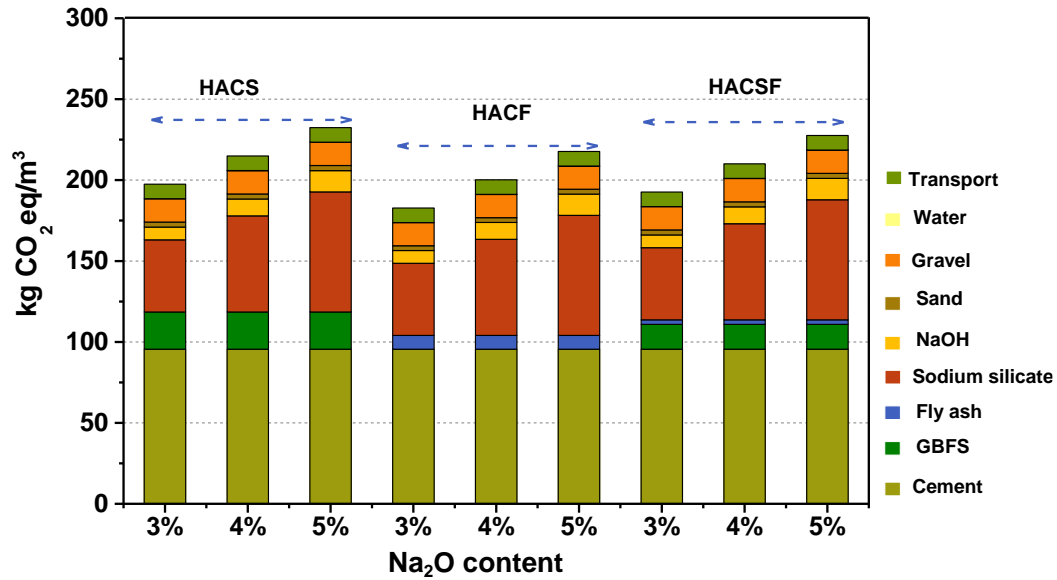


Figure 7-2. Summary of GWP100 for 1 m<sup>3</sup> HAC concretes with different precursors and different alkali contents.

### 7.3.3 Comparative analysis of HACs with different alkali activators

The alkali activators have an impact on the carbon emissions of HAC concrete due to their different production processes and sources, which are worthy to analyze. Figure 7-3 depicts the GWP100 of OPC and HAC concrete with different alkali activators. The waterglass, solid sodium silicate, sodium hydroxide activated HAC and one-part HAC are investigated in this study. One -part HAC is the HAC which directly adds water in the application process, which can ensure that the HAC components are stable and easy to control the operation. As can be seen in Figure 7-3, HACs concrete activated by different activators all shows lower carbon emissions than that of OPC concrete, approximately 50%. It is obvious that HAC concrete with sodium hydroxide exhibits the lowest GWP100, while the carbon emissions of HAC concrete activated by waterglass is relatively high in the HAC system. HAC concrete with solid sodium silicate and one-part HAC concrete has slightly lower carbon emissions than that of waterglass activated concrete. In conclusion, the type and state of alkali activator has an obvious influence on the carbon emission of HACs. It is suggested to choose the alkali activator with low carbon emission to activate the HAC without affecting the strength and operation. One-part HAC concrete is recommended because of its low

carbon footprint and precise, controllable and easy operation.

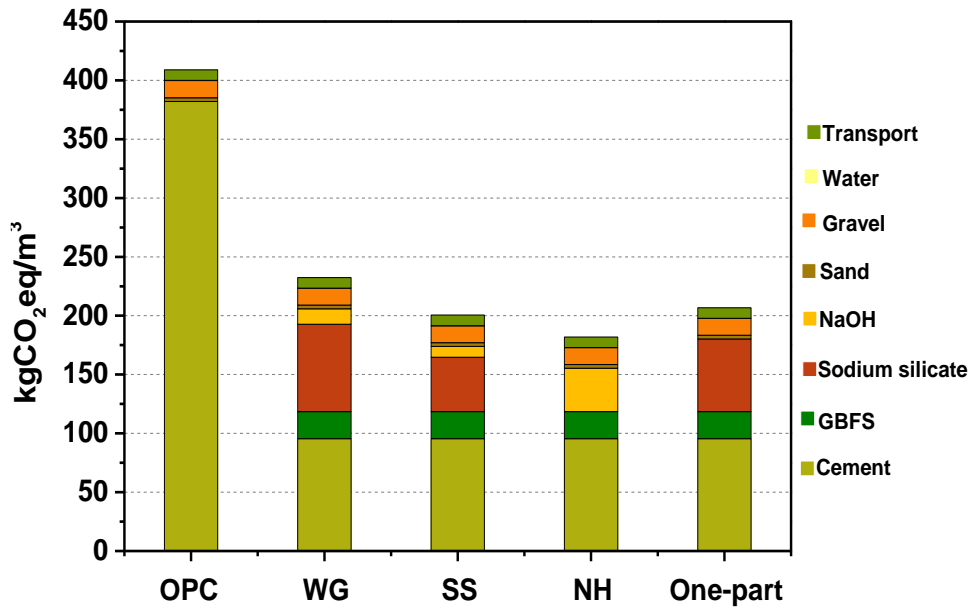


Figure 7-3. Comparison of GWP100 for 1 m<sup>3</sup> OPC and HAC concretes with different alkali activators.

### 7.4 Conclusions

In this chapter, the GWP impact is employed to evaluate and quantify the manufacturing parameters for carbon dioxide emissions of one cubic HAC concrete, including raw materials, curing regime and transport. Meanwhile, the GWP impact of HACs is compared with OPC concrete, geopolymer concrete and other AAC concrete. The CO<sub>2</sub> footprint of HAC concrete is approximately 43-55% less than comparable concrete containing 100% OPC binder, whereas the carbon footprint of HACs is slightly higher than that of geopolymer concrete and other AAC concretes with the same alkali content. It is well understood that activator is the biggest source of GWP. The carbon emission of HAC decreases when the fly ash is substituted for GBFS. Increasing the alkali contents of HAC results in an increase in carbon emissions. In terms of type of activator, HAC activated by waterglass shows the highest carbon emission, while HAC with sodium hydroxide has the lowest carbon footprint. In conclusion, HAC can be considered as a low-carbon alternative to OPC due to its lower impact on global warming.

## CHAPTER:8 CONCLUSIONS AND PERSPECTIVES

### 8.1 Conclusions

This thesis aims to understand the hydration kinetics and shrinkage behavior of HACs and thus the hydration and shrinkage control to promote the engineering application. It includes the influence of precursors, alkali contents, alkali activator and curing regimes on mechanical properties, hydration and microstructure on HACs. HACs have much more complex hydration mechanisms compared to normal Portland cement, in terms of hydration process and products. Based on the results presented, the following main conclusions can be drawn:

In Chapter 4, the type of precursors and alkali content that govern the hydration kinetics and thus determine the microstructure of HAC were investigated, thus the workability and compressive strength of HAC can be controlled by a specific amount of alkali content when a particular precursor was used.

The Na<sub>2</sub>O content of HACs was negatively associated with the setting times of HACs but positively correlated with compressive strength. Slag-based HAC showed the shortest initial setting time, and the inclusion of fly ash could delay setting time slightly but will significantly reduce compressive strength. It was shown that increasing the Na<sub>2</sub>O content improved the reaction extent and the compactness of microstructure gradually despite the hydration process being delayed in the first few hours. Fly ash - based HAC exhibited the minimum reaction extent and a relatively porous microstructure with a large amount of unreacted fly ash grains. The partial replacement of slag by fly ash hardly affects the reaction degree and microstructure of HACs.

The early gels of slag-based HAC are mainly C-S-H and C-(A)-S-H, and the gelation component proportion varies with the alkali content, while the early gel composition for fly ash-based is principally C-(A)-S-H and N-A-S-H. When fly ash and slag are blended in HAC, the gels are C-S-H, C-(A)-S-H and N-A-S-H. According to deconvolution results of <sup>29</sup>Si NMR spectra, the increased alkali content results in a more polymerization and crosslinking in the C-(A)-S-H gel in HACs. When fly ash

and slag are both applied in HAC, the formed gels seem to have an increased degree of polymerization.

Chapter 5 investigated the influence of gypsum on setting time, hydration products and microstructure of HACs. The gypsum could prolong the initial and final setting times of HACs. Increasing the dosage of gypsum resulted in longer setting time of HACs, and both initial and final setting time reached the maximum value when the gypsum content is 20%. The calorimetric analysis indicated that the incorporation of gypsum led to the decrease of reaction rate and reaction products of HAC, and also changes the basicity of the system. The HACs with gypsum exhibit a relative loose microstructure due to the reduction in the number of cations in the matrix. And HAC with 20% gypsum shows the loosest microstructure. The SEM-EDS analysis confirmed that the retarding mechanism of gypsum on HACs is the decreased ions dissolution rate rather than coverage theory.

The retardation mechanism of gypsum on hybrid cement can be attributed to two aspects: the basicity of the system is reduced due to the decrease in the concentration of Na ions reacting with  $\text{SO}_4^{2-}$ . Another is the decreased dissolution rates of Ca and Al ions induced by gypsum.

In Chapter 6, the drying shrinkage behavior of HAC mortars was evaluated, including the effect of precursors, curing regimes and activator states. Meanwhile, the shrinkage characteristics of HAC mortars were compared with those of OPC and AAC mortars. AAC mortar exhibits the largest magnitude of drying shrinkage, followed by HAC mortar, and the shrinkage value of OPC mortar is the lowest. Slag-based HAC mortar shows the highest drying shrinkage. The incorporation of fly ash could temper the magnitude of drying shrinkage. The drying shrinkage of HACs is not concerned with water loss. The larger capillary pores size is likely to explain the lower shrinkage of fly ash-based HAC mortar according to Laplace equation. The main reason lies in the more crystalline phase in fly ash-based HAC due to the more inert crystalline phase in fly ash.

The drying shrinkage of slag-based HAC mortar was lower in magnitude under steam curing compared to standard curing. The types and composition of hydration products under the two curing regimes were similar except for differences in Ca/Si ratio in gel. The lower drying shrinkage with steam curing could be attributed to the stiffer and denser microstructure and higher Ca/Si ratio gel than that curing under standard conditions. The magnitude of drying shrinkage for slag-based HAC mortar decreased when a solid activator instead of liquid. Whereas, alkali activator state did not affect the type and quantify of the reaction products in addition to higher Ca/Si ratio hydration gel with solid activator. The reason may be attributed to a larger proportion of capillary pores and larger pore size which could decrease the capillary stress, ultimately resulting in lower drying shrinkage.

Finally, the CO<sub>2</sub>-e of HACs with different precursors, alkali contents and activators were analyzed and compared with that of Portland cement and other alkali activator materials. The GWP impact was employed to evaluate and quantify the carbon dioxide emissions of one cubic HAC concretes, including raw materials, curing regime and transport. The CO<sub>2</sub> footprint of HAC concrete was approximately 43-55% less than comparable concrete containing 100% OPC binder, whereas the carbon footprint of HACs was slightly higher than that of geopolymer concrete and AAC concrete with the same alkali content. The carbon emission of HAC decreases when the fly ash is substituted for GBFS. Increasing the alkali contents of HAC results in an increase in carbon emissions. In terms of activator, HAC activated by waterglass shows the highest carbon emission, while HAC with sodium hydroxide has the lowest carbon footprint. In conclusion, HAC can be considered as a low-carbon cementitious material due to its lower impact on global warming.

## **8.2 Perspectives**

Regarding the durability, the carbonation mechanisms of HACs under different conditions must be well studied because of the high alkalinity of this type of cement. The influences of the types and proportions of cementitious materials, the types and

modulus of activator on the carbonization behavior of HACs needs to be further studied. In terms of eliminating efflorescence, the capability of HAC hydrates formed from different precursors and under different curing regimes to bind alkali cations must be studied, so a proper precursor selection and proportion can be justified.

There are still doubts of ASR risk for engineering applications due to the higher concentration of alkalis, although the current studies in literature show that expansion value of ASR in HACs is smaller than that of OPC. It is likely that the high amount of fly ash and metakaolin contain high concentration of Al, which lowers the reaction of ASR in HAC, and the quantitative relationship between these parameters, such as reactive Al, free alkalis and water access and status, should be studied in the future to further lower the risk of ASR by better proportioning of raw materials, or improve the public confidence of using HAC.

In terms of precursors, seeking future SCMs that can replace fly ash and slag to prepare new HACs is also a vital topic for further research.

## REFERENCES

- Abdollahnejad, Z., Hlavacek, P., Miraldo, S., Fernando, P.T., & Aguiar, José Luís Barroso de. 2014. Compressive strength, microstructure and hydration products of hybrid alkaline cements. *Materials Research*, 17(4), 829-839.
- Acevedo-Martinez, E., Gomez-Zamorano, L. Y., & Escalante-Garcia, J. I. 2012. Portland cement-blast furnace slag mortars activated using waterglass: - Part I: Effect of slag replacement and alkali concentration. *Construction and Building Materials*, 37, 462-469.
- Alarcon-Ruiz, L., Platret, G., Massieu, E., & Ehrlacher, A. 2005. The use of thermal analysis in assessing the effect of temperature on a cement paste. *Cement and Concrete Research*, 35, 609-613.
- Alahrache, S., Winnefeld, F., Champenois, J. B., Hesselbarth, F., & Lothenbach, B. 2016. Chemical activation of hybrid binders based on siliceous fly ash and Portland cement. *Cement and Concrete Composites*, 66, 10-23.
- Al-Kutti, W., Nasir, M., Megat Johari, M. A., Islam, A. B. M. S., Manda, A. A., & Blaisi, N. I. 2018. An overview and experimental study on hybrid binders containing date palm ash, fly ash, OPC and activator composites. *Construction and Building Materials*, 159, 567-577.
- Al-Otaibi, S. 2008. Durability of concrete incorporating GGBS activated by waterglass. *Construction and Building Materials*, 22(10), 2059-2067.
- Althaus H.-J., Chudacoff, M., Hischer, R., & Jungbluth, N. 2007. Life Cycle Inventories of Chemicals. Final reportecoinvent data volume 2.0 No. 8., Dübendorf, CH.
- Angulo-Ramírez, D. E., Mejía de Gutiérrez, R., & Medeiros, M. 2018. Alkali-activated Portland blast furnace slag cement mortars: Performance to alkali-aggregate reaction. *Construction and Building Materials*, 179, 49-56.
- Angulo-Ramírez, D. E., Mejía de Gutiérrez, R., & Puertas, F. 2017. Alkali-activated Portland blast-furnace slag cement: Mechanical properties and hydration. *Construction and Building Materials*, 140, 119-128.
- Angulo-Ramirez, D. E., Mejía de Gutiérrez, R., Valencia-Saavedra, W. G., De Medeiros, M. H. F., & Hoppe-Filho, J. 2019. Carbonation of hybrid concrete with high blast furnace slag content and its impact on structural steel corrosion. *Materiales de Construccion*, 69(333), 1-10.

Askarian, M., Tao, Z., Adam, G., & Samali, B. 2018. Mechanical properties of ambient cured one-part hybrid OPC-geopolymer concrete. *Construction and Building Materials*, 186, 330-337.

Aperador, W.C., Ruiz, J.H.B., & Gómez, R. 2012. Corrosion of reinforcing bars embedded in alkali-activated slag concrete subjected to chloride attack. *Materials Research*, 15(1), 57-62.

Báčuvčík, M., Martauz, P., & Janotka, I. 2018. NTCC 2017: Long-term observation of the resistance of novel hybrid cement exposed to sulphate solution. *Key Engineering Materials*, 761, 163-168.

Bažant, Z.P. 2001. Prediction of concrete creep and shrinkage: past, present and future. *Nuclear Engineering and Design*, 203 (1), 27-38.

Bernal, S.A., & Provis, J. L. 2014. Durability of alkali-activated materials: progress and perspectives, *Journal of American Ceramics Society*. 97, 997-1008.

Bernal, S.A., Provis, J.L., Walkley, B., Nicolas, R. S., Gehman, J. D., Brice, D. G., Kilcullen, A. R., Duxson, P., & Van. Deventer, J. S. J. 2013. Gel nanostructure in alkali-activated binders based on slag and fly ash, and effects of accelerated carbonation. *Cement and Concrete Research*, 53, 127-144.

Bernal, S.A., San Nicolas, R., Provis, J.L., Mejía de Gutiérrez, R., & Deventer, J.S.J.V. 2014. Natural carbonation of aged alkali-activated slag concretes. *Materials and Structures*, 47(4), 693-707.

Bilim, C. 2011. Properties of cement mortars containing clinoptilolite as a supplementary cementitious material. *Construction and Building Materials*, 25, 3175-3180.

Bilim, C., & Ati, C. D. 2012. Alkali activation of mortars containing different replacement levels of ground granulated blast furnace slag. *Construction and Building Materials*, 28(1), 708-712.

Bissonnette, B., Pierre, P., & Pigeon, M. 1999. Influence of key parameters on drying shrinkage of cementitious materials. *Cement and Concrete Research*, 29 (10), 1655–1662.

Boesch, M.E., & Hellweg, S. 2010. Identifying improvement potentials in cement production with life cycle assessment. *Environmental & Science Technology*, 44, 9143-9149.

Borges, P.H.R., Costa, J.O., Milestone, N.B., Lynsdale, C.J., & Streatfield, R.E. 2010.

Carbonation of CH and C-S-H in composite cement pastes containing high amounts of BFS. *Cement and Concrete Research*, 40 (2), 284-292.

Brough, A.R., Holloway, M., Sykes, J., & Atkinson, A. 2000. Sodium silicate - based alkali activated slag mortars: Part II. The retarding effect of additions of sodium chloride or malic acid. *Cement and Concrete Research*, 30(9), 1375-1379.

Cao, R., Zhang, S., Banthia, N., Zhang, Y., & Zhang, Z. 2020. Interpreting the early-age reaction process of alkali-activated slag by using combined embedded ultrasonic measurement, thermal analysis, XRD, FTIR and SEM. *Composite Part B: Engineering*, 186, 107840.

Cao, Y., Wang, Y., Zhang, Z., Ma, Y., & Wang, H. 2021. Recent progress of utilization of activated kaolinitic clay in cementitious construction materials. *Composite Part B: Engineering*, 211, 108636.

Chang, J. 2003. A study on the setting characteristics of sodium silicate-activated slag pastes. *Cement and Concrete Research*, 33, 1005-1011.

Chen, Y., Pu, X., Yang, C., & Ding Q.J. 2002. Alkali aggregate reaction in alkali slag cement mortars. *Journal of Wuhan University Technology*, 17, 60-62.

Cheung, J., Jeknavorian, A., Roberts, L., & Silva, D. 2011. Impact of admixtures on the hydration kinetics of Portland cement. *Cement and Concrete Research*, 41, 1289-1309.

Chi, M., & Huang, R. 2013. Binding mechanism and properties of alkali-activated fly ash/slag mortars. *Construction and Building Materials*, 40, 291-298.

Collins, F., & Sanjayan, J. G. 2000. Effect of pore size distribution on drying shrinkage of alkali-activated slag concrete. *Cement and Concrete Research*, 30(9), 1401-1406.

Damidot, D., & Glasser, F. P. 1993. Thermodynamic investigation of the CaO-Al<sub>2</sub>O<sub>3</sub>-CaSO<sub>4</sub>-H<sub>2</sub>O system at 25°C and the influence of Na<sub>2</sub>O. *Cement and Concrete Research*, 23, 221-238.

Dan, X., Li, Y., Wang, S., & Fan, X. 2014. Study on retardation of preparing grouting material by alkali-activated fine slag powder. *Concrete*, 10, 81-85.

Davidovits, J., Comrie, DC., Paterson, J.H., & Ritcey, D.J., 1990. Geopolymeric concretes for environmental protection. *ACI Concrete International*, 12, 30-40.

Deschner, F., Winnefeld, F., Lothenbach, B., Seufert, S., Schwesig, P., Dittrich, S.,

Goetz-Neunhoeffler, F., & Neubauer, J. 2012. Hydration of portlandite cement with high replacement by siliceous fly ash, synthesis of high strength ambient. *Cement and Concrete Research*, 42,1389-1400.

Donatello, S., Fernández-Jimenez, A., & Palomo, A. 2013a. Very high volume fly ash cements. Early age hydration study using Na<sub>2</sub>SO<sub>4</sub> as an activator. *Journal of the American Ceramic Society*, 96(3), 900-906.

Donatello, S., García-Lodeiro, I., Fernandez-Jimenez, A., & Palomo, A. 2014a. Some durability aspects of hybrid alkaline cements. *MATEC Web of Conferences*, 11, 01008.

Donatello, S., Maltseva, O., Fernandez-Jimenez, A., & Palomo, A. 2014b. The early age hydration reactions of a hybrid cement containing a very high content of coal bottom ash. *Journal of the American Ceramic Society*, 97(3), 929-937.

Donatello, S., Palomo, A., & Fernández-Jiménez, A. 2013b. Durability of very high volume fly ash cement paste and mortars in aggressive solutions. *Cement and Concrete Composites*, 38, 12-20.

Duchesne, J., & Reardon, E.J. 1995. Measurement and prediction of portlandite solubility in alkaline solutions. *Cement and Concrete Research*, 25, 1043-1053.

Duran Atiş, C., Bilim, C., Çelik, Ö., & Karahan, O. 2009. Influence of activator on the strength and drying shrinkage of alkali-activated slag mortar. *Construction and Building Materials*, 23(1), 548-555.

Durdzinski, P.T. 2016. Hydration of multi-component cements containing cement clinker, slag, calcareous fly ash and limestone. *Water Resources Research*, 22-23.

Duxson, P., Provis, J.L., Lukey, G.C., & Van Deventer, J.S.J. 2007. The role of inorganic polymer technology in development of “green concrete”. *Cement and Concrete Research*, 37, 1590-1597.

Elahi, A., Khan, Q.U.Z., Barbhuiya, S.A., Basheer, P.A.M., & Russell, M.I. 2012. Hydration Characteristics of Cement Paste Containing Supplementary Cementitious Materials. *Arabian Journal for Science and Engineering*, 37 (3), 535-544.

El-Yamany, H. E., El-Salamawy, M. A., & El-Assal, N. T. 2018. Microstructure and mechanical properties of alkali-activated slag mortar modified with latex. *Construction and Building Materials*, 191, 32-38.

Escalante-Garcia, J. I., Castro-Borges, P., Gorokhovskiy, A., & Rodriguez-Varela, F. J. 2014. Portland cement-blast furnace slag mortars activated using waterglass: Effect

of temperature and alkali concentration. *Construction and Building Materials*, 66, 323-328.

Escalante-García, J.I., & Sharp, J.H. 2000. The effect of temperature on the early hydration of Portland cement and blended cements. *Advances in Cement Research*, 121-130.

Fernández-jiménez, A., & García-lodeiro, I. 2013. Hybrid alkaline cements-Part III: Durability and industrial applications. *Romanian Journal of Materials*, 43(2), 195-200.

Fernández-Jiménez, A., García-Lodeiro, I., Donatello, S., Maltseva, O., & Palomo, Á. 2014. Specific Examples of Hybrid Alkaline Cement. *MATEC Web of Conferences*, 11(March 2015), 01001.

Fernández-Jiménez, A., García-Lodeiro, I., Maltseva, O., & Palomo, A. 2019. Hydration mechanisms of hybrid cements as a function of the way of addition of chemicals. *Journal of the American Ceramic Society*, 102(1), 427-436.

Fernandez-Jimenez, A., García-Lodeiro, I., & Palomo, A. 2007. Durability of alkali-activated fly ash cementitious materials. *Journal of Materials Science*, 42(9), 3055-3065.

Fernández-Jiménez, A., Pastor, J. Y., Martín, A., & Palomo, A. 2010. High-temperature resistance in alkali-activated cement. *Journal of the American Ceramic Society*, 93(10), 3411-3417.

Fernández-Jiménez, A., & Puertas, F. 2001. Setting of alkali-activated slag cement. Influence of activator nature. *Advanced in Cement Research*, 13, 115-121.

Gao, X., Yu, Q.L., Brouwers, & H.J.H. 2016. Assessing the porosity and shrinkage of alkali activated slag-fly ash composites designed applying a packing model. *Construction and Building Materials*, 119, 175-184.

Gao, X., Yu, Q. L., & Brouwers, H. J. H. 2017. Apply  $^{29}\text{Si}$ ,  $^{27}\text{Al}$  MAS NMR and selective dissolution in identifying the reaction degree of alkali activated slag-fly ash composites. *Ceramics International*, 43(15), 12408-12419.

García-Lodeiro, I., Boudissa, N., Fernandez-Jimenez, A., & Palomo, A. 2018a. Use of clays in alkaline hybrid cement preparation. The role of bentonites. *Materials Letters*, 233, 134-137.

García-Lodeiro, I., Carcelen-Taboada, V., Fernández-Jiménez, A., & Palomo, A. 2016a. Manufacture of hybrid cements with fly ash and bottom ash from a municipal solid waste incinerator. *Construction and Building Materials*, 105, 218-226.

García-Lodeiro, I., Donatello, S., Fernández-Jiménez, A., & Palomo, A. 2013a. Basic Principles of Hybrid Alkaline Cements. *Chemistry and Materials Research*, 4(November), 27-30.

García-Lodeiro, I., Donatello, S., Fernández-Jiménez, A., & Palomo, A. 2016b. Hydration of hybrid alkaline cement containing a very large proportion of fly ash: A descriptive model. *Materials*, 9(8), 1-16.

García-Lodeiro, I., Fernández-Jiménez, A., & Palomo, A. 2013b. Hydration kinetics in hybrid binders: Early reaction stages. *Cement and Concrete Composites*, 39, 82-92.

García-Lodeiro, I., Fernández-Jiménez, A., & Palomo, A. 2013c. Variation in hybrid cements over time. Alkaline activation of fly ash-Portland cement blends. *Cement and Concrete Research*, Vol. 52, 112-122.

García-Lodeiro, I., Fernández-Jiménez, A., & Palomo, A. 2018b. Hybrid Alkaline Cements: Bentonite-Opc Binders. *Minerals*, 8(4), 137.

García-Lodeiro, I., Palomo, A., Fernández-Jiménez, A., & MacPhee, D. E. 2011. Compatibility studies between N-A-S-H and C-A-S-H gels. Study in the ternary diagram  $\text{Na}_2\text{O}-\text{CaO}-\text{Al}_2\text{O}_3-\text{SiO}_2-\text{H}_2\text{O}$ . *Cement and Concrete Research*, 41(9), 923-931.

García-Lodeiro, I., Palomo, A., Maltseva, O., & Fernández-Jiménez, A. 2013d. Hybrid Alkaline Cements: Part I. Fundamentals. *Romanian Journal of materials*, 43(1), 74-80.

García-Lodeiro, I., Taboada, V. C., Fernández-Jiménez, A., & Palomo, A. 2017. Recycling Industrial By-Products in Hybrid Cements: Mechanical and Microstructure Characterization. *Waste and Biomass Valorization*, 8(5), 1433-1440.

GB 175-2007, Common Portland Cement, Inspection and Quarantine of the People's Republic of China, Beijing, 2007.

GB/T 1596-2017, Fly ash used for cement and concrete, Inspection and Quarantine of the People's Republic of China, Beijing, 2017.

GB/T 18046-2017, Ground granulated blast furnace slag for cement, mortar and concrete, Inspection and Quarantine of the People's Republic of China, Beijing, 2017.

Gebregziabih, B. S., Thomas, R., & Peethamparan, S. 2015. Very early-age reaction kinetics and microstructural development in alkali-activated slag. *Cement and Concrete Composites*, 55, 91-102.

Gruskovnjak, A., Lothenbach, B., Winnefeld, F., Figi, R., S.-Ko, C., Adler, M., & Mäder, U. 2008. Hydration mechanisms of super sulphated slag cement. *Cement and*

Concrete Research, 38, 983-992.

Gruskovnjak, A., Lothenbach, B., Holzer, L., Figi, R., & Winnefeld, F. 2006. Hydration of alkali-activated slag: Comparison with ordinary Portland cement. *Advances in Cement Research*, 18(3), 119-128.

Gruyaert, E., Van den Heede, P., & De Belie, N. 2013. Carbonation of slag concrete: Effect of the cement replacement level and curing on the carbonation coefficient-effect of carbonation on the pore structure. *Cement and Concrete Composites*, 35 (1), 39-48.

Gu, Y., & Fang, Y. 2012. Shrinkage, cracking, shrinkage-reducing and toughening of alkali-activated slag cement-a short review. *Journal of the Chinese Ceramic Society*, 40, 76-84.

Guo, S., Zhang, Y., Wang, K., Bu, Y., Wang, C., & Ma, C. 2019. Delaying the hydration of Portland cement by sodium silicate: Setting time and retarding mechanism. *Construction and Building Materials*, 205, 543-548.

He, J., Gao, Q., Wu, Y., He, J., & Pu, X. 2018. Study on improvement of carbonation resistance of alkali-activated slag concrete. *Construction and Building Materials*, 176, 60-67.

Hossain, M. M., Karim, M.R., Hossain, M.K., Slam, M.N., & Zain, M.F.M. 2015. Durability of mortar and concrete containing alkali-activated binder with pozzolans: A review. *Construction and Building Materials*, 93, 95-109.

Hou, D., Ma, H., & Li, Z. 2015. Morphology of calcium silicate hydrate (CSH) gel: a molecular dynamic study, *Advanced Cement Research*, 27(3), 135-146.

Hubler, M.H., Thomas, J.J., & Jennings, H.M. 2011. Influence of nucleation seeding on the hydration kinetics and compressive strength of alkali activated slag paste. *Cement and Concrete Research*, 41, 842-846.

Ichikawa, T. 2009. Alkali-silica reaction, pessimum effects and pozzolanic effect. *Cement and Concrete Research*, 39, 716-726.

Ismail, I., Bernal, S. A., Provis, J.L., San Nicolas, R., Hamdan, S., & Van Deventer, J.S. 2014. Modification of phase evolution in alkali-activated blast furnace slag by the incorporation of fly ash. *Cement and Concrete Composites*, 45, 125-35.

Janotka, I., Martauz, P., & Testing, B. 2014. Chemical Resistance of Novel Hybrid Cement in Various Aggressive Solutions. *RILEM International Workshop on Performance-Based Specification and Control of Concrete Durability*, (June), 17-24.

Jelenic, I., Panovic, A., Halle, R., & Gacesa, T. 1977. Effect of gypsum on the hydration and strength development of commercial Portland cements containing alkali sulphates. *Cement and Concrete Research*, 7, 239-246.

JGJ 55-2011, Specification for mix proportion design of ordinary concrete, Ministry of Housing and Urban-Rural Development of the People's Republic of China, Beijing, 2011.

Jia, Z., Yang, Y., Yang, L., Zhang, Y., & Sun, Z. 2018. Hydration products, internal relative humidity and drying shrinkage of alkali activated slag mortar with expansion agents. *Construction and Building Materials*, 158, 198-207.

Jiao, Z., Wang, Y., Zheng, W., & Huang, W. 2018. Effect of dosage of sodium carbonate on the strength and drying shrinkage of sodium hydroxide based alkali-activated slag paste. *Construction and Building Materials*, 179, 11-24.

Jiao, Z., Wang, Y., Zheng, W., & Huang, W. 2019. Effect of the activator on the performance of alkali-activated slag mortars with pottery sand as fine aggregate. *Construction and Building Materials*, 197, 83-90.

Juenger, M. C. G., Winnefeld, F., Provis, J. L., & Ideker, J. H. 2011. Advances in alternative cementitious binders. *Cement and Concrete Research*, 41(12), 1232-1243.

Kaja, A. M., Lazaro, A., & Yu, Q. L. 2018. Effects of Portland cement on activation mechanism of class F fly ash geopolymer cured under ambient conditions. *Construction and Building Materials*, 189, 1113-1123.

Kellenberger D.K.T., Althaus, H.-J., & Jungbluth, N. 2004. Life Cycle Inventories of Building Products. Final report ecoinvent data volume 2.0 No. 7, Dübendorf, CH.

Kong, D.L.Y., & Sanjayan, J.G. 2010. Effect of elevated temperatures on geopolymer paste, mortar and concrete. *Cement and Concrete Research*, 40 (2), 334-339.

Krivenko, P., Drochytka, R., Gelevera, A., & Kavalerova, E. 2014. Mechanism of preventing the alkali-aggregate reaction in alkali activated cement concretes. *Cement and Concrete Composites*, 45, 157-165.

Krivenko, P., Kovalchuk, G., & Kovalchuk, O. 2013. Hybrid fly ash-based alkali activated cements. *Conference Paper, Brno*, 66-72.

Law, D.W., Adam, A.A., Molyneaux, T.K., & Patnaikuni, I. 2012. Durability assessment of alkali activated slag (AAS) concrete. *Materials and Structures*, 45, 1425-1437.

- Le Saoût, G., Ben Haha, M., Winnefeld, F., & Lothenbach, B. 2011. Hydration degree of alkali-activated slags: A  $^{29}\text{Si}$  NMR study, *Journal of American Ceramics Society*, 1-7
- Lecomte, I., Henrist, C., Liégeois, M., Maseri, F., Rulmont, A., & Cloots, R. 2006. (Micro)-structural comparison between geopolymers, alkali-activated slag cement and Portland cement. *Journal of the European Ceramic Society*, 26(16), 3789–3797.
- Lee, N.K., & Lee, H. K. 2015. Reactivity and reaction products of alkali-activated, fly ash/slag paste. *Construction and Building Materials*, 81, 303-312.
- Lee, N. K., & Lee, H. K. 2016. Influence of the slag content on the chloride and sulfuric acid resistances of alkali-activated fly ash/slag paste. *Cement and Concrete Composites*, 72, 168-179.
- Li, N., Shi, C., & Zhang, Z. 2019. Understanding the roles of activators towards setting and hardening control of alkali-activated slag cement. *Composites Part B: Engineering*, 171(January), 34-45.
- Li, W., Hong, J., Zhu, X., Yang, D., Bai, Y., Liu, J., & Miao, C. 2018. Retardation mechanism of anionic asphalt emulsion on the hydration of Portland cement. *Construction and Building Materials*, 163,714-723.
- Martauz, P., Janotkav, I., Strigáč, J., & Bačuvčík, M. 2016. Fundamental properties of industrial hybrid cement: utilization in ready-mixed concretes and shrinkage-reducing applications. *Materials De Construction*, 1-12.
- Martinez-Ramirez, S., & Palomo, A. 2001. OPC hydration with highly alkaline solutions. *Advances in Cement Research*, 13(3), 123-129.
- Mastali, M., Kinnunen, P., Dalvand, A., Mohammadi Firouz, R., & Illikainen, M. 2018. Drying shrinkage in alkali-activated binders - A critical review. *Construction and Building Materials*, 190, 533-550.
- Mataalkah, F., Salem, T., Shaafaey, M., & Soroushian, P. 2019. Drying shrinkage of alkali activated binders cured at room temperature. *Construction and Building Materials*, 201, 563-570.
- Martauz, P., & team. 2019. Evaluation of existing technology for the production of hybrid alkaline cement, 15th International Congress on the Chemistry of Cement, Prague, September 15.

McLellan, B. C., Williams, R. P., Lay, J., Van Riessen, A., & Corder, G. D. 2011. Costs and carbon emissions for geopolymer pastes in comparison to ordinary portland cement. *Journal of Cleaner Production*, 19, 1080-1090.

Mehta, P.K., & Monteiro, P.J.M. 1993. *Concrete Structures, Properties and Materials*.

Mehta, P. K., & Monteiro, P. J. M. 2006. *Concrete: microstructure, properties, and materials*. McGraw-Hill.

Mejía, J. M., Rodríguez, E., Mejía de Gutiérrez, R., & Gallego, N. 2015. Preparation and characterization of a hybrid alkaline binder based on a fly ash with no commercial value, *Journal of Cleaner Production*, 104, 346-352.

Mejía-Arcila, J., Valencia-Saavedra, W., & Mejía de Gutiérrez, R. 2020. Eco-efficient alkaline activated binders for manufacturing blocks and pedestrian pavers with low carbon footprint: Mechanical properties and LCA assessment. *Materiales de Construcción*, 70(340), 1-15.

Melo Neto, A. A., Cincotto, M. A., & Repette, W. 2008. Drying and autogenous shrinkage of pastes and mortars with activated slag cement. *Cement and Concrete Research*, 38(4), 565-574.

Najafi Kani, E., Allahverdi, A., & Provis, J. L. 2012. Efflorescence control in geopolymer binders based on natural pozzolan. *Cement and Concrete Composites*, 34(1), 25-33.

Nath, P., & Sarker, P. K. 2015. Use of OPC to improve setting and early strength properties of low calcium fly ash geopolymer concrete cured at room temperature. *Cement and Concrete Composites*, 55, 205-214.

Pacheco-Torgal, F., Abdollahnejad, Z., Camões, A.F., Jamshidi, M., & Ding, Y. 2012. Durability of alkali-activated binders: A clear advantage over Portland cement or an unproven issue?. *Construction and Building Materials*, 30, 400-405.

Palomo, A., Fernández-Jiménez, A., Kovalchuk, G., Ordoñez, L. M., & Naranjo, M. C. 2007. Opc-fly ash cementitious systems: Study of gel binders produced during alkaline hydration. *Journal of Materials Science*, 42(9), 2958-2966.

Palomo, A., Monteiro, P., Martauz, P., Bilek, V., & Fernandez-Jimenez, A. 2019. Hybrid binders: A journey from the past to a sustainable future (opus caementicium futurum). *Cement and Concrete Research*, 124(March), 105829.

- Palomo, Á., Maltseva, O., García-lodeiro, I., & Fernández-jiménez, A. N. A. 2013. Hybrid Alkaline Cements. Part II : The Clinker Factor. *Romanian Journal of Materials*, 43(1), 74-80.
- Palomo, A., Grutzeck, M. W., & Blanco, M. T. 1999. Alkali-activated fly ashes: A cement for the future. *Cement and Concrete Research*, 29(8), 1323-1329.
- Partha Sarathi Deb, P. S., Nath, P., & Sarker, P. K. 2015. Drying shrinkage of slag blended fly ash geopolymer concrete cured at room temperature. *Procedia Engineering*, 125, 594-600.
- Pratiwi, W. D., Fansuri, H., Ekaputri, J. J., & Triwulan. 2017. Effect of Activators on Strength of Hybrid Alkaline Cement. *IOP Conference Series: Materials Science and Engineering*, 196(1), 1- 6.
- Provis, J. L., Palomo, A., & Shi, C. 2015. Advances in understanding alkali-activated materials. *Cement and Concrete Research*, 78, 110-125.
- Puertas, F., Palacios, M., & Vázquez, T. 2006. Carbonation process of alkali-activated slag mortars. *Journal of Materials Science*, 41, 3071-3082.
- Puertas, F., Varga, C., Palacios, M., Pellerin, B., Eychenne-Baron, C., Babayan, D., & Elkhadiri, I. 2011. Alkali-Activation of Slag Cements: Activation Process, Microstructure and Mechanical Properties. 13th ICCG, Madrid, (July), 1-7.
- Qiu, X., Sasaki, K., Takali, Y., Hirajima, T., Ideta, K., & Miyawali, J. 2015. Mechanism of boron uptake by hydrocalumite calcined at different temperatures. *Journal of Hazardous Materials*, 287, 268-277.
- Qu, B., Martin, A., Pastor, J. Y., Palomo, A., & Fernández-Jiménez, A. 2016. Characterisation of pre-industrial hybrid cement and effect of pre-curing temperature. *Cement and Concrete Composites*, 73, 281-288.
- Rivera, J. F., De Gutierrez, R. M., Mejia, J. M., & Gordillo, M. 2014. Hybrid cement based on the alkali activation of by-products of coal. *Revista de La Construccion*, 13(2), 31-39.
- Ríos, A., González, M., Montes, C., Vázquez, J., & Arellano, J. 2020. Assessing the effect of fly ash with a high SO<sub>3</sub> content in hybrid alkaline fly ash pastes (HAFAPs). *Construction and Building Materials*, 238, 117776.
- Robayo-Salazar, R., Mejía-Arcila, J., Mejía de Gutiérrez, R., & Martínez, E. 2018. Life cycle assessment (LCA) of an alkali-activated binary concrete based on natural

volcanic pozzolan: A comparative analysis to OPC concrete. *Construction and Building Materials*, 176, 103-111.

San Nicolas, R., Bernal, S. A., Mejía De Gutiérrez, R., Van Deventer, J. S. J., & Provis, J. L. 2014. Distinctive microstructural features of aged sodium silicate-activated slag concretes. *Cement and Concrete Research*, 65, 41-51.

San Nicolas, R., & Provis, J.L. 2012. Interfacial transition zone in alkali-activated slag concrete, Twelfth International Conference on Recent Advances in Concrete Technology and Sustainability Issues, American Concrete Institute, Prague, Czech Republic (CD-ROM proceedings)

Schneider, M., Romer, M., Tschudin, M., & Bolio, H. 2011. Sustainable cement production—present and future. *Cement and Concrete Research*, 41, 642-650.

Scrivener, K.L., Juilland, P., & Monteiro, P.J.M. 2015. Advances in understanding hydration of Portland cement. *Cement and Concrete Research*, 78, 38-56.

Scrivener, K., Snellings, R., & Lothenbach, B. A practical guide to microstructural analysis of cementitious materials. CRC Press, Oxon, UK, 2016, 188-198.

Scrivener, K. L., Füllmann, T., Gallucci, E., Walenta, G., & Bermejo, E. 2004a. Quantitative study of Portland cement hydration by X-ray diffraction/Rietveld analysis and independent methods. *Cement and Concrete Research*, 34(9), 1541-1547.

Scrivener, K. L. 2004b. Backscattered electron imaging of cementitious microstructures: Understanding and quantification. *Cement and Concrete Composites*, 26(8), 935-945.

Shi, C., Jiménez, A. F., & Palomo, A. 2011. New cements for the 21st century: The pursuit of an alternative to Portland cement. *Cement and Concrete Research*, 41(7), 750-763.

Shi, C., Krivenko, P.V., & Roy, D.M. *Alkali-Activated Cements and Concretes*, Taylor & Francis, Abingdon, UK, 2006

Shi, C., Shi, Z., Hu, X., Zhao, R., & Chong, L. 2015a. A review on alkali-aggregate reactions in alkali-activated mortars/concretes made with alkali-reactive aggregates. *Materials and Structures*, 48(3), 621-628.

Shi, C., & Xie, P. 1998. Interface between cement paste and quartz sand in alkali-activated slag mortars. *Cement and Concrete Research*, 28, 887-896.

Shi, H., & Liu, H. 2008. Resource recovery of flue gas desulphurization gypsum in slag cement. *Journal of Tongji University (Nature Science)*, 36(1), 66-70.

Shi, Z., Shi, C., Zhao, R., & Wan, S. 2015b. Comparison of alkali–silica reactions in alkali-activated slag and Portland cement mortars. *Materials and Structures*, 48(3), 743-751.

Shi, Z., Shi, C., Wan, S., & Ou, Z. 2017. Effect of alkali dosage on alkali-silica reaction in sodium hydroxide activated slag mortars. *Construction and Building Materials*, 143, 16-23.

Shi, Z., Shi, C., Wan, S., & Zhang, Z. 2018a. Effects of alkali dosage and silicate modulus on alkali-silica reaction in alkali-activated slag mortars. *Cement and Concrete Research*, 111(February), 104-115.

Shi, Z., Shi, C., Zhang, J., Wan, S., Zhang, Z., & Ou, Z. 2018b. Alkali-silica reaction in waterglass-activated slag mortars incorporating fly ash and metakaolin. *Cement and Concrete Research*, 108, 10-19.

Shimada, Y., & Young, J. F. 2004. Thermal stability of ettringite in alkaline solutions at 80°C. *Cement and Concrete Research*, 34, 2261-2268.

Singh, M., & Siddique, R. 2014. Compressive strength, drying shrinkage and chemical resistance of concrete incorporating coal bottom ash and partial or total replacement of sand. *Construction and Building Materials*, 68, 39-48.

Škvára, F., Kopecký, L., Šmilauer, V., Alberovska, L., & Bittner, Z. 2009a. Material and structural characterization of alkali activated low-calcium brown coal fly ash. *Journal of Hazardous Materials*, 168, 711-720.

Škvára, F., Kopecký, L., Myšková, L., Šmilauer, V. Í. T., Alberovská, L., & Vinšová, L. 2009b. Aluminosilicate polymers -Influence of elevated temperatures, efflorescence. *Ceramics - Silikaty*, 53(4), 276-282.

Slowik, V., Schmidt, M., & Fritzsche, R. 2008. Capillary pressure in fresh cement-based materials and identification of the air entry value. *Cement and Concrete Composites*, 30 (7), 557–565.

Stengel, T., Reger, J., & Heinz, D. 2009. LCA of geopolymers concrete - what is the environmental benefit? In: *Proceedings Concrete 09, 24th Biennial Conf Australian Concrete Institute, Sydney, Concrete Institute of Australia*, 54-62.

Strigáč, J., & Martauz, P. 2014. Novel hybrid cement based on different mechanisms of setting and hardening. *RILEM International workshop on performance-based specification and control of concrete durability (June)*, 25-31.

- Talling, B., & Brandstetr, J. 1989. Present state and future of alkali-activated slag concretes. ACI Special Publication, 114, 1519-1546.
- Tang, F. J., & Gartner, E. M. 1988. Influence of sulphate source on Portland cement hydration. *Advances in Cement Research*, 1, 67-74.
- Taylor, H. F. W. *Cement Chemistry* (2<sup>nd</sup> edition). Thomas Telford Publishing, London, 1997.
- Teh, S. H., Wiedmann, T., Castel, A., & De Burgh, J. 2017. Hybrid life cycle assessment of greenhouse gas emissions from cement, concrete and geopolymer concrete in Australia. *Journal of Cleaner Production*, 152, 312-320.
- Tennis, P. D., & Jennings, H. M. 2000. A model for two types of calcium silicate hydrate in the microstructure of Portland cement pastes. *Cement and Concrete Research*, 30(6), 855-863.
- Thomas, J. J., Rothstein, D., Jennings, H. M., & Christensen, B. J. 2003. Effect of hydration temperature on the solubility behavior of Ca-, S-, Al-, and Si- bearing solid phases in Portland cement pastes. *Cement and Concrete Research*, 33, 2037-2047.
- Thomas, M. 2011. The effect of supplementary cementing materials on alkali-silica reaction: A review. *Cement and Concrete Research*, 41, 1224-1231
- Thomas, R. J., Lezama, D., & Peethamparan, S. 2017. On drying shrinkage in alkali-activated concrete: Improving dimensional stability by aging or heat-curing. *Cement and Concrete Research*, 91, 13-23.
- Torres, J., Mejía de Gutiérrez, R., Castelló, R., & Vizcayno, C. 2008. Proceso de Hidratación de Pastas de OPC Adicionadas Con Caolín Tratado Térmicamente. *Rev. Fac. Ing. Univ. Antioquia* 43(2008) 77-85.
- Turner, L. K., & Collins, F. G. 2013. Carbon dioxide equivalent (CO<sub>2</sub>-e) emissions: A comparison between geopolymer and OPC cement concrete. *Construction and Building Materials*, 43, 125-130.
- Vargas, P., Restrepo-Baena, O., & Tobón, J. I. 2017. Microstructural analysis of interfacial transition zone (ITZ) and its impact on the compressive strength of lightweight concretes. *Construction and Building Materials*, 137, 381-389.
- Wang, Y., Cao, Y., Zhang, P., Ma, Y., Zhao, T., Wang, H., & Zhang, Z. 2019. Water absorption and chloride diffusivity of concrete under the coupling effect of uniaxial compressive load and freeze-thaw cycles. *Construction and Building Materials*, 209, 566-576.

- Walkley, B., & Provis, J. L. 2019. Solid-state nuclear magnetic resonance spectroscopy of cements. *Materials Today Advances*, 1(May), 100007.
- Xue, L., Zhang, Z., & Wang, H. 2021. Hydration mechanisms and durability of hybrid alkaline cements (HACs): A review. *Construction and Building Materials*, 266, 121039.
- Yang, N. 2018. *Non-tradition Cementitious Materials Chemistry*. Wuhan University of Technology Press, China.
- Ye, H., Cartwright, C., Rajabipour, F., & Radlińska, A. 2017. Understanding the drying shrinkage performance of alkali-activated slag mortars. *Cement and Concrete Composites*, 76, 13-24.
- Ye, H., & Radlińska, A. 2016. Shrinkage mechanisms of alkali-activated slag. *Cement and Concrete Research*, 88, 126-135.
- Yip, C. K., & Van Deventer, J. S. J. 2003. Microanalysis of calcium silicate hydrate gel formed within a geopolymeric binder. *Journal of Materials Science*, 38(18), 3851-3860.
- Yu, Q., Zhao, S., Huang, J., Qiao, F., Guo, W., Yin, S., Wen, Z., & Gu, G. 2005. Retardation of gelation and improvement of flow ability for alkali activated carbonation-slag cementitious grouting material. *Journal of the Chinese Ceramic Society*, 33(7), 871-875.
- Yu, X., Yu, C., Ran, Q., & Liu, J. 2018. Retarding mechanism of hydroxy carboxylic acid retarder on cement hydration. *Journal of Chinese Ceramics Society*, 46, 181-186.
- Yuan, R. *Cementitious Materials Science (2<sup>nd</sup> edition)*. Wuhan University of Technology Press, China, 1996.
- Zah, R., & Hischer, R. 2007. *Life Cycle Inventories of Detergents. Final report ecoinvent data volume 2.0, No. 12*, Dübendorf, CH.
- Zeng, Q., Li, K., Fen-Chong, T., & Dangla, P. 2012. Pore structure characterization of cement pastes blended with high-volume fly-ash. *Cement and Concrete Research*, 42, 194-204.
- Zhang, Z., Provis, J. L., Reid, A., & Wang, H. 2014a. Geopolymer foam concrete: An emerging material for sustainable construction. *Construction and Building Materials*, 56, 113-127.

Zhang, J., Shi, C., Zhang, Z., & Ou, Z. 2017. Durability of alkali-activated materials in aggressive environments: A review on recent studies. *Construction and Building Materials*, 152, 598-613.

Zhang, Z., Li, L., Ma, X., Wang, H., & Si, A. 2016. Compositional, microstructural and mechanical properties of ambient condition cured alkali-activated cement. *Construction and Building Materials*, 113, 237-245.

Zhang, Z., Provis, J.L., Ma, X., Reid, A., & Wang, H. 2018. Efflorescence and sub-florescence induced microstructural and mechanical evolution in fly ash-based geopolymers. *Cement and Concrete Composites*, 92, 165-177.

Zhang, Z., Provis, J. L., Reid, A., & Wang, H. 2014b. Fly ash-based geopolymers: The relationship between composition, pore structure and efflorescence. *Cement and Concrete Research*, 64, 30-41.

Zheng, W., Zou, M., & Wang, Y. 2019. Literature review of alkali-activated cementitious materials. *Journal of Building Structures*, 40 (1), 28-39.

## APPENDIX

### A1. Setting time and hydration heat of HAC with solid alkali activator

Solid alkali activator is used to control the initial setting time. The setting times of OPC and HACs with liquid activator (HACS) and solid activator (HACS\*) are given in Figure A-1. It can be found that HACs show much shorter initial and final setting times than that of OPC. HAC with solid activator reacts slowly than that of liquid activator. The reason is explained as that the solid activator has to dissolve before reacting, while the liquid activator reacts directly. However, the final setting time is not very long.

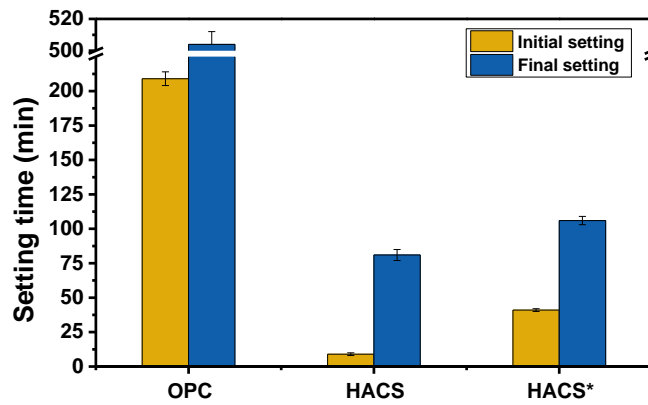


Figure A-1. Setting times of OPC and HACs with different activator states

The initial setting times of HAC activated by solid activator with different alkali contents and modulus are shown in Figure A-2.

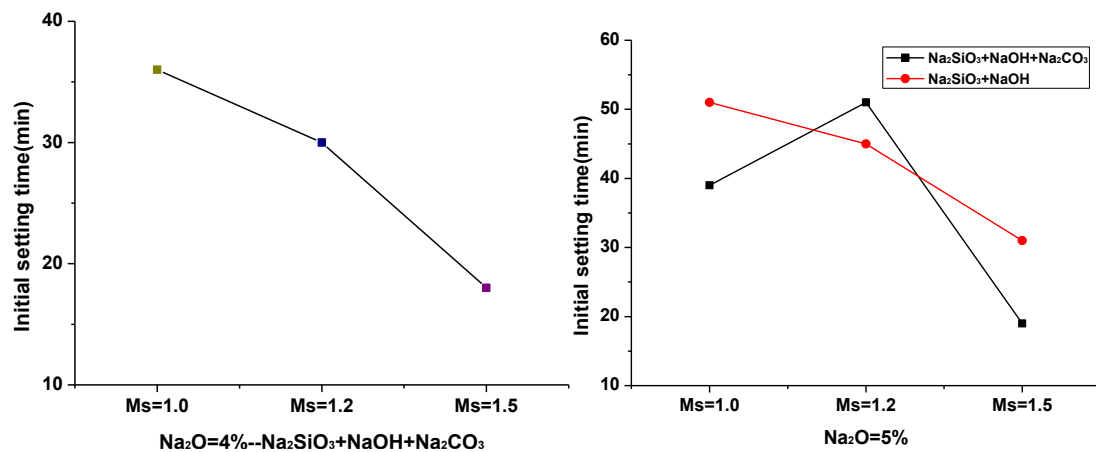


Figure A-2. Initial setting time of HAC with solid activator

In Figure A-2, it can be seen that the initial setting time is shortened with the increase of solid activator modulus. The HAC shows longer initial setting time when the Na<sub>2</sub>O

content is 5% and modulus of activator is equals to 1.2. Compared with Figure A-1, the HAC activated by solid activator exhibits longer initial setting time than liquid activator when the modulus is 1.0-1.2.

The profiles of heat flow and cumulative heat vs time graphs for the HACs pastes with different activator states are shown in Figure A-3.

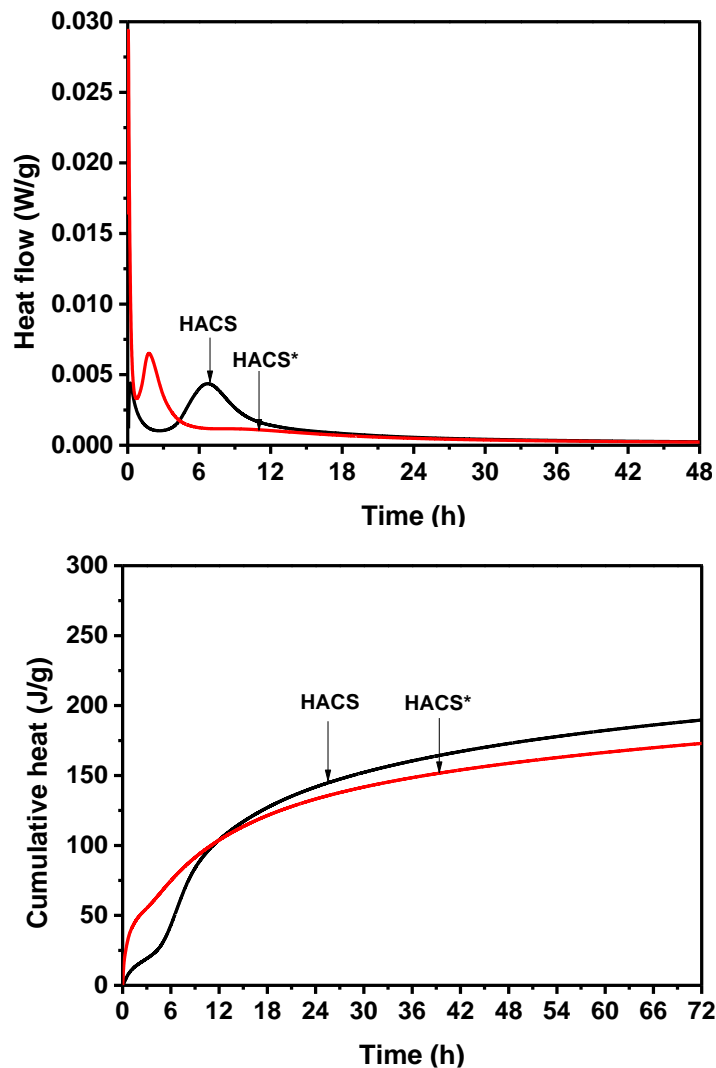


Figure A-3. Heat flow and cumulative heat of HACs activated by liquid and solid activators

It can be seen that the HACs\* also shows two exothermic peaks as HACs, including one initial sharp strong peak for a very short time and one lower and wider peak. However, the second peak of HACs\* appears earlier than HACs. In addition, the cumulative heat release of HACs\* is greater than HACs in the first 12 hours, but then the situation reverses after 12 hours. The cumulative heat of HAC activated by solid

activator is ultimately less than that of with liquid activated. It was reported that the cumulative heat could be an indicator of the amount of hydration products because the heat of hydration was generated from the formation of hydration products, and thus the total heat of hydration could be used to reflect the hydration degree. Therefore, it can be deduced from the cumulative heat curve that the HACs\* generates less hydration products than HACs, resulting in lower compressive strength (see Figure A-4).

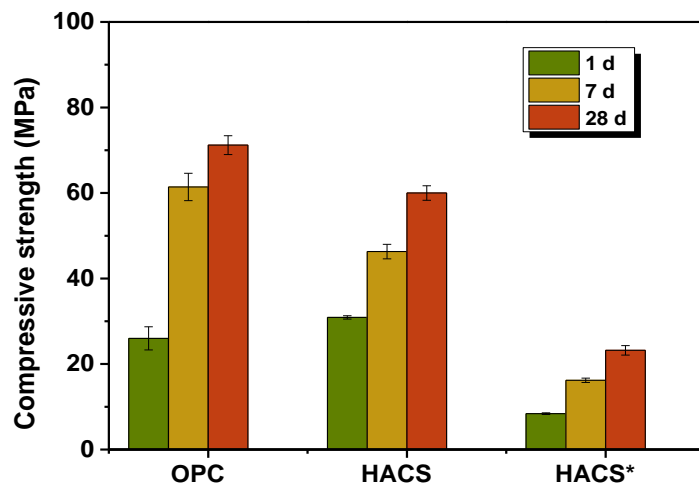
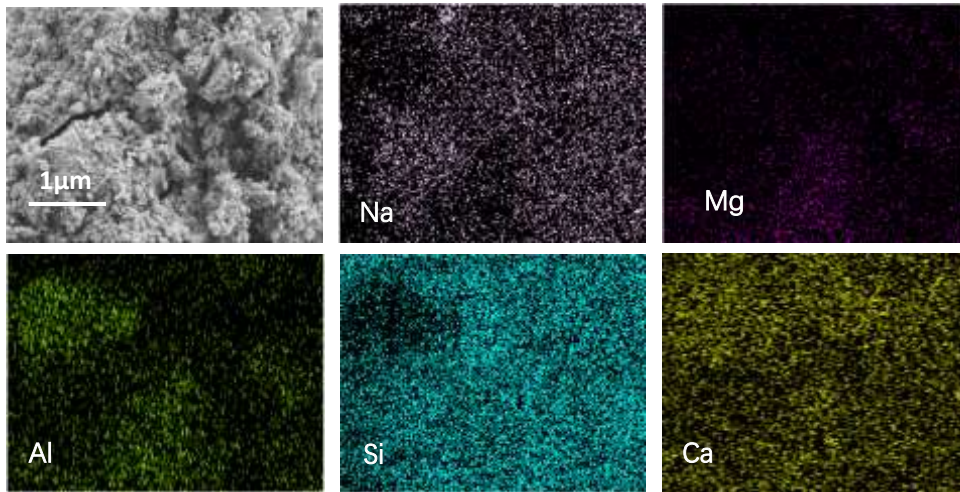


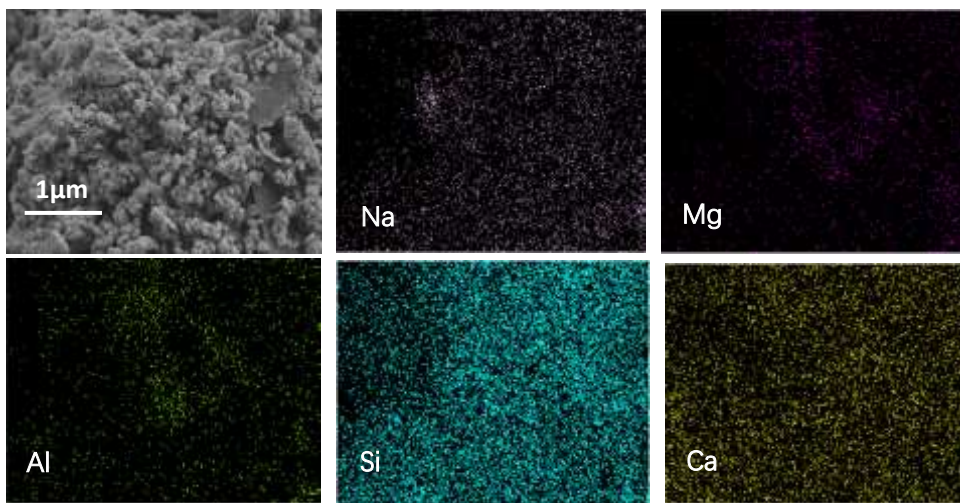
Figure A-4. Compressive strengths of OPC and HACs with liquid and solid activator at different curing ages

## **A2. Electron-mapping of HAAC with various gypsum dosages**

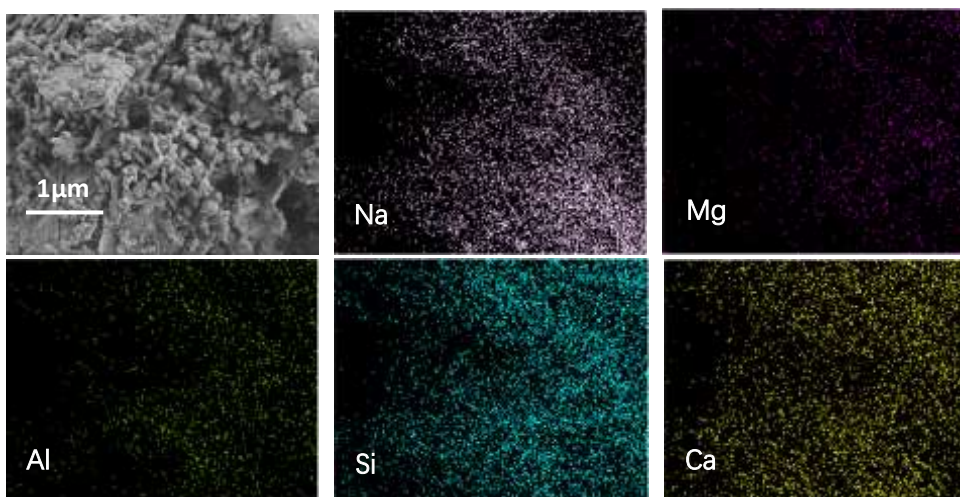
Figure A-5 shows the electron-mapping of some elements of HAAC with various gypsum dosages to further determine the element distribution. The element distribution of HAACs at initial setting time shows that the Na, Si and Ca element dosages are different during the HAACs incorporating gypsum. The Na concentration in the HAAC20 is the least, which is compatible with the above EDS analysis. There is no significant difference in Mg and Al contents in the HAACs with various amounts of gypsum. In terms of HAACs paste cured for 24 hours, although the concentration of Na is lower than that of initial setting time, it still shows the most sparse distribution when the gypsum was 20%. Moreover, the Ca and Si display a similar distribution to Na. This further illustrates that Ca ions dissolution is inhibited to the maximum extent when HAAC is mixed with 20% gypsum, resulting in the longest setting time and the loosest microstructure. The distribution change of Na ions is also explained by reacting with sulfate ions to form  $\text{Na}_2\text{SO}_4$ .



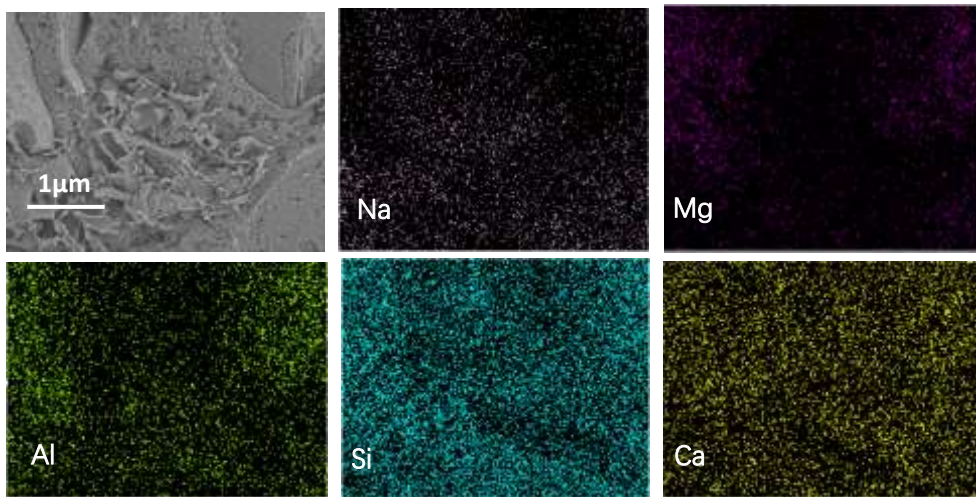
(a) HAAC10 at initial setting time



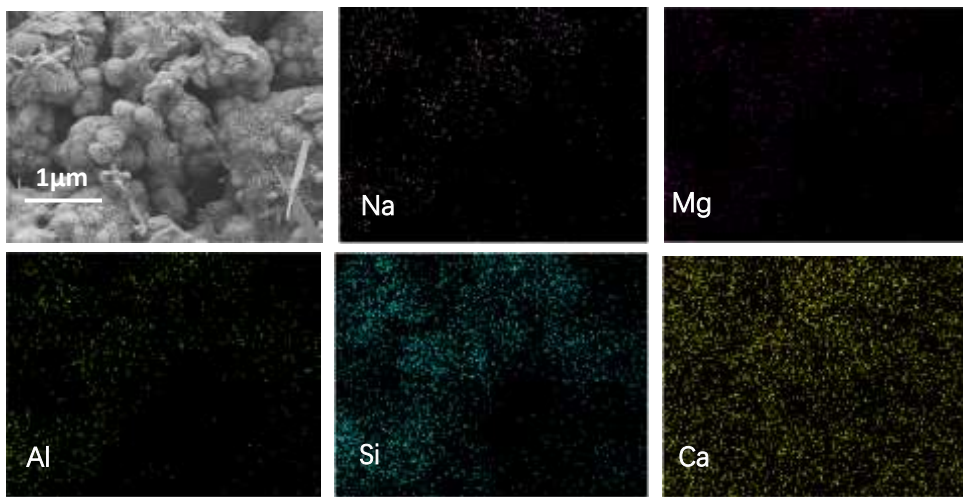
(b) HAAC20 at initial setting time



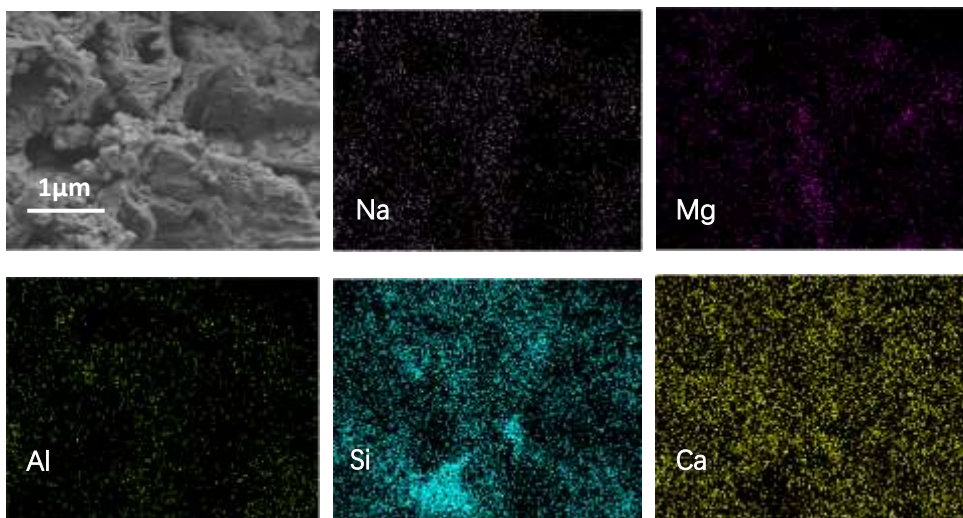
(c) HAAC30 at initial setting time



(d) HAAC10 for 24 hours of curing



(e) HAAC20 for 24 hours of curing



(f) HAAC30 for 24 hours of curing

Figure A-5. Elemental distribution mapping of HAACs at different curing ages